Exploring Interactions between Force, Repetition and Posture on Low Back Joint Loading and Intervertebral Disc Injury

by

Chad E. Gooyers

A thesis
presented to the University of Waterloo
in fulfillment of the
thesis requirement for the degree of
Doctor of Philosophy
in
Kinesiology

Waterloo, Ontario, Canada, 2014

AUTHOR'S DECLARATION

I hereby declare that I am the sole author of this thesis. This is a true copy of the thesis, including any required final revisions, as accepted by my examiners.

I understand that my thesis may be made electronically available to the public.

x_____

Abstract

Background & Purpose

Low back pain (LBP) affects approximately 80% of the population at some point in their lives, with 65% of cases becoming chronic pain sufferers. Approximately 40% of LBP cases are attributed to intervertebral disc (IVD) disruption, which can be characterized by damage to the annulus fibrosus (AF) or cartilaginous endplates. Although the medical community strives to treat and rehabilitate these injuries, there is immense opportunity for primary prevention, given that most problems will continue to persist until the underlying mechanical risk factors are resolved. The most commonly accepted mechanical exposures linked to low back injury include: (i) high force demands, (ii) frequent repetition and (iii) awkward postures. However, these demands have typically been examined in isolation, and are often assumed to function independently regarding injury risk. As such our understanding of the combined effects of external task demands on internal joint loading, and their influence on fatigue injury pathways in the lumbar spine may be limited, overly simplified, and underestimate the potential risk of injury. Therefore, using a combination of both *in vivo* modeling of human movement and *in vitro* mechanical testing of porcine IVD tissue, the global purpose of this thesis was twofold: (i) explore interactions between external task demands on *in vivo* joint loading in the lumbar spine, and (ii) characterize the combined effects of each of these mechanical exposures on fatigue injury pathways in the IVD. In-line with these global purposes, four independent studies were conducted, each with their own focused objectives.

Study I: Exploring interactions between external task demands in lifting on low back joint loads in vivo.

Background: The most commonly accepted mechanical risk factors linked to low back injury include: (i) high force demands; (ii) frequent repetition; and (iii) deviated postures. However, our understanding of the interactions that exist between each of these factors on the resultant *in vivo* joint loads that occur in the lumbar spine during manual materials handling remains limited.

Objectives: The primary objective of this study was to explore interactions between: (i) the magnitude of the external load, (ii) speed of lifting movement, and (iii) symmetry of initial

load placement (i.e. posture) on estimates of *in vivo* joint loading at L4/L5 during simulated occupational lifting.

Methods: Thirty-four participants with manual materials handling experience were recruited. Three-dimensional motion data were captured together with foot-ground contact forces and activation of six bilateral trunk muscle groups while participants performed lifts with two loads ("light" and "heavy"), at two movement speeds ("controlled" and "fast"), and using two initial load placements ("symmetric" and "asymmetric"; i.e. posture). Inverse dynamics analyses were conducted, and outputs were incorporated into a three-dimensional EMG-assisted musculoskeletal model of the lumbar spine to generate L4/L5 joint compression and shear force-time histories.

Results: Significant interactions between load, speed and posture emerged in virtually every dependent measure that was used to characterize the time-varying estimates of load in the lumbar spine. Significant two-way interactions between load and speed ($p = 0.0035$), as well as speed and posture ($p = 0.0004$) were revealed in peak measures of L4/L5 compressive forces. A significant three-way interaction between load, speed and posture ($p = 0.0477$) was revealed in the cumulative measure of compressive loading at L4/L5 during the ascending portion of the lifting trials. A significant main effect of load ($p < 0.0001$) and a significant two-way interaction between speed and posture ($p = 0.0384$) was revealed in peak measures of peak L4/L5 anterior/posterior (AP) joint shear.

Conclusions: Results from this investigation provide strong evidence that known mechanical risk factors linked to low back injury should not be viewed in isolation. Stated differently, the influence of external demands on *in* vivo estimates of joint loading was not additive. Therefore, future injury prevention efforts should consider the complex interactions that exist between external task demands and their combined influence on internal (musculoskeletal) joint loading.

Study II: Exploring the combined effects of force, repetition and posture on injury pathways in isolated functional spinal units from sub-acute-failure magnitudes of cyclic compressive force.

Background: Previous research suggests that when the magnitude of peak compressive force applied during cyclic loading exceeds 30% of a functional spinal unit's (FSU) estimated

ultimate compressive tolerance (UCT), endplate fracture will occur before intervertebral disc (IVD) herniation. However, the amount of tissue damage imposed to the IVD of "survivor" specimens from these investigations remains unknown, as this threshold has been established through the detection of fatigue injury or using radiographic measures used to track the nucleus pulposus through layers of the AF.

Objectives: The primary objective of this study was to explore interactions between: (i) the magnitude of the applied compressive force, (ii) cycle rate and (iii) degree of postural deviation on known fatigue injury pathways in FSUs at sub-acute-failure magnitudes of peak compressive force. The secondary purpose was to characterize the micro-structural damage imposed to the AF in "survivor" specimens using histological staining methods.

Methods: A total of 126 FSUs were initially included in the study. Three levels of peak compressive force (10, 20 and 40% of specimens' UCT), three cycle rates (5, 10 and 30 cycles per minute) and two dynamic postural conditions (100 and 300% neutral zone range; NZ) were examined using a full-factorial design. Cyclic compressive force was applied using a modified material testing apparatus, using a time-varying waveform with synchronous flexion/extension rotation that was based on *in vivo* estimates of lumbar compression and spine posture during an occupation lifting task. All FSUs were cyclically loaded for 5000 cycles or until fatigue failure occurred. AF tissue from 36 "survivor" FSUs was excised for histological analysis across experimental conditions. Three tissue samples, consisting of the outermost 10 lamellae, were obtained from the anterior and posterior-lateral regions of the IVD from each specimen. To characterize the micro-structural damage in the AF, frozen tissue samples mounted in OCT compound were serially sectioned using a cryostat microtome, H&E stained and visualized with a brightfield microscope linked to a digital camera. Characteristic images of the micro-structural damage were captures at 10X.

Results: Of the 123 specimens that were considered for analysis, 99 (80%) survived 5000 cycles of cyclic compressive loading. Twenty-four FSUs experienced a fatigue related injury, which could be classified into three primary injury pathways: (i) endplate fracture, (ii) avulsion of the superior endplate and (iii) fracture of the pars interarticularis. A marked difference of the magnitude of peak compressive force was noted in the Kaplan-Meier survival function of experimental conditions that induced fatigue injury in less than 5000 cycles, with a higher probability of survival at 20% UCT. Overall, in the 40% UCT load

condition, the probability of survival was less than 67%. When considering the representative images across each of the 10 and 20% UCT experimental conditions, it is noteworthy that a qualitative depiction of emerging interactions could be detected. The micro-structural damage detected in excised samples of AF tissue consisted of clefts and fissures within the intra-lamellar matrix, as well as delamination within the inter-lamellar matrix. There was no consistent trend in the amount of damage that was observed between 10% and 20% UCT loading conditions. However, a moderate effect of posture was noted, with increased disruption observed in tissue samples exposed to 300% NZ postural deviation.

Conclusions: Consistent with previous research, our findings support a threshold of peak compressive force of 30% UCT, where cyclic loading above this level is likely to lead to fatigue injury of the cartilaginous endplate in less than 5000 cycles of *in vitro* mechanical loading. However, findings from our histological analyses demonstrate that considerable IVD disruption occurred in specimens that "survived" 5000 cycles of cyclic loading at 10 and 20% UCT. Therefore, it is strongly recommended that future efforts in injury prevention consider more than just the magnitude of the applied load when evaluating risk of low back injury.

Study III: Exploring interactions between force, repetition and posture on intervertebral disc height loss and bulging in isolated functional spinal units from sub-maximal cyclic compressive loading.

Background: Most *in vitro* studies are limited in the ability to partition intervertebral disc (IVD) height loss from total specimen height loss since the net changes in the actuator position of the materials testing system used for testing simply reflect net changes to the entire osteoligamentous system of FSUs used for testing. Moreover, previous research conducted to characterize changes in IVD bulging has been limited to static compressive loading for 15 minutes or less.

Objectives: To explore interactions between: (i) the magnitude of the applied compressive force, (ii) cycle rate and (ii) degree of postural deviation on IVD height loss, as well as

pre/post changes in annulus fibrosus (AF) bulging in order to better understand the structural changes that occur in the IVD under cyclic loading conditions.

Methods: A total of 99 porcine cervical FSUs were included in the study. Three levels of peak compressive force (10, 20 and 40% UCT), three cycle rates (5, 10 and 30 cycles per minute) and two dynamic postural conditions (100 and 300% of specimens' neutral zone range) were examined using a full-factorial design. Compressive force was applied using a time-varying waveform based on estimates of *in vivo* loading using a dynamic EMG-assisted model of the lumbar spine during a floor to waist height lift, which was synchronous paired with dynamic flexion/extension. All FSUs were cyclically loaded for 5000 cycles or until fatigue failure occurred. Surface scans from the anterior aspect of the IVD were recorded in a both a neutral and flexed posture before and after the cyclic loading protocol using a 3D laser scanner. The peak anterior bulge of the AF at the midline of the IVD in the frontal plane was computed from the 3D surface profiles, pre/post testing. To facilitate the comparison of AF bulging measurements between specimens and improve the anatomical interpretation of this measure, the maximum anterior bulge perpendicular to a vector defined by the endpoints of the superior and inferior endplates has been reported.

Results: A significant three-way interaction (p = 0.0092) between the magnitude of peak compressive force, cycle rate and degree of postural deviation was observed in cycle-varying specimen height loss data. However, a significant main effect of peak compressive force (p=0.0003) was observed in IVD height loss obtained from the 3D surface profiles, pre/post testing. A wide range of Pearson product-moment correlation between total specimen height loss and IVD height loss (r = -0.54 to 0.95) was observed across experimental conditions, with the relative contribution of IVD height loss to total specimen height loss, ranging from 19 to 58%. Significant main effects of postural deviation (p=0.0016) and time (p=0.0423) were observed in peak measures of AF bulging. A wide range of Pearson product-moment correlation was also observed (r = -0.44 to 0.78) between IVD height loss and IVD bulging across experimental conditions.

Conclusions: This investigation provides evidence that total specimen height loss is not an accurate depiction of cycle-varying changes in the IVD across a range of *in vivo* scenarios that were replicated during *in-vitro* testing of FSUs. The magnitude of the applied compressive load was the only exposure variable that significantly influenced IVD height

loss, as measured from the 3D surface profiles. Interestingly, postural deviation was the only factor that significantly affected the magnitude of peak AF anterior bulge, pre/post testing.

Study IV: Exploring interactions between the magnitude of tissue stretch and cycle rate on the mechanical properties of the annulus fibrosus during cyclic, biaxial tensile loading.

Background: Previous research has shown that the intervertebral disc (IVD) undergoes multidirectional tensile strain under *in vivo* loading conditions. *In vitro* testing has found that biaxial tensile testing of excised samples of AF tissue results in higher stresses at considerably lower magnitudes of strain compared to uniaxial testing methods. However, the cycle-varying changes in the mechanical properties of the AF have yet to be studied under cyclic biaxial tensile loading conditions.

Objectives: The primary objective of this study was to explore interactions between: (i) the magnitude of peak tissue stretch and (ii) cycle rate on cycle-varying changes in the mechanical properties of the AF tissue during cyclic biaxial tensile loading. A secondary purpose was to examine whether the mechanical response of multilayer AF tissue samples would be different about each axis of loading or across radial locations of the IVD.

Methods: Ninety-six AF tissue samples, consisting of 3-5 lamellae, were excised from two radial locations on the IVD, including: (i) the anterior and (ii) posterior-lateral regions. Each tissue sample was randomly assigned to 1 of 12 experimental conditions to examine interactions between the magnitude of peak tissue stretch and cycle rate on the mechanical properties of isolated multilayer AF tissue samples, during cyclic biaxial tensile loading. Three levels of peak biaxial tissue stretch (circumferential-axial), including: (i) 6-10%, (ii) 9-15% and (iii) 12-20% and two cycle rates (5 and 10 cycles per minute) were examined using a full factorial design. Biaxial tensile load was applied in displacement control using a BioTester tensile loading apparatus in a temperature (29° C ± 1) and humidity (90% ± 5) controlled local testing environment. Top-down digital images of the tissue's surface were captured during both the stretch portion of cycles 1, 10 and 100 using an overhead CCD camera.

Results: A significant three-way interaction between the radial location on the IVD, magnitude of tissue stretch and cycle rate ($p = 0.0053$) and a significant two-way interaction between the axis of loading and magnitude of tissue stretch ($p < 0.0001$) was observed in measures of peak tensile stress. Similarly, significant two-way interactions were observed in the S-S moduli between: (i) magnitude of tissue stretch and cycle rate ($p = 0.0004$), as well as (ii) magnitude of tissue stretch and axis of loading ($p < 0.0001$). Significant two-way interactions between: (i) the magnitude of tissue stretch and axis of tensile loading ($p < 0.0001$), (ii) cycle rate and axis of tensile loading ($p = 0.0174$) and (iii) transverse location of the IVD and cycle rate ($p = 0.0005$) were observed in cycle-varying measures of peak surface strains that were calculated using a virtual gauge region defined on the surface of each tissue sample.

Conclusion: Results from this study emphasize the cycle-varying tensile stress response of the AF, which changed across loading axis and region of the IVD. However, it is interesting that no significant changes were observed in S-S moduli after 100 cycles of cyclic biaxial tensile loading. These findings provide novel insight into the cycle-varying stress-relaxation that occurs in multilayer samples of AF tissue, which may be linked to the known mechanism of IVD tissue failure (i.e. development of fissures and clefts) under chronic loading conditions.

Global Summary

Collectively, the findings from this thesis indicate the combined effects of magnitude of the applied load, cycle rate (which inevitably affects movement speed) and postural deviation interact to modulate both the resultant load in the lumbar spine (*in vivo*), as well as the mechanical response (and resultant injury pathways) of the intervertebral disc under cyclic loading conditions. Stated differently, the influence of force repetition and posture on estimates of low back joint loading and intervertebral disc injury were not simply additive. Future injury prevention efforts need to consider the complex interactions that exist between mechanical risk factors that have been linked to musculoskeletal injury.

Acknowledgements

First I would like to acknowledge the ongoing mentorship and support that I have received from my Ph.D. supervisor and friend, Dr. Jack Callaghan. Jack, you have provided me with the most amazing learning environment over the last five years. I feel very fortunate to have had the opportunity to work with such a well-respected and productive scientist. I will forever be indebted to you for the countless hours of academic and professional guidance that you offered throughout my degree.

I would also like to thank my thesis committee members, Drs. Wayne Brodland, Stu McGill, Rob Parkinson, and Richard Wells. I am grateful for the feedback that you provided in the early stages of this work, as well the thought provoking conversations that we have had over the last two years. In particular, I would like to acknowledge the guidance and support that I have received from my friend and mentor Dr. Rob Parkinson during the final stages of my degree. Similarly, I am very appreciative for some of the unique perspectives and insight that were provided by my external examiner, Dr. Sean Gallagher.

Next, I would to acknowledge the financial support that I have received from the Ontario Graduate Scholarship Program and the Centre for Research Expertise for the Prevention of Musculoskeletal Disorders (CRE-MSD) seed grant program.

I would like to thank all of my collaborators, Drs. Tyson Beach, David Frost, Sam Howarth and Joe Quadrilatero, as well as Elliott McMillan and Mamiko Noguchi. Although I am the sole author on this document, in no way was my research conducted under solitary effort.

Lastly, I would like to acknowledge the rest of my 'Callaghan Spine Lab' friends. In particular, Dr. Diana De Carvalho, Nick Frank, Thomas Karakolis, Kaitlin Gallagher and Kristina Gruevski. We have shared a number of laughs over the last five years! It has been a pleasure to work with such amazing people.

Dedication

To my beautiful wife, Erica. Without your love and support, I am not sure how I would have completed a project of this magnitude. You mean everything to me.

To my parents, Ed & Lorna Gooyers. From an early age you instilled in me the necessary dedication and drive to succeed no matter what the challenge. Thank you for always believing in me! I honestly couldn't have asked for better parents…

Table of Contents

List of Figures

List of Tables

Chapter 1

Introduction

1.1 Scope of the Problem

Low back pain (LBP) affects approximately 80% of the population at some point in their lives, with 65% of these cases becoming chronic pain sufferers (Cassidy, Carroll & Côté, 1998). Approximately 40% of LBP cases are attributed to intervertebral disc (IVD) disruption, which can be characterized by damage to the annulus fibrosus (AF) or cartilaginous endplate (Dammers & Koehler, 2002; DePalma, Ketchum & Saullo, 2011; Schwarzer et al., 1995). In Ontario, the low back is the most frequently injured region of the body, representing 20% of all lost time claims (*The Workplace Safety and Insurance Board of Ontario Statistical Supplement to the 2013 Annual Report,* 2013). Although the medical community strives to treat and rehabilitate these injuries, there is immense opportunity in primary prevention, given that most problems will continue to persist until the underlying mechanical risk factors are resolved.

Several reports from the epidemiological literature have noted that occupational mechanical exposures are closely associated with the reporting of low back pain (Andersson, 1981; Marras et al., 1995; Norman et al., 1998). In particular, manual materials handling (MMH) activities have been identified as a significant occupational risk factor (Hoogendoorn, van Poppel, Bongers, Koes & Bouter, 1999; Kuiper et al., 1999; Marras et al., 1995; Norman et al., 1998). The most commonly accepted mechanical exposures linked to low back injury include: (i) high force demands, (ii) frequent repetition and (iii) awkward postures (Bernard, 1997). However, as noted by Gallagher and Heberger (2013), these exposures have typically been examined in isolation, and are often assumed to function independently regarding injury risk. As such, our understanding of the combined effects of external task demands on internal joint loading, and their influence on fatigue injury pathways in the lumbar spine may be limited, overly simplified, and underestimate the potential risk of injury.

1.2 Global Purpose & Focused Objectives

Mechanical overload of musculoskeletal tissues in the low back is considered to be one of the most significant and preventable causes of injury (Marras, 2000). Therefore, the global purpose of this thesis was twofold: (i) explore interactions between external task demands on *in vivo* joint loading in the lumbar spine, and (ii) characterize the combined effects of each of these mechanical exposures on fatigue injury pathways in the IVD, a common source of LBP (Dammers & Koehler, 2002; Schwarzer et al., 1995). Using a combination of both *in vivo* modeling of human movement and *in vitro* mechanical testing of porcine IVD tissue, the following focused objectives defined the scope of this work:

i. Explore the complex interactions that exist between: (i) magnitude of external load, (ii) speed of movement, and (iii) postural symmetry on estimates of *in vivo* low back joint loading during a simulated occupational lifting task (**study I**).

ii. Examine the combined effects of: (i) the magnitude of the applied compressive force, (ii) frequency of loading (i.e. cycle rate) and (ii) degree of postural deviation on known fatigue injury pathways in porcine cervical functional spinal units (FSUs) at sub-acute-failure magnitudes of peak compressive force and to characterize the micro-structural damage imposed to the IVD in "survivor" specimens using histological staining methods (**study II)**.

iii. Characterize interactions between: (i) the magnitude of the applied compressive force, (ii) cycle rate and (ii) degree of postural deviation on IVD height loss, as well as pre/post changes in AF bulging to better understand the structural changes that occur in the IVD with cyclic compressive loading (**study III)**.

iv. Explore interactions between the magnitude of peak tissue stretch and cycle rate on cycle-varying changes in the mechanical properties of the annulus fibrosus (AF) tissue during cyclic, biaxial tensile loading (**study IV)**.

1.3 Thesis Overview

This thesis is comprised of four studies (**Figure 1-1**), each focused on elucidating the complex interactions between external task demands (or mechanical loading factors) and known mechanisms of low back injury.

Study one provides insight into the *in vivo* low back joint loading across various external task demands during occupational lifting. Using data collected from a sample of participants with manual materials handling experience (Beach, 2011; Frost, 2012), this investigation explored interactions between: (i) the magnitude of the external load, (ii) movement speed and (iii) symmetry of initial load placement (i.e. posture) on estimates of L4/L5 joint compression and shear using a dynamic, EMG-assisted, three-dimensional dynamic model of the lumbar spine (Cholewicki & McGill, 1996).

Using a biofidelic time-varying waveform that was based on the *in vivo* estimate of compressive loading in the lumbar spine during an occupation lifting task, study two characterizes the combined effects of: (i) the magnitude of the applied compressive force, (ii) cycle rate and (ii) degree of postural deviation on known fatigue injury pathways in porcine cervical FSUs at sub-acute-failure magnitudes of peak compressive force. Further, using histological staining methods, this investigation examines the micro-structural damage imposed to the IVD in "survivor" specimens (i.e. those that did not experience fatigue injury during the 5000 cycles of cyclic compressive loading).

Using a 3D laser scanner, study three explores interactions between: (i) the magnitude of the applied compressive force, (ii) cycle rate and (ii) degree of postural deviation on IVD height loss and AF bulging in the same sample of porcine cervical FSUs that were included in study II. Three-dimensional surface profiles of the anterior aspect of the IVD were captured from each specimen pre/post testing, which enabled local IVD height loss to be partitioned from net changes in specimen height, as calculated from the vertical position of the materials testing system actuator. Moreover, pre/post changes in AF bulging are explored across loading conditions.

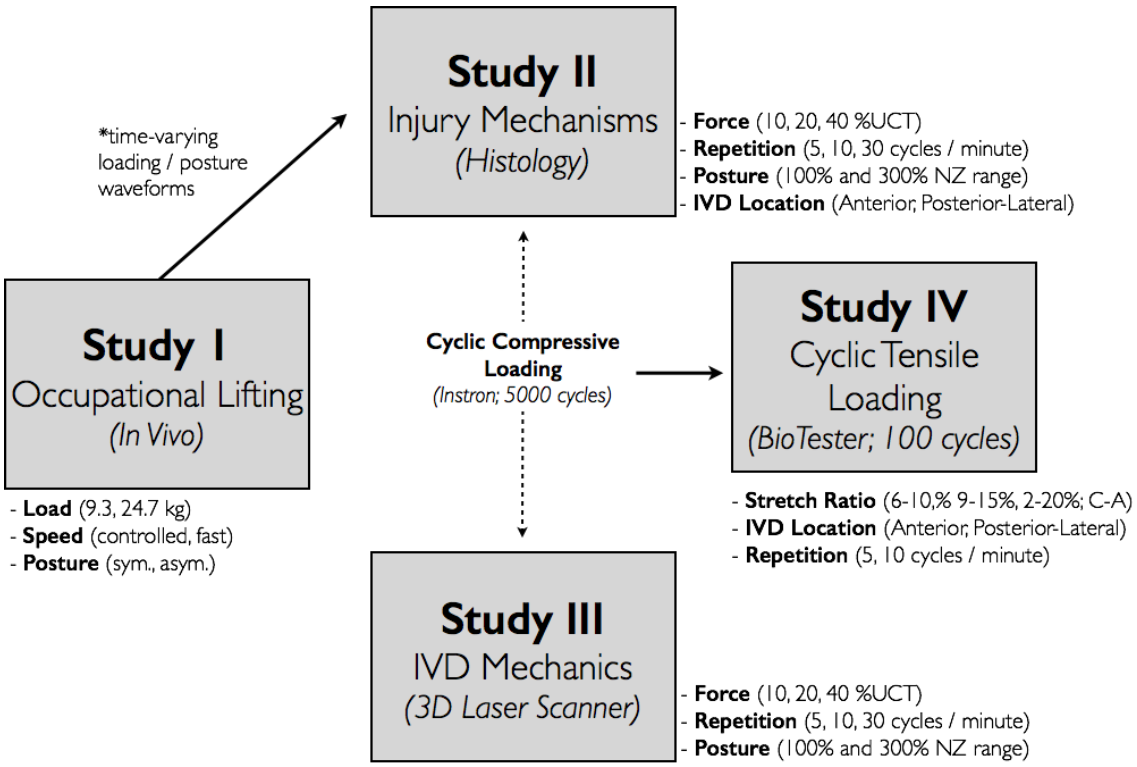

Figure 1-1: Overview schematic of the four studies included in the thesis.

Study four, the final investigation included in this thesis, builds on the insight gained from studies II and III on IVD mechanics by characterizing interactions between: (i) the magnitude of peak tissue stretch and (ii) cycle rate on cycle-varying changes in the mechanical properties of the AF tissue during cyclic, biaxial tensile loading. Specifically, cycle-varying changes in the stress stretch-ratios (S-S) profile are compared across both axial and circumferential axes of loading in isolated multilayer AF tissue samples excised from both the anterior and posterior-lateral regions of the IVD.

1.4 Global Hypotheses

The general hypothesis for this thesis was that a significant interaction between external task demands would emerge in estimates of *in vivo* joint loading in the lumbar spine and that the combined influence of these exposures would have a significant effect on the mechanical response and fatigue injury pathways in the IVD. In-line with the global purpose of this thesis, the following null hypotheses were tested:

i. There will be no significant interactions between the magnitude of the external load, movement speed, and postural symmetry on estimates of *in vivo* joint loading in the lumbar spine (**study I**).

ii. The mechanism of fatigue injury in isolated FSUs will not differ across levels of peak compressive force, cycle rate and postural deviation with cyclic compressive loading paired with dynamic flexion/extension (**study II**).

iii. There will be no differences in the magnitude of micro-structural tissue damage imposed to the AF across cyclic loading conditions paired with dynamic flexion/extension (**study II)**.

iv. There will be no differences in IVD height loss or AF bulging across cyclic loading conditions paired with dynamic flexion/extension (**study III)**.

v. There will be no cycle-varying changes in the mechanical properties of isolated AF tissue exposed to cyclic, biaxial tensile loading (**study IV**).

Although specific hypothesis are provided for each of the four studies in the subsequent chapters, the global hypotheses have been presented as “null” so that each of them can be tested on the basis of data/research that has been conducted in the thesis. Each hypothesis will be revisited in Chapter 7.

Chapter 2

Literature Review

2.1 Overview

This chapter has been organized into three main sections, which will review the scientific foundation for the research that is presented in this thesis. These sections include: (i) low back structure and function, (ii) low back injury, and (iii) methodological considerations affecting both *in vivo* and *in vitro* experimental techniques that were employed in this research.

2.2 Low Back Structure & Function

2.2.1 Vertebrae

The human lumbar spine typically consists of 5 vertebrae, named L1 to L5 in descending order (cranial to caudal). The function of these irregular bones serve to protect the spinal cord and nerve roots, support the weight of the body, and provide attachment for surrounding musculature, which play an important role in posture and locomotion.

Conceptually, each vertebra can be divided into three functional components, including: (i) the vertebral body, (ii) the pedicles and (iii) the posterior elements - consisting of the laminae and their processes (**Figure 2-1**) (Bogduk, 2005). Each of these components serves a unique function, but contributes to the overall structure of an intervertebral joint. The vertebral body plays an important role in weight bearing, and its structure reflects this purpose (Bogduk, 2005). Each lumbar vertebral body is composed of cancellous bone, which consists of a highly organized network of trabeculae, surrounded by a thin shell of cortical bone (Bogduk, 2005). The superior and inferior surfaces of the vertebral body are capped with cartilaginous endplates, which are composed of both hyaline cartilage and fibrocartilage (Bogduk, 2005). These endplates serve as the junction between the vertebral bodies and the intervertebral disc.

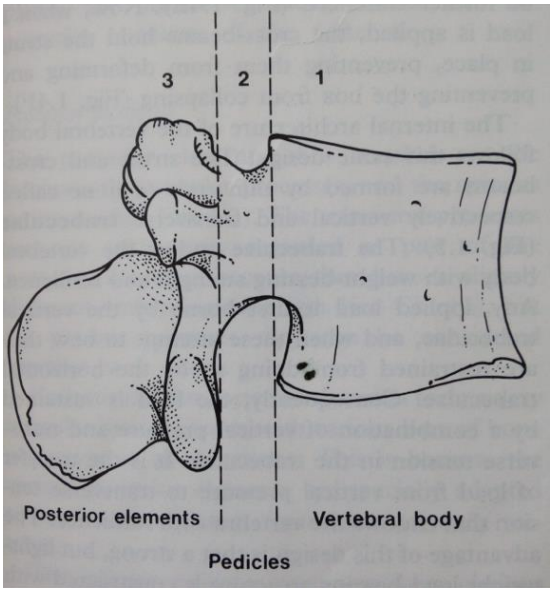

Figure 2-1: Three functional components of the human lumbar vertebrae, including: (i) the vertebral body, (ii) the pedicles and (iii) the posterior elements consisting of the laminae and their processes. *Image from:* (Bogduk, 2005).

The pedicles on lumbar vertebrae are the only connection between the posterior elements and the vertebral bodies. All forces sustained by any of the posterior elements are transmitted to the vertebral body through these bony connections. Not surprisingly, their structure is designed to sustain these forces (Bogduk, 2005). The external structure of the pedicle is a thick pillar of bone; however, in cross-section they have been compared to the walls of a cylinder that enables them to resist bending in multiple directions (Bogduk, 2005).

The posterior elements of a vertebra include: (i) the laminae, (ii) the articular processes and (iii) the spinous process. Although in some cases the transverse processes are not regarded as part of the posterior elements of the vertebrae (Bogduk, 2005), for the purpose of this review their function will be discussed here. The inferior articular processes lock into the superior articular processes of the adjacent vertebra that is directly below to form the zygapophysial (i.e. facet) joint. The primary function of these synovial joints, which are also covered with articular cartilage, is to resist forward sliding and twisting motions of the vertebral bodies (Bogduk, 2005). Conversely, the primary roles of the spinous, transverse, accessory and mammillary processes provide surface area for muscle attachment. In particular, the longer processes (e.g. spinous and transverse) supply a substantial lever-arm that enhances the mechanical advantage of the surrounding muscles that attach to them (Bogduk, 2005). It is noteworthy that almost every muscle that acts on the lumber spine attaches to the posterior elements of the vertebrae. Only parts of the psoas muscle attach directly to the vertebral body (Bogduk, 2005).

2.2.2 Intervertebral Disc

The intervertebral disc (IVD) consists of three basic components: (i) the nucleus pulposus (NP), which is surrounded by (ii) the annulus fibrosus (AF) (Bogduk, 2005). Although the NP is quite distinct in the central region the IVD (as is the AF towards the periphery) there is no clear boundary between either of the two components in human adult IVDs. A third component of the IVD, already mentioned above, are the two cartilaginous endplates that form the top and bottom of each disc, and act as a barrier to separate the fluid content of the NP from the adjacent vertebral bodies (Bogduk, 2005).

The primary function of the IVD is to allow movement in the spine, and transmit load between adjacent vertebrae (Bogduk, 2005). It is important to note that both the NP and AF make important contributions in each of these roles. As a semi-fluid mass, the NP is deformable but its volume cannot be compressed. Thus, an axial load applied to the IVD will result in a reduction in disc height that causes the NP to expand laterally, exerting radial pressure on the inner layers of the AF and vertically exerting pressure on the cartilaginous endplates, which causes them to deflect (Bogduk, 2005). As such, the NP plays an important role in transmitting load to the surrounding structures in the IVD. The vertical pressure exerted on the cartilaginous endplates serves to transmit a portion of the applied load from one vertebrae to the next, thus reducing the amount of force that is supported by the AF (Bogduk, 2005). In addition, the radial pressure that is exerted on the AF prevents it from buckling, thus increasing its capacity to bear load and absorb/store mechanical energy (Bogduk, 2005). As the NP tries to expand laterally, this energy is used to stretch the collagen fiber bundles in the AF, which is stored as elastic strain energy (up to a certain point) (Bogduk, 2005). Once the load that is applied to the IVD is removed, the elastic recoil of the elastin and collagen fibers release energy back to the NP, restoring any deformation that it may have experienced (Bogduk, 2005). For this reason, the fluid content of the NP is of critical importance to IVD's mechanical integrity. Since the amount of fluid in IVD is a function of its proteoglycan content, normal mechanics are often considered dependent on proteoglycan proteins (Bogduk, 2005).

2.2.2.1 Nucleus Pulposus

In a healthy IVD the NP has a gel-like consistency, with collagen fibrils dispersed in a semi-fluid medium (Inoue, 1981). The NP contains primarily type II collagen fibers, is rich with proteoglycans (Hayes, Benjamin & Ralphs, 2001) and contains chondrocyte-like cells similar to those seen in articular cartilage (Bruehlmann, Rattner, Matyas & Duncan, 2002). The type II collagen that is synthesized by these cells is thought to play an important role in resisting compressive load, pressurizing the endplates vertically and the annulus fibrosus (AF) laterally (Hayes et al., 2001). The high proteoglycan content has been attributed to the semi-fluid nature of the NP, due to the negatively charged environment that they create

(Bogduk, 2005). This promotes an influx of fluid into the IVD, which helps to maintain its hydrostatic pressure.

2.2.2.2 Annulus Fibrosus

The AF is a complex fibrocartilage structure composed of highly organized sheets (approximately 15-25 layers; Tampier, Drake, Callaghan & McGill, 2007) of collagen fibers (lamellae) that are arranged in concentric rings surrounding the NP (Bogduk, 2005). However, the concentric sheets of collagen fibers often form incomplete layers, such that two adjacent layers will merge into one (Marchand & Ahmed, 1990; Schollum, Robertson & Broom, 2008; Tsuji et al., 1993). Previous work by Tsuji and colleagues (1993) has identified an increased number of incomplete lamellae in the posterior region of the AF. Within each lamella, the collagen fibers are arranged in a parallel fashion, approximately 45 to 65 degrees from vertical (i.e. compressive) axis of the spine (Marchand & Ahmed, 1990; Tampier et al., 2007), often spanning the entire distance between vertebrae. While the fiber angle is thought to be similar within each lamella, the direction of this inclination alternates between layers (**Figure 2-2**).

The inner layers of the AF are composed of primarily type II collagen and proteoglycans, while the outer layers are composed of primarily type I collagen (Eyre & Muir, 1976; Hayes et al., 2001). In between lamellae lies an adhesive layer of disc-shaped, flat cells, which have projecting processes that form a stellate pattern (Bruehlmann et al., 2002). These processes interconnect in a complex lattice formation, similar to what has been found surrounding ligaments (Lo, Chi, Ivie, Frank & Rattner, 2002). Interestingly, the inner AF lamellae attach directly to the cartilaginous endplates to form a closed vessel for the NP; however, the most superficial (i.e. outer) layers attach directly to the bone of the vertebral bodies (Bogduk, 2005). This difference in attachment site may suggest there are functional differences between the inner and outer layers of the AF (Marchand & Ahmed, 1990).

Along with the organized architecture of collagen fibers within the AF, there is also a complex network of elastin fibrils (Schollum et al., 2008; Yu, Fairbank, Roberts & Urban,

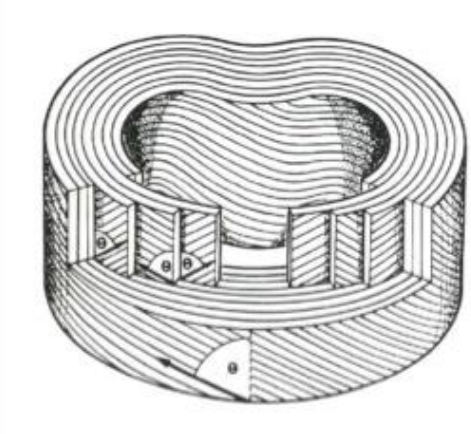

Figure 2-2: Annulus fibrosus collagen fiber angle across layers of the annulus fibrosus in the intervertebral disc. *Image from: (*Bogduk, 2005)

2005; Yu, Winlove, Roberts & Urban, 2002). Although elastin is only a minor structural component, comprising approximately 2% of the dry weight of the AF (Olczyk, 1994), previous research suggests that the elastic fiber network may play an important role in reinforcing the mechanical integrity of the collagen matrix, facilitating its elastic recoil (Yu et al., 2005; Yu et al., 2007; Yu et al., 2002). A dense network of elastic fibers has been identified between adjacent lamellae, while within individual lamellae elastic fibers have been shown to run parallel to the collagen fiber bundles (Yu et al., 2007). In addition, there is evidence that elastic fibers form cross-bridges that connect collagen bundles across layers in the AF (Yu et al., 2007; Yu et al., 2002). Using a combination of immunohistochemical and light microscopy techniques, Smith and Fazzalari (2006) illustrated regional variation in the elastic fiber density in the AF of the human IVD. The density of elastic fibers was shown to be significantly higher in the lamellae of the posterior-lateral samples of the AF compared to the anterior-lateral region, and significantly higher in the outer layers compared to those found in the deep layers (Smith & Fazzalari, 2006). Considering these findings, the authors hypothesized that the arrangement of elastic fibers in the IVD was proportional to the magnitude of tensile deformations experienced in bending and torsion (Smith & Fazzalari, 2006). Later work by the same group (Smith, Byers, Costi & Fazzalari, 2008) using enzymatic digestion of elastic fiber network showed a significant reduction in the elastic modulus and a significant increase in the extensibility of radially oriented AF tissue samples subject to tensile loading.

In 2008, Schollum and colleagues (2008) conducted a microscopic investigation into the translamellar bridging network (i.e. collagen cross-bridges) that had previously been identified in earlier work (Pezowicz, Robertson & Broom, 2005; Pezowicz, Schechtman, Robertson & Broom, 2006; Yu et al., 2002). Using differential interference contrast optics, a three-dimensional reconstruction of this secondary network (spanning several lamellae) in ovine lumbar IVDs was developed, showing much greater complexity in the interlamellar structure than had been previously recognized (**Figure 2-3**) (Schollum et al., 2008). Interestingly, a close association between this translamellar bridging network and incomplete lamellae was observed (Schollum et al., 2008). Based on these findings, the authors speculated that structural damage to this network may result in annular weakening, potentially causing the IVD to fail (Schollum et al., 2008). Moreover, it was speculated that

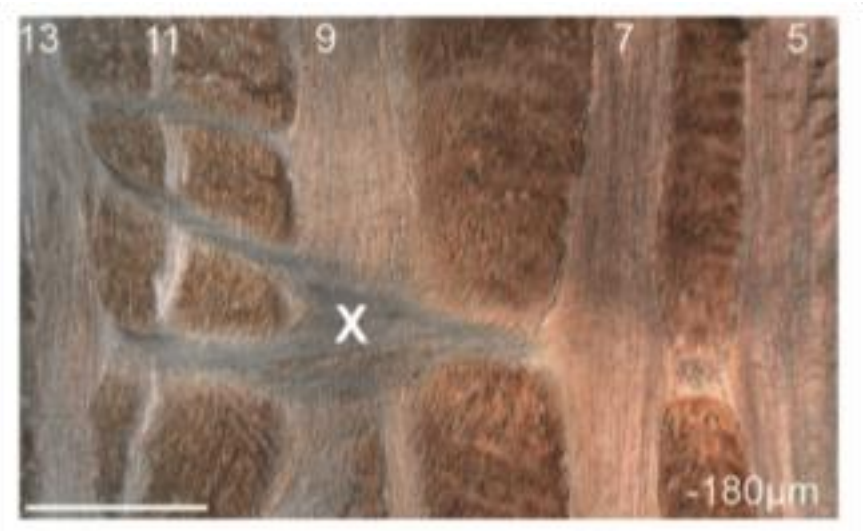

Figure 2-3: Translamellar bridging network shown in an oblique slice of annulus fibrosus tissue (layers 5 to 13) harvested from an ovine lumbar intervertebral disc. *Image from:* (Schollum et al., 2008).

the translamellar bridging network's response to mechanical loading might be an important factor influencing known mechanisms of fatigue injury of the AF (e.g. formation of clefts, delamination), as the architecture of this secondary network appeared to prevent excessive sliding between adjacent lamellae (Schollum et al., 2008). Moreover, it was hypothesized the strength and stiffness of the translamellar bridging system was reinforced by the collagen component and not the elastin cross-bridge fibers that had previously been suggested (Yu et al., 2005; Yu et al., 2007; Yu et al., 2002).

Research conducted by Melrose and colleagues (2008) has identified that these cross-bridges were distinct from the surrounding collagenous lamellae in having a matrix rich in type VI collagen in adult AF tissue. Although previous work has suggested these cross-bridges may be the result of adaptive remodeling to changes in the micro-mechanical environment in the IVD with age or follow injury (Melrose, Smith, Appleyard & Little, 2008; Schollum et al., 2008). Smith and Elliott (2011) have recently theorized that this may not be the case, since the adult AF has a limited capacity for remodeling and repair (due to is avascular blood supply). Instead, they have hypothesized that the cross-bridges found in the translamellar bridging network are pathways left by receding blood vessels, which remain only in the periphery of the AF during adulthood (Smith & Elliott, 2011). Moreover, it has been posited that the micro-structural disruption in the lamellar architecture never fully regenerates following vascular regression and thus transitions into translamellar cross-bridges (Smith & Elliott, 2011). This theory was based on observations in L1/L2 ovine lumbar IVDs that during fetal development blood vessels penetrate deep within the AF and recede during post-natal growth, perhaps due to increasing mechanical stresses in the surrounding matrix (Smith & Elliott, 2011).

2.2.3 Ligaments

There are two primary ligaments that interconnect the vertebral bodies in the lumbar spine, including: (i) the anterior and (ii) posterior longitudinal ligaments, which serve to resist vertical separation and excessive sagittal plane rotations of adjacent vertebrae (Bogduk, 2005). Structurally, the anterior longitudinal ligament consists of several sets of collagen fibers (Bogduk, 2005). There are both short fibers that span each intervertebral joint,

attaching to the anterior surface of the vertebral bodies, as well as longer collagen fiber bundles that span two or three (sometimes more) vertebral levels, with loose attachment to the outer layers of the AF (Bogduk, 2005). The anterior longitudinal ligament's primarily function during extension movements of the vertebral joint (Bogduk, 2005).

In the lumbar spine, the posterior longitudinal ligament forms a narrow band over the posterior aspect of vertebral bodies, but expands laterally over the back of each IVD (Bogduk, 2005). The collagen fibers of the posterior longitudinal ligament mesh with the posterior, outer layers of the AF but attach to the posterior margins of each vertebrae. The shortest (deep) fibers of the posterior longitudinal ligament span two intervertebral joints (Bogduk, 2005). Longer collagen fibers, which are typically more superficial, can span three to five vertebral levels (Bogduk, 2005). Other ligaments that help to resist motion and provide stability, include: (i) the ligamentum flavum, (ii) interspinous, (iii) supraspinous ligaments, as well as the (iv) facet joint capsule (Bogduk, 2005) (**Figure 2-4**).

2.3 Low Back Injury

2.3.1 Injury Pathways

The underlying theory for mechanical injury to musculoskeletal tissues in the low back occurs when the applied load exceeds the capacity of a tissue. There are two primary pathways in which tissues can be overloaded, including: both (i) acute (i.e. overexertion) and (ii) chronic (i.e. overuse) mechanisms for injury (McGill, 1997). Although forthright in principle, differentiating between overexertion and overuse injury mechanisms can be quite difficult in practice (Gooyers, Frost, McGill & Callaghan, 2013). Discretion must be exercised when a low back injury is attributed to a specific occupational task, unless the tissue's short- and long-term loading history is known (McGill, 1997).

2.3.1.1 Acute Injury Model

The first mechanism, often described as an acute or overexertion injury (**Figure 2-5**) occurs when a single load exposure exceeds a tissue's failure tolerance. Acute injury mechanics can be used to describe the mechanism of tissue failure that occurs during

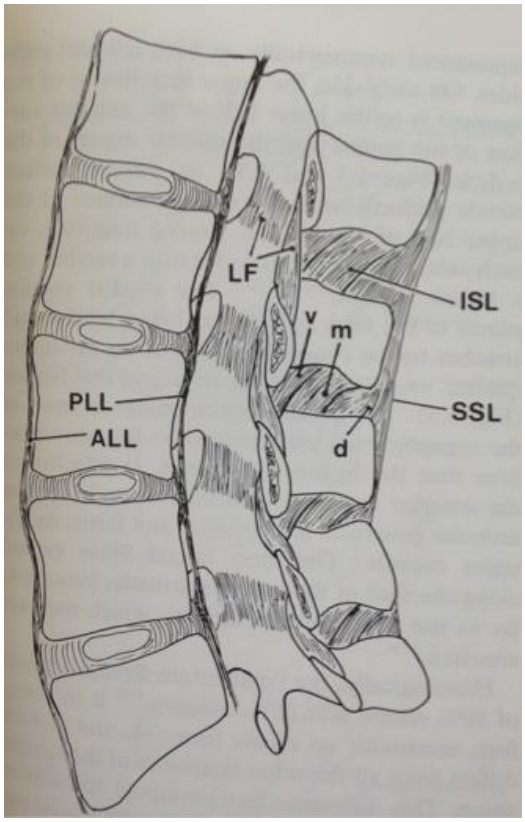

Figure 2-4: Ligaments in the human lumbar spine (sagittal view).

ISL - interspinsous; **SSL** - supraspinous; **LF** - ligamentum flavum;
PPL - posterior longitudinal; **ALL** - anterior longitudinal, ligaments.

Image from: (Bogduk, 2005).

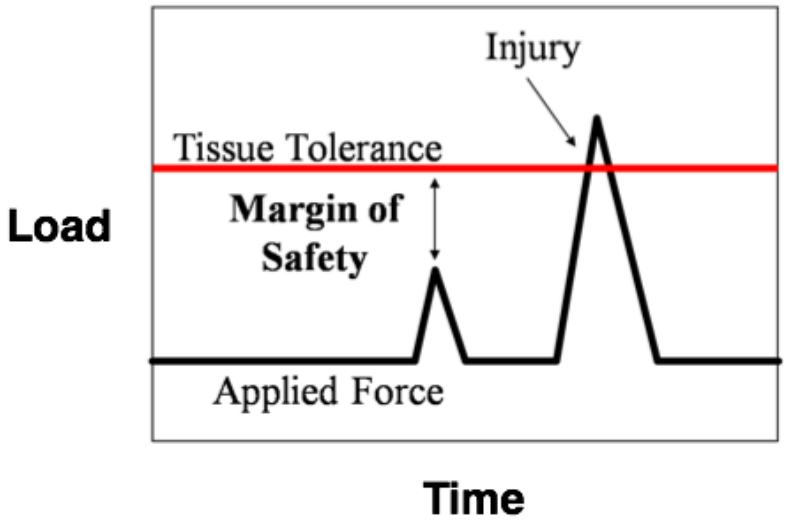

Figure 2-5: A theoretical model to describe acute (i.e. overexertion) injury mechanisms in the low back. Failure occurs when the magnitude of applied load exceeds the tolerance of the tissue. *Image adapted from:* (McGill, 1997).

common workplace accidents (e.g. slips, trips and falls). In such cases, the loads that are applied to the body often exceed the capacity of individual tissues, which can result in injury. One common example of an acute injury in the lumbar spine is rupture of the interspinous ligament when falling and landing on one's behind, which drives the pelvis forward during impact, creating a posterior shearing of the lumbar joints in a flexed posture (McGill, 2007).

2.3.1.2 Chronic Injury Model

A second way that musculoskeletal tissues can be damaged is through repeated (or sustained) application of loads that are of sub-acute-failure magnitude (**Figure 2-6**). This cumulative injury pathway (often attributed to overuse) reduces a tissue's capacity to bear load, which over time will result in failure when the accumulation of damage outpaces the rate of recovery (Kumar, 1990; McGill, 1997). A common cumulative injury mechanism in the lumbar spine is IVD herniation, which has been observed with repeated application of dynamic flexion-extension under modest amounts of compressive load (Callaghan & McGill, 2001; Tampier et al., 2007).

2.3.2 Mechanical Risk Factors for Low Back Pain and Injury

Several reports from the epidemiological literature (Andersson, 1981; Bernard, 1997; Marras et al., 1995; Norman et al., 1998) have noted that occupational mechanical exposures are closely associated with the reporting of low back pain and injury. In particular, manual materials handling (MMH) activities have been identified as a significant occupational risk factor (Hoogendoorn et al., 1999; Kuiper et al., 1999; Marras et al., 1995; Norman et al., 1998). From this body of work, a number of mechanical risk factors for low back injury have been identified, including: (i) work intensity, (ii) static work postures, (iii) frequent bending and twisting, (iv) lifting, pushing or pulling and (v) repetitive (i.e. cyclic) mechanical exposure.

One of the first investigations to perform an epidemiological analysis of low back injury using quantitative biomechanical measures was conducted by Marras and colleagues (1995), who surveyed 400 industrial lifting tasks across 48 different industries.

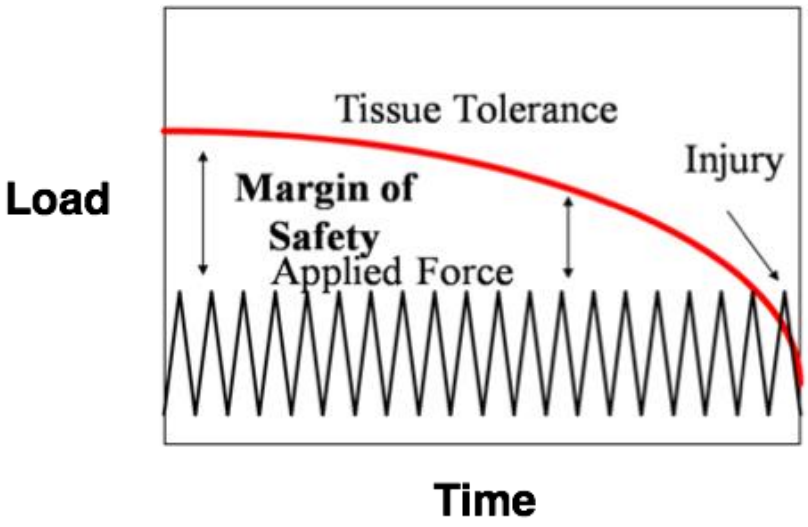

Figure 2-6: A theoretical model to describe chronic (i.e. overuse) injury mechanisms in the low back. Failure occurs when the accumulation of tissue damage outpaces the rate of recovery. *Image adapted from:* (McGill, 1997)

Based on a thorough review of medical records for each industry, the investigators classified each task as having low, medium or high risk of causing low back injury (Marras et al., 1995). A triaxial electrogoniometer (i.e. lumbar motion monitor) was worn by participants, which recorded the angular position, velocity and acceleration of the lumbar spine for each task. Interestingly, the most powerful single variable for predicting jobs with a high risk of low back injury was peak low back moment (Odds ratio; OR = 3.32; low vs. high risk groups) (Marras et al., 1995). Other variables that had notable predictive capacity for low back injury (between low and high risk groups) were average measures of sagittal plane trunk velocity (OR = 2.48) and maximum weight handled (OR = 2.42) (Marras et al., 1995). From a multiple logistic regression analysis, the combinations of five trunk motion and workplace factors were successful in predicting both medium and high risk tasks. These factors included: (i) lifting frequency, (ii) load moment, (iii) trunk lateral velocity, (iv) trunk twisting velocity and (v) trunk sagittal plane angle (Marras et al., 1995). Varying the magnitudes of each of these factors was shown to decrease the high-risk group membership by over ten times (OR = 10.6) (Marras et al., 1995). This investigation is a foundational paper in the biomechanics literature, as it was one of the first studies to highlight that mechanical exposures were linked to the risk of low back injury using epidemiological analysis techniques.

In 1998, Norman and colleagues (1998) published a second important case-control epidemiological study, which provided further support for the importance of mechanical risk factors for the reporting of low back pain (LBP) in an automotive assembly plant. Over the two-year span during which the study was collected, the authors conducted analyses on 104 cases and 130 randomly selected controls (Norman et al., 1998). Cases were defined as any full-time worker who reported LBP to a nursing station, who had not previously submitted a report within the previous 90 days (Norman et al., 1998). It is important to highlight that there were no significant differences in demographic (e.g. age, height, weight, etc.) between cases and controls. Additionally, cases showed significantly higher loading across all biomechanical variables that were examined (Norman et al., 1998). However, based on a conservative analysis of these data, four independent mechanical risk factors for LBP were identified, including: (i) integrated lumbar moment (OR = 1.4), (ii) usual hand force (OR = 1.7), (iii) peak shear force at L4/L5 (OR = 1.5) and (iv) peak trunk velocity (OR = 1.6)

(Norman et al., 1998). An important contribution from this work was the strong empirical evidence that highlighted the importance of cumulative load as risk factors for the reporting of LBP. Although this notion had previously been raised by Professor Kumar (Kumar, 1990) in a sample of institutional aides, a more thorough set of biomechanical analyses were applied by Norman and colleagues (1998); as Kumar (1990) used a recall interview of static postures and then interpolated postures between each recall position. Nonetheless, Professor Kumar's paper (1990) also showed that the cumulative compressive load exposure of institutional aides who reported LBP was significantly higher than in the no-pain group.

A recent study conducted by Coenen and colleagues (2013) investigated the prospective relationship between cumulative low back loads with the reporting of LBP. Physical exposures of 1,086 workers were monitored using video observation and direct force measurements. These data were used to calculate cumulative low back loads (net joint moments) at L5/S1 using a static, top-down modeling approach (Coenen et al., 2013). Cumulative loading in the lumbar spine was assessed by calculating the area under the squared-moment curve (Coenen et al., 2013). At baseline and at every year of the 3-year follow up, the incidence of LBP was assessing using a self-administered modified version of the Nordic Questionnaire (Kuorinka et al., 1987). The results of this investigation showed that cumulative mechanical exposures were a significant risk factor for LBP (OR = 2.06; 95% CI = 1.32 to 3.20) (Coenen et al., 2013). Moreover, using logistic regression analyses, cumulative loading appeared to reflect both the effects of working in a trunk flexed position and the number of lifts performed. However, lifting ≥ 25 kg > 15 times in an 8 hour shift (as a risk factor) proved to have additional predictive ability in identifying workers with LBP (OR = 2.03; 95% CI = 1.23-3.36) (Coenen et al., 2013).

A series of recent systematic review papers (Roffey, Wai, Bishop, Kwon & Dagenais, 2010a; , 2010b; , 2010c; Wai, Roffey, Bishop, Kwon & Dagenais, 2010a; , 2010b; , 2010c) have concluded that a there is insufficient evidence to support an independent causal relationship between physical occupational exposures and the reporting of LBP. Specifically, these authors analyzed existing literature on: (i) bending and twisting (Wai et al., 2010a) (ii) awkward postures (Roffey et al., 2010a), (iii) pushing and pulling (Roffey et al., 2010b), (iv)

lifting (Wai et al., 2010b), (v) carrying (Wai et al., 2010c) and (vi) manual handling (Roffey et al., 2010c) and reported that overall there was weak to moderate evidence to suggest that any of these occupational mechanical exposures met the necessary criteria for causation that were established by Bradford-Hill (Hill, 1965). In total, five of the Bradford-Hill's criteria were evaluated, including: (i) association (i.e. strength of significant associations), (ii) dose response, (iii) experiment, (iv) temporality and (v) biological plausibility (Hill, 1965).

Not surprisingly, these papers gained significant attention among biomechanics researchers across the globe (Kuijer et al., 2011; McGill, 2011; van Dieën et al. 2012; Takala, 2010), particularly since these systematic reviews are highly respected publications in the scientific community and are often used to influence policy. Additionally, since basic science investigations (e.g. *in vitro* cadaver studies) were not included in their review, and much of existing literature (e.g. cross-sectional or case control studies) was highly criticized for the possibility of recall bias and the fact that both the risk factor and outcome were measured simultaneously, many groups did not feel that the conclusions drawn by in these systematic review papers were appropriate. As summarized by Professor Takala (2010) in a letter to the editor of *The Spine Journal*, epidemiological studies have very limited ability to investigate "biological plausibility" and choosing to exclude the rich body of basic science spine biomechanics literature that shows numerous short-term effects between mechanical exposures and outcomes linked to LBP was inappropriate. Additionally, Bradford-Hill's aspects related to causality are often incorrectly classified as necessary criteria, which have been discussed in a recent epidemiological report (Ward, 2009). In a subsequent letter to the editor of *The Spine Journal* from Professor Kuijer and colleagues (2011) it was further discussed that the Bradford-Hill criteria were not intended for evaluation of individual studies, rather they were meant to be used to assess the level of evidence for causality of Factor A with Disease B across all scientific evidence in the literature. By the nature of the Bradford-Hill criteria, it would not be possible for one observational study to provide strong evidence for each of the required categories (Kuijer et al., 2011). Rather, the authors opined that the application of the Bradford-Hill criteria for causality requires a combination of observational and experimental studies and a synthesis of the findings into a consistent evaluation of the likelihood of causality (Kuijer et al., 2011)

Professor McGill also followed up with a letter to the editor of *The Spine Journal* highlighting that back pain is not a homogenous condition, and that we should not expect to observe a cause and effect relationship from a systematic review conducted on nonspecific low back pain (McGill, 2011). As such, the complex interactions between structure and injury biomechanics were ignored by grouping the different mechanisms for LBP together, instead of considering very specific types of low back injuries that are linked to specific occupational mechanical exposures (McGill, 2011). Additionally, the magnitude of the occupational exposure (e.g. load lifted) is not a sufficient metric to examine links with LBP, as the way a person lifts dominates the loading that is applied to specific tissues in the low back. A similar letter submitted to the editor of the *Lancet*, by Professor van Dieën and colleagues (2012) highlights that the mechanical exposures considered for analysis in these review papers was incomplete (i.e. not specifying intensity, frequency and duration) and were based on proxy measures.

2.4 Methodological Considerations

2.4.1 *In Vitro* Techniques

2.4.1.1 Use of Porcine Functional Spinal Units for Mechanical Testing

A human osteoligamentous intervertebral joint is composed of two adjacent vertebrae, the intervening IVD and a series of ligaments. Within the spine biomechanics literature, an isolated vertebral joint has been called a functional spinal unit (FSU) (Oxland, Panjabi, Southern & Duranceau, 1991; Yingling, Callaghan & McGill, 1999). This joint is capable of flexion/extension, lateral bend and axial twist motions, and has the capacity to tolerate both shear and compressive loading. Although much has been learned about the lumbar spine from *in vitro* testing of human cadaver specimens, there are numerous research questions for which human specimens are not preferred (Yingling et al., 1999). Young, healthy, human specimens are extremely rare, since typical donors are elderly and sick or were from younger donors who sustained substantial trauma. Additionally, when considering experimental design and scientific control of *in vitro* studies, it is virtually impossible to collect a sample of similar human specimens. However, this type of control is possible using a homogenous sample of healthy animal tissue, specifically controlling for the

genetic makeup, age, weight, physical activity levels and diet of specimens. However, a potential limitation of using an animal model is its relevance for application to human mechanics. Previous research has confirmed both structural and functional similarities between the porcine cervical spine (i.e. c34, c56) and the human lumbar spine (Oxland et al., 1991; Yingling et al., 1999). However, two slight differences have been identified in the porcine cervical FSU. These include: (i) the presence of anterior processes, which appear to have no significant mechanical role, and (ii) the endplates are smaller in the porcine model (Yingling et al., 1999).

2.4.1.2 Effects of Freezing on the Mechanical Properties of Functional Spinal Units

FSUs thawed from a frozen state continue to be used for *in vitro* biomechanical testing, despite the conflicting evidence that exists regarding the impact of freezing on the mechanical properties of FSUs. Previous research has shown that freezing does not affect the tensile properties of human AF tissue (Hirsch & Galante, 1967). Additionally, Smeathers and Joanes (1988) have shown that the compressive stiffness and hysteresis in human lumbar specimens were altered by less than 1% between fresh and thawed testing conditions, under repetitive sub-acute-failure magnitude (750 ± 250 N) compressive loads. Callaghan and McGill (1995) have shown that the ultimate compressive failure load of thawed porcine FSUs was increased by 24% and the energy absorbed to failure by 33% in comparison to fresh specimens. Interestingly, research conducted by Dhillon and colleagues (2001) has shown that freezing introduces an increase in IVD disc height, but recovers to pre-frozen values during the thawing process. Therefore, the potential limitations of freezing for the research proposed in this thesis must be acknowledged; however, it is still not feasible to procure and store a sufficient quantity of fresh specimens for *in vitro* testing in our spine biomechanics laboratories at the University of Waterloo.

2.4.1.3 Regional Differences in the Mechanical Properties of the Annulus Fibrosus

Previous research has examined regional differences in the tensile properties of single (Holzapfel, Schulze-Bauer, Feigl & Regitnig, 2005; Skaggs, Weidenbaum, Iatridis, Ratcliffe & Mow, 1994) and multilayer samples (Ebara et al., 1996) of AF tissue. Adams and

Green (1993) were one of the first groups to compare the tensile strength of human AF tissue between anterior and posterior regions of the IVD. Results from this study demonstrate that the estimated *in situ* strength (in the vertical direction) was greater in the posterior annulus (8.6 MPa) compared to anterior samples (3.0 MPa). Interestingly, despite the high incidence of incomplete layers in the lamellar structure of the posterior annulus, results from this work showed that the structural irregularities did not appear to weaken this region of the IVD (Green, Adams & Dolan, 1993). Later work conducted by Skaggs and colleagues (1994) examined the tensile properties of single human lamellae and found that when stretched parallel to the direction of the collagen fibers, ultimate failure stresses for anterior samples of the AF were higher than posterior-lateral lamellae, as well as in outer-layer samples compared to those harvested from deep regions (i.e. inner layers). The average (standard deviation; SD) reported failure stresses for each region were: 10.3 MPa (8.4) in the anterior-outer samples, 3.6 MPa (2.0) in the anterior-inner samples, 5.6 MPa (3.2) in the posterior-outer samples and 5.8 (2.9) in the posterior inner regions (Skaggs et al., 1994). Ebara and colleagues (1996) reported similar regional differences in the mechanical properties in multilayer samples of AF tissue, stretched circumferentially (i.e. parallel to the cartilaginous endplates). Results from this work showed that anterior tissue samples had larger tensile moduli and failure stresses compared to posterior-lateral specimens (Ebara et al., 1996). In addition, the outer regions of the AF had greater moduli and failure stresses and lower failure strains than the inner layers.

Holzapfel and colleagues (2005) were one of the first groups to examine the tensile strength of individual lamellae from human lumbar IVDs about multiple axes of loading. In this investigation, the authors examined the uniaxial tensile strength of AF tissue samples parallel to the collagen fiber direction (within a layer), as well as perpendicular to the collagen fiber bundles (Holzapfel et al., 2005). For inline testing (i.e. parallel to collagen fibers) both superficial and deep layers of the AF were examined separately from the anterior and posterior regions of the IVD. However, for perpendicular testing only the anterior-lateral region (at an intermediate depth) was examined (Holzapfel et al., 2005). Similar to previous work (Skaggs et al., 1994; Stokes, 1987) when the tensile force was applied in-line with the direction of the collagen fibers, the superficial layers were found to have a larger modulus than the deep specimens; however, there were no significant

differences found in the tensile moduli between the anterior-lateral and posterior regions. Interestingly, the tensile moduli transverse to the collagen fiber direction was shown to be two orders of magnitude smaller (0.22 MPa ± 0.2) than the inline tests conducted parallel to the collagen fiber bundles (e.g. posterior internal layers; 3.80 MPa ± 5.02) (Holzapfel et al., 2005).

More recently, Gregory and Callaghan (2011) were some of the first investigators to compare the uniaxial tensile properties of porcine AF tissue in to biaxial tensile testing conditions, since healthy IVDs are subject to multidirectional tensile loads *in vivo* (Heuer, Schmidt, Claes & Wilke, 2008a; Stokes, 1987). Bi-layer samples of AF tissue were isolated from porcine cervical IVDs across four separate locations: (i) anterior-superficial (layers 1 to 4), (ii) anterior-deep (layers 5 to 10), (iii) posterior-superficial and (iv) posterior-deep (Gregory & Callaghan, 2011). Results from this work showed that the maximal stress and stress-stretch ratio moduli determined from biaxial testing conditions were significantly higher than those from uniaxial tests (97% and 118% respectively). However, there were no significant differences found between regions on the IVD (Gregory & Callaghan, 2011).

2.4.1.4 Non-Contact Methods for Measuring Intervertebral Disc Bulging

Bulging of the IVD is a direct parameter of the outer AF strain distribution on the IVD and is an indirect parameter of the internal stress environment (Heuer, Schmidt, Claes & Wilke, 2007). Previous studies have proposed methods to quantify to the propagation of AF bulging to elucidate potential mechanisms of injury in the lumbar spine (Reuber, Schultz, Denis & Spencer, 1982; Stokes, 1988). However, these methods were limited in the resolution of their measurement systems due to the need for direct contact with the specimen, which could deform the surface of the AF and introduce measurement error. Several non-contact measurements techniques (e.g. Fredericson et al., 2001; Moon, Abramowitch & Woo, 2006) have been reported in the literature, which digitize the three-dimensional surface of the IVD while under load. However, these methods are limited by the time is require to characterize the surface profile of the IVD, since creep deformation while the specimen is under load will introduce errors into the measurement data.

For this reason, Heuer and colleagues (2007) developed a non-contact laser scanning method to characterize the three-dimensional surface of the IVD, which was paired with a modified material testing systems for *in vitro* spine biomechanics research. Initially, Heuer et al. (2007) employed a commercially available laser displacement sensor (OWLF4007, Welotec, Germany) to measure the proximity between a specimen and the rotating stage (accuracy of 5 µm inside of 40 mm). On average a surface scan could be collected in 40 seconds (or less), and it was assumed that any viscoelastic changes of the IVD would be so small that they wouldn't influence their results. The accuracy this non-contact laser-scanning device was assessed using manufactured steel bars with different cross-sectional profiles (e.g. triangle, square, hexagon, circular) (Heuer et al., 2007). Results from this work showed errors of 2% (or less) in the measured cross-sectional areas (compared to theoretical values). Interestingly, when using the device to characterize an initial seven human lumbar FSUs (L4/L5; with their posterior elements removed) statically loaded with 500 N of compression for 15 minutes, it was found that the average IVD height loss was 1.3 mm, with the largest magnitude of AF bulge in the anterior-lateral regions (0.86 mm). More recently, the same group (Heuer, Schmidt, Claes & Wilke, 2008b) improved their device by exchanging the single point sensor with a two-dimensional (2D) laser (scanControl 2800-25, MicroEpsilon, Ortenburg, Germany). This device is now capable of recording the surface profile of an IVD with a resolution of 10 µm in the transverse (i.e. bulging) and 25 µm in vertical (i.e. IVD height) direction in approximately 4 seconds (Heuer, et al., 2008b).

2.4.1.5 Histological Staining Techniques used to Visualize Micro-Structural Damage in the Annulus Fibrosus from Mechanical Exposures.

Numerous histological staining methods for isolated AF tissue have been reported in the scientific literature, including: alcian blue-fast red (Smits, 2003), safranin-O-fast green (Chubinskaya et al., 2007; Lü, Shono, Oda, Abumi & Kaneda, 1997; Sahlman et al., 2001) and the more standard hematoxylin-eosin (H&E) staining method (Tampier et al., 2007). More recently, staining methods using multiple dyes (Gruber, Ingram & Hanley, 2002; Ho, Leung, Cheung & Chan, 2008; Leung, Chan, Hung, Cheung & Chan, 2009) have been employed to increase the resolution of visual analysis. For example, in 2009 Leung and

colleagues (2009) developed a histological staining procedure (FAST staining) using four dyes (fast green, alcian blue, safranin-o and tartrazine) to generate an enhanced resolution of the IVD's structure. This method has proven to be effective for characterizing micro-structural damage and matrix properties of the IVD (Leung et al., 2009). Research conducted by our own group (Tampier et al., 2007) has shown that hematoxylin and eosin (H&E) was an effective method for characterizing micro-structural damage imposed to the AF from a repetitive flexion/extension loading protocol that has previously been used to induce herniation (Callaghan & McGill, 2001). Hematoxylin stains the cell nuclei and ground substance in the AF blue, but only when it is present in large amounts such as in cartilage matrix or remnants of the nucleus pulposus (Tampier, 2006). Conversely, eosin is an anionic and combines electrostatically with various tissues as the following colours: (i) bright red with elastic fibers, (ii) pink with collagen and myelinated nerve fibers and (iii) orange with red blood cells (Tampier, 2006). Collectively, H&E staining methods have been used extensively to study connective tissues, and has been proven successful for visualizing disruption to the IVD (Gunzburg et al., 1992; Hasegawa, An, Inufusa, Mikawa & Watanabe, 2000; Tampier et al., 2007; Yasuma, Arai & Yamauchi, 1993; Yasuma, Koh, Okamura & Yamauchi, 1990).

2.4.2 *In Vivo* Modeling of Lumbar Spine Kinetics

2.4.2.1 EMG-Assisted Musculoskeletal Model of the Lumbar Spine

Although the *in vivo* modeling approach employed in this thesis has been thoroughly described in the literature (e.g. Cholewicki & McGill, 1996; McGill, 1992; McGill & Norman, 1986) a brief review of the underlying theory is provided here. Contributions to the net L4/L5 joint moments from passive tissues (e.g. ligaments, IVDs, etc.) are approximated using three-dimensional kinematics of the lumbar spine (i.e. orientation of ribcage with respect to the pelvis). With the assumption that each intervertebral joint contributes an equal proportion to the total lumbar spine angular displacement (McGill, 1992; McGill & Norman, 1986) the moment contributions from a lumped passive tissues component is calculated using joint displacement-load relationships described previously (McGill, Seguin & Bennett, 1994). Next, the remaining contributions to the restorative moment are then partitioned

amongst the surrounding musculature, in combining the three-dimensional anatomical model of Cholewicki and McGill with the distribution-moment (DM) equations proposed by Ma and Zahalak (1991), which provide individual force and stiffness profiles for each muscle based on normalized linear enveloped EMG data. An alternative approach to calculate muscle force using a Hill-type muscle model has also been employed in previous research (Brown & Potvin, 2007). Muscle attachment data reported by Cholewicki and McGill (1996) are combined with measurements of the three-dimensional kinematics of the lumbar spine to calculate instantaneous muscle lengths and contraction velocities used in either the DM or Hill-type muscle model equations. Muscle groups not directly accessible for surface EMG recording are assigned activation profiles from anatomically and functionally similar muscle groups (McGill, Juker & Kropf, 1996). Each muscle's maximum force-producing capability (i.e. maximum muscle stress multiplied by the physiological cross-sectional area of the muscle) is then incorporated into either the DM equations (Cholewicki & McGill, 1996) or the Hill-type muscle model.

To compensate for potential errors associated with the transformation of EMG signals into estimates of muscle force and stiffness, a calibration procedure is typically used to fit the EMG-assisted model to each subject (or experimental condition). Specifically, a single gain factor (G) is computed by finding the value for G that minimizes the total sum of squared differences between instantaneous estimates of the net L4/L5 joint moment derived from the linked-segment model (LSM) and the equivalent restorative moment predicted by the EMG-driven biomechanical model. By multiplying instantaneous muscle force estimates by G, these quantities are adjusted at each instant in time during the experimental trials to account for between-subject differences in factors that can influence EMG-to-force transformations (Cholewicki & McGill, 1996). Passive tissue and adjusted muscle forces acting at the L4/L5 joint are then combined with LSM-derived L4/L5 reaction forces to quantify joint compression and shear forces. Hence, the resultant L4/L5 joint forces incorporate contributions from passive tissues, muscle, external forces and moments, and the gravitational-inertial forces associated with moving body segments.

2.5 Summary

Considering this body of literature, there is considerable evidence in the biomechanics literature that occupational mechanical exposures are closely associated with low back injury. Using a combination of both engineering and administrative controls, modern practices for injury prevention have been moderately successful in preventing acute injuries in the workplace. However, our understanding of the interactions that exist between external task demands on low back joint loading and fatigue injury (i.e. progressive tissue breakdown) could be improved. In particular, when considering the prevalence of low back pain and injury in today's workforce, there remains considerable opportunity to further refine our understanding of how workers load their spines across various external task demands (e.g. load, speed, postural symmetry; **study I**) and how these mechanical exposures influence known fatigue injury mechanisms in the lumbar spine (**study II**). In particular, for cyclic exposure to sub-acute-failure magnitudes of applied force, the mechanical and structural changes that occur in the IVD have yet to be characterized in intact joints across loading conditions (**study III**) or on isolated AF tissue (**study IV**; cyclic biaxial tension). This was the primary motivation for the collection of studies that comprise this thesis.

Chapter 3

Study I: Exploring interactions between external task demands in lifting on low back joint loads *in vivo*.

3.1 Overview

Study Design: An experiment was conducted to explore the interaction effects of mechanical low back injury risk factors on *in vivo* estimates of L4/L5 joint loading during a laboratory-simulated occupational lifting task.

Background: The most commonly accepted mechanical risk factors linked to low back injury include: (i) high force demands; (ii) frequent repetition; and (iii) deviated postures. However, our understanding of the interactions that exist between each of these factors on the resultant *in vivo* joint loads that occur in the lumbar spine during manual materials handling remains limited.

Objectives: The primary objective of this study was to explore interactions between: (i) the magnitude of the external load, (ii) speed of lifting movement, and (iii) symmetry of initial load placement (i.e. posture) on estimates of *in vivo* joint loading at L4/L5 during simulated occupational lifting.

Methods: Thirty-four participants with manual materials handling experience were recruited. Three-dimensional motion data were captured together with foot-ground contact forces and activation of six bilateral trunk muscle groups while participants performed lifts with two loads ("light" and "heavy"), at two movement speeds ("controlled" and "fast"), and using two initial load placements ("symmetric" and "asymmetric"; i.e. posture). Inverse dynamics analyses were conducted, and outputs were incorporated into a three-dimensional EMG-assisted musculoskeletal model of the lumbar spine to generate L4/L5 joint compression and shear force-time histories.

Results: Significant interactions between load, speed and posture emerged in virtually every dependent measure that was used to characterize time-varying estimates of load in the lumbar spine. Significant two-way interactions between load and speed ($p = 0.0035$), as well as speed and posture ($p = 0.0004$) were revealed in peak measures of L4/L5 compressive forces. A significant three-way interaction between load, speed and posture ($p = 0.0477$) was revealed in the cumulative measure of compressive loading at L4/L5 during

the ascending portion of the lifting trials. A significant main effect of load ($p < 0.0001$) and a significant two-way interaction between speed and posture ($p = 0.0384$) was revealed in peak measures of peak L4/L5 anterior/posterior (AP) joint shear.

Conclusions: Results from this investigation provide strong evidence that known mechanical risk factors linked to low back injury should not be viewed in isolation. Stated differently, the influence of external demands on *in* vivo estimates of joint loading was not simply additive. Therefore, future injury prevention efforts should consider the complex interactions that exist between external task demands and their combined influence on internal (musculoskeletal) joint loading.

Keywords: low back, joint loading, external demands, movement speed, posture

3.2 Introduction

The most commonly accepted mechanical risk factors linked to low back injury include: (i) high force demands; (ii) frequent repetition; and (iii) awkward postures (Bernard, 1997). However, as noted by Gallagher and Heberger (2013) these exposures have typically been examined in isolation, and are often assumed to function independently concerning injury risk. As such, our understanding of the combined effects of different external task demands on low back joint loading and injury may be limited.

A review of workplace lifting conditions indicates that virtually all manual materials handling (MMH) tasks involve asymmetric lifting (Marras et al., 1995;, 1993). Previous research has demonstrated that trunk strength is significantly affected by both asymmetrical postures and increased angular velocity (i.e. movement speed) (Lavender, Li, Andersson & Natarajan, 1999; Marras & Mirka, 1989). Early work conducted by Marras and Mirka (1992) demonstrated increased co-activation of the trunk musculature due to increased trunk velocity and asymmetrical postures during simulated occupational lifting, which resulted in an increased spinal loading. Later, Gallagher et al. (1994), comparing both symmetric and asymmetrical lifting tasks, showed that the average lumbar compression was greater in purely sagittal plane lifting tasks, although both anterior-posterior (AP) and lateral shear forces acting on the lumbar spine were increased during asymmetrical trials. Interestingly, analysis of individual muscle recruitment indicated that the external demands of asymmetrical lifting were shifted to ancillary muscles (i.e. muscles other than the erector spinae or latissimus dorsi) with smaller cross-sectional areas, which may be at an elevated risk of overexertion injury during MMH tasks (Gallagher, Hamrick, Love & Marras, 1994).

Marras and Davis (1998) also examined the three-dimensional lumbar spine loads at L5/S1 associated with asymmetrical lifting using an EMG-assisted musculoskeletal model. Simulated occupational lifts were performed with asymmetrical load placement (0, 30 or 60 degrees in the mid-sagittal plane) on both sides of the body. Results from this study demonstrate that spinal compression and lateral shear forces increased as the lift origin became more asymmetric; however, the observed differences increased by approximately 200% when the lifts were conducted from the left side of the body when compared to the right side (Marras & Davis, 1998). Posterior L5/S1 joint shear forces were also shown to

decrease as the magnitude of asymmetry (i.e. deviation away from the mid-sagittal plane of the body) increased, due to the partitioning of the resultant joint load across both the anterior-posterior and mediolateral axes (Marras & Davis, 1998). Based on these results, the authors concluded that the trade-offs between the direction of the resultant joint force in the lumbar spine must be considered across various types of lifting tasks (Marras & Davis, 1998).

Previous research by Lavender et al. (2003) has examined the combined effects of the magnitude of the load, movement speed, and initial lift height on low back kinetics. Results from this study showed that peak L5/S1 flexion reaction moments were dependent upon a combination of these aforementioned factors, with the largest moments observed in the high-load, high-speed trials that were initiated from ground height. More recently, Greenland et al. (2013) also explored interactions between the magnitude of the load and lifting speed across three different lifting heights on the resultant loading in the lumbar spine using a single equivalent muscle model. Results from their study demonstrate that, on average, there was an 18.3% increase in the compressive forces in the in the high-load (9 kg), high-speed lifts compared to the low-load (2.25 kg), low-speed trials.

Therefore, the primary motivation for this study was to explore interactions between: (i) magnitude of external load, (ii) movement speed, and (iii) symmetry of initial load placement (i.e. posture) on estimates of *in vivo* low back joint loading during a simulated occupational lifting task. In-line with this objective, the following hypotheses were formulated:

i. significant interactions between the magnitude of the external load, movement speed and posture would emerge in peak measures of compression and anterior-posterior (AP);
ii. significant increases in AP shear loading would be observed in asymmetrical lifting trials;
iii. cumulative compression (calculated per lift) would also be significantly influenced by significant interactions between all external demands.

3.3 Materials & Methods

3.3.1 Study Design

An experiment conducted to explore the combined effects of known mechanical risk factors for low back injury on *in vivo* estimates of L4/L5 joint loading. Different levels of external task demands were evaluated during a simulated occupational lifting task by varying the: (i) mass of the load lifted, (ii) movement speed (*i.e.* time required to execute the ascending portion of the lift) and (iii) symmetry of initial load placement (i.e. posture).

3.3.2 Participants

Thirty-four participants with an average [SD] of 9 [10] years of manual materials handling experience (mean [SD] age = 37 [10] years; height = 1.80 [0.06] m; and body mass = 86 [10] kg) were recruited for this study. The inclusion criteria for participation specified that all participants reported that they were free of any known musculoskeletal injury and pain at the time of testing. All participants signed an informed consent document that outlined the study's protocols and associated risks. The study was approved by the University of Waterloo's Office of Research Ethics.

3.3.3 Instrumentation

3.3.3.1 Kinematics

Three-dimensional kinematic data were measured at 160 Hz using a 10-camera optoelectronic motion capture system (Vicon, Centennial, CO, USA). Sets of four and five reflective markers, fixed to rigid pieces of plastic were secured to the body with Velcro® straps, and used to track the position and orientation of the 15 body segments that were modeled. For each participant, reflective markers were placed on 23 anatomical landmarks that were used to define the proximal and distal endpoints of the feet, shanks, thighs, pelvis, trunk, head, upper-arms, forearms and hands. Functional joint centers for the hips (HJC) and knees (KJC) were determined using similar methods to those described by Begon et al. (2007) and Schwartz and Rozumalski (2005). Briefly, participants were asked to perform 10 repetitions of open chain: (i) knee flexion/extension; (ii) hip flexion/extension; (iii) hip

ab/adduction; and (iv) hip circumduction. From these trials, Visual 3D™ software (Version 5.0, C-Motion, Inc., Germantown MD, USA) was used to compute the frontal planes of the thigh and shank segment-fixed coordinate systems. A standing (static) calibration trial was collected such that the orientation of each segments' local coordinate system, as defined by the anatomical landmarks and segment endpoints, could be determined through a transformation from the coordinate system established for each rigid body. The anatomical markers were removed following the calibration procedure. Lastly, end-range trunk flexion and extension movement trials were collected (3 repetitions each) to facilitate normalization of trunk posture during subsequent lifting trials.

3.3.3.2 Kinetics

Two in-ground force platforms (FP6090: 60 x 90 cm; Bertec, Columbus, OH, USA) mounted side-by-side were used to measure interactive forces and moments between the feet and ground. Participants were required to keep their feet on both force plates and the load was repositioned to the same position, in one of two locations (i.e. in front of the body or rotated to the left side) after every trial. The four-corners of each force platform were located in the collection volume using a calibration wand (Vicon, Centennial, CO, USA), such that its local coordinate system could be transformed into the global reference frame. The analog signals from each force platform were synchronized with the kinematic data, and sampled at a rate of 2400 Hz using Vicon software (Nexus version 1.4, Centenial, CO, USA).

3.3.3.3 Electromyography

Pairs of pre-gelled, surface electromyography (EMG) recording electrodes (3 cm inter-electrode spacing; Medi-Trace, Kendall-LTP, Chicopee, MA, USA) were adhered to the skin bilaterally over the following six trunk muscle groups: (i) upper erector spinae; approximately 5 cm lateral to the T9 spinous process, (ii) lower erector spinae; approximately 3 cm lateral to the L3 spinous process, (iii) rectus abdominus; approximately 3 cm lateral to the umbilicus, (iv) external abdominal obliques; approximately 15 cm lateral to the umbilicus, (v) internal abdominal obliques; midway between the anterior superior iliac

spine and symphysis pubis, and (vi) latissimus dorsi; lateral to the T9 spinous process over the muscle belly (Cholewicki & McGill, 1996). EMG signals were bandpass filtered (10-500 Hz) and differentially amplified (CMRR > 100 dB at 60 Hz; input impedance > 100 MΩ) (TeleMyo 2400 G2 Telemetry System, Noraxon Inc., Scottsdale, AZ, U.S.A.) prior to analog-to-digital conversion (16-bit resolution) at 2400 Hz. Surface EMG signals were collected synchronously with the force platform and kinematic data using Vicon software (Nexus version 1.4, Centennial, CO, USA).

Before the simulated occupational lifting trials were collected, maximum voluntary isometric contractions (MVICs) were performed for each of the aforementioned muscle groups. Briefly, with their lower body restrained, subjects performed a series of standardized maximal trunk flexion, extension, lateral bend and axial twist exertions, as well as left and right isometric "pull-downs" (for latissimus dorsi) while a research assistant provided matching external resistance (McGill, 1991). Three repetitions of each MVIC were collected, with one minute of rest provided between each trial.

3.3.4 Protocol

Each participant initially performed three lifting trials (box dimensions; 30.5 x 30.5 x 30.5 cm) that represented a low-demand condition (*i.e.* 9.3 kg mass, low movement speed, symmetrical positioning of load). Once these low-exposure trials were collected, the external demands of the lifting task were modified according to one of the following parameters using a full-factorial design: (i) magnitude of external load; low = 9.3 kg, high = 24.7 kg (Waters, Putz-Anderson, Garg & Fine, 1993), (ii) movement-speed; participants were instructed to either perform the lift in a *"controlled manner"* or *"as quickly as comfortable"* and (iii) symmetry of initial load placement (i.e. posture); the load was placed either in front of participants or at 45 degrees to the left of participants' mid-sagittal plane. This comprised a total of 24 lifting trials for each participant that were evenly distributed across each of the eight experimental conditions (i.e. three trials per condition collected in a block-randomized order). Approximately 15 seconds and 60 seconds of rest were provided between each trial and condition, respectively. In the case where a participant stepped-off the force platforms, an additional trial was collected after 15 seconds of rest. No feedback

was provided to participants regarding their task performance at any point throughout the investigation. Each participant wore a pair of tight shorts, a fitted T-shirt, and their preferred athletic footwear during data collection.

3.3.5 Data Processing

All kinematic and kinetic signals were padded with one second of data (Howarth, Beach, Pearson & Callaghan, 2009) using an end-point reflection method (Smith, 1989) and smoothed using a second-order, lowpass (dual-pass) digital Butterworth filter with an effective cutoff frequency of 10 Hz (Bisseling & Hof, 2006). EMG signals were full-wave rectified and lowpass filtered using a second-order (single-pass) digital Butterworth filter with a cutoff frequency of 2.5 Hz to produce linear envelopes for each muscle (Brereton & McGill, 1998). All surface EMG signals collected during simulated occupational lifting trials were subsequently normalized to the peak amplitude recorded during the three MVIC trials. Angular displacement of the lumbar spine was described by the relative orientation between the pelvis and trunk/ribcage. The rotation matrix describing the relative three-dimensional orientation between these adjoining segments was decomposed using a rotation sequence of: (i) flexion/extension, (ii) lateral bend, and (iii) axial rotation (McGill, 1997).

Instantaneous reaction forces and net joint moments of force (about the axes located at the origin of the pelvis coordinate system) were computed using a bottom-up, inverse dynamics approach with Visual3D™ software. The origin of the pelvis-segment coordinate system was calculated as the midpoint between iliac crests and a least-squares plane fit to the locations of the iliac crests and greater trochanters represented the frontal plane of the pelvis segment (Beach, Frost & Callaghan, 2014). The component of the reaction force acting perpendicular to the frontal plane of the pelvis was assumed to have been equivalent to the anterior/posterior shear force acting at L4/L5. Default parameters within the Visual3D™ software for segmental mass and inertial properties (scaled for individual participants based using height and mass) were used in the inverse dynamics calculations. Reaction forces and moments derived from the inverse dynamics analyses, lumbar spine angular kinematics, and the normalized EMG signals were entered into a three-dimensional, dynamic, EMG-assisted musculoskeletal model of the lumbar spine (**Figure 3-1**) to quantify

L4/L5 joint compression and shear forces (Cholewicki & McGill, 1996). A Hill-type muscle model was used to estimate the force generated by each of the 118 muscle fascicles in the model (**Equation 3-1**) (McGill & Norman, 1986).

Equation 3-1

$$F_m = G[(EMG/EMG_{MAX}) \times (PCSA \times \sigma_{MAX}) \times (L_0) \times (V_0) + F_{PEC}]$$

where:

F_m	=	*force in the muscle (N)*
G	=	*common gain factor*
EMG	=	*linear envelope (instantaneous recording)*
EMG_{MAX}	=	*maximum amplitude from MVIC trial (linear envelope)*
$PCSA$	=	*physiological cross-sectional area of muscle (cm^2)*
σ_{MAX}	=	*maximum muscle stress (N/cm^2)*
L_0	=	*force length multiplier*
V_0	=	*force velocity multiplier*
F_{PEC}	=	*force from passive elastic components*

To compensate for potential errors associated with the transformation of EMG signals into estimates of muscle force, a calibration procedure was used to balance the internal muscle moments with the reaction moments for each subject. Specifically, a single gain factor (*G*) for each of the 8 experimental conditions was computed for each subject by finding the value for *G* that minimized the total sum of squared differences between the L4/L5 reaction moments (about all three axes) derived from the linked-segment model (M_{LSM}) and the internal muscle moment determined by the EMG-driven model (M_{EMG}) (**Equation 3-2**). Data collected over the entire duration of all three trials in each experimental condition were used to resolve *G*.

Equation 3-2

$$\sum_{f=1}^{Frame} \min\left(M_{LSM(x,y,z)}(f) - \left[G \times M_{EMG(x,y,z)}(f)\right]\right)^2$$

where:

$M_{LSM\ (x,y,z)}$	=	*moments about the origin of the pelvis coordinate system from link segment model (Nm)*
$M_{EMG\ (x,y,z)}$	=	*restorative muscle moments (Nm)*
G	=	*common gain factor*

Multiplying the instantaneous muscle forces by the gain factor (*G*) effectively adjusted the resultant compressive joint force at L4/L5 at each instant of time during the experimental trials to account for between-subject differences in factors that can influence EMG-to-force transformations (e.g. anthropometry, assumed physiological cross-sectional area of each muscle fascicle included in the model, *etc.*) (Cholewicki & McGill, 1996). The net individual adjusted muscle and passive tissue forces acting at the L4/L5 joint were then added to the LSM-derived reaction forces to quantify L4/L5 joint compression and shear forces during the simulated occupational lifting trials (Potvin, McGill & Norman, 1991). Hence, estimates of joint load considered contributions from passive tissue forces, muscles forces, external forces and moments, and the gravitational-inertial forces associated with moving body segments.

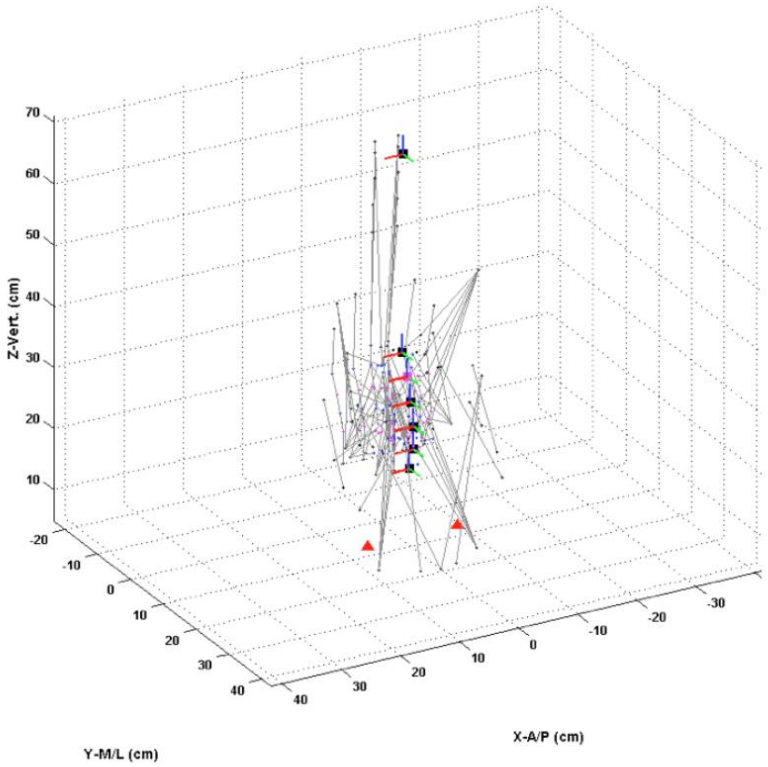

Figure 3-1: Three-dimensional representation of the McGill musculoskeletal model in the MATLAB virtual environment. The red triangles represent the two hip joint centres. Local coordinates systems are shown at the joint centres of L1/L2, L2/L3, L3/L4, L4/L5, L5/S1 and C7/T1. Individual muscle fascicles included in the model are shown as grey vectors (with the exception of transverse abdominis, which has not been graphed).

3.3.6 Data Reduction

All trials were truncated to include only the ascending phase of the lifting motion based on the vertical trajectory of participants' link-segment model centre of mass. Our decision to only focus on the ascending portion of the lift was made *a priori* since the participants were only provided instructions on the speed of the lift and not the entire movement. Therefore, inclusion of the other phases of the trial may have attenuated any effect of speed (as an independent factor) on the results that have been present in this study.

Seven dependent measures were computed, including: (i) total lift time for the ascent; (ii) lifting speed; calculated using the vertical trajectory of the link-segment model, (iii) average common gain factor for each experimental condition that was used to balance the EMG-assisted musculoskeletal model; (iv) peak L4/L5 compression; (v) lumbar flexion angle at the time of peak compressive loading; (vi) cumulative L4/L5 compression during the ascending portion of the lift; calculated using trapezoidal integration and (vii) peak L4/L5 posterior joint shear.

3.3.7 Statistical Analyses

All statistical analyses were computed using SAS software (version 9.2, SAS Institute Inc., Cary, NC) with a significance level of 0.05 that was determined *a priori*. To examine interactions between the magnitude of the external load, speed of movement, and symmetry of initial load placement (i.e. posture) on the dependent measures, a within-subject, three-factor general linear model was employed. Tukey's *post hoc* test was used to further explore all significant main effects. In cases where a significant interaction was found, simple effects were analyzed (e.g. impact of posture on the interaction between load and speed). Effect sizes for all significant comparisons were evaluated using Cohen's *d* (Cohen, 1988).

3.4 Results

3.4.1 Lift time – Ascending

Significant two-way interactions between load and speed ($p < 0.0001$), as well as load and posture ($p = 0.0002$) emerged in the total time required to complete the ascending phase of the lifting task. Subsequent analysis of simple effects revealed that there were no significant differences between the time required to execute low-load, low-speed trials compared to high-load, low-speed trials ($p = 0.3665$); however, the high-speed lifts with asymmetrical load placement were associated with significantly longer lift times ($p < 0.0001$; $d > 0.98$; mean difference = 0.13 seconds) compared to the high-speed symmetrical trials. A summary of all lifting times across experimental conditions is provided in **Table 3-1**.

3.4.2 Lifting Speed – Link Segment Model Centre of Mass

Significant two-way interactions between load and speed ($p < 0.0001$), load and posture ($p = 0.0350$) and speed and posture ($p = 0.0006$) were revealed in the average vertical velocity of the link-segment model centre of mass. Subsequent analysis of simple effects revealed that significantly greater velocities ($p < 0.0001$; $d = 0.70$; average difference = 0.1 m/s) were observed in the symmetrical, low-load, high-speed trials compared to the similar asymmetrical load placement condition. The symmetrical, high-load lifting velocities were also significantly greater than the asymmetrical trials at both the controlled ($p = 0.0015$; $d = 0.80$; average difference = 0.07 m/s) and fast lifting speeds ($p < 0.0001$; $d = 0.72$; average difference = 0.1 m/s). A summary of all lifting velocities across experimental conditions is provided in **Figure 3-2**.

3.4.3 Common Gain Factor Used with EMG-Assisted Model

Significant main effects of load ($p < 0.0001$), speed ($p = 0.0002$) and posture ($p < 0.0001$) were revealed in the average common gain factor that was used across participants to balance the estimates of the net L4/L5 joint moments derived from the linked-segment model and the equivalent quantity predicted by the EMG-driven model. Tukey's *post hoc* test revealed that a significantly larger common gain factor was required for the high load

condition ($p < 0.0001$; $d = 0.42$), the controlled lifting speed ($p = 0.0002$; $d = 0.27$) and symmetrical load placement ($p < 0.0001$; $d = 0.63$). A summary of all common gain factors across experimental conditions is provided in **Table 3-2**.

3.4.4 Peak L4/L5 Compressive Loading

Significant two-way interactions between load and speed ($p = 0.0035$), as well as speed and posture ($p = 0.0004$) were revealed in peak measures of L4/L5 compressive loading. Subsequent analysis of simple effects revealed significantly greater magnitudes of peak compressive loading for fast lifting trials with 9.3 kg of external load compared to the controlled speed trials ($p < 0.0001$; $d = 0.72$; average difference = 588 N); however, there was no significant difference between the controlled and fast lifting trials performed with 24.7 kg of external load ($p = 0.5586$). Interestingly, there were significantly greater magnitudes of peak compressive force in the high-speed trials with asymmetrical load placement compared to the low speed condition ($p < 0.0001$; $d = 0.34$; average difference = 580 N); however, there was no significant difference observed between the high and low speed trials for the asymmetrical condition ($p = 0.5699$). A summary of peak compressive loading at L4/L5 across all experimental conditions is provided in **Figure 3-3**. Profile plots that illustrate the significant two-way interactions between load and speed, as well as speed and posture are provided in **Figures 3-4** and **Figure 3-5**, respectively.

3.4.5 Lumbar Flexion at the Time of Peak Compressive Loading

A significant main effect of posture ($p < 0.0001$) was revealed in normalized measures of lumbar flexion angle at the time of peak compressive loading. There was no significant main effect of load ($p = 0.4297$) or speed ($p = 0.1963$) found. Tukey's *post hoc* test revealed that, on average, participants assumed more lumbar spine flexion at the time of peak compressive loading with asymmetrical load placement ($p < 0.0001$; $d = 0.66$; average difference = 8.5% full flexion). A summary of spine flexion angle at the time of peak compressive loading across all experimental conditions is provided in **Figure 3-6**.

3.4.6 Cumulative L4/L5 Compressive Loading (per lift)

A significant three-way interaction between load, speed and posture ($p = 0.0477$) was revealed in the cumulative measure of compressive loading at L4/L5 during the ascending portion of the lifting trials. Subsequent analysis of the interaction between load and speed across both symmetrical and asymmetrical load placement trials revealed a significant main effect of load ($p < 0.0001$; $d = 1.39$; average difference = 724.7 Ns) and speed ($p < 0.0001$; $d = 0.95$; average difference = 561.5 Ns) in trials with symmetrical load placement; however, there was a significant interaction between load and speed ($p = 0.0006$) for asymmetrical trials. Tukey's *post hoc* test revealed that both the low- and high-load conditions were significantly different ($p < 0.0001$), although a more pronounced difference (1030.6 Ns) was observed at the controlled movement speed. A summary of the cumulative L4/L5 compressive load across all experimental conditions is provided in **Figure 3-7**. A profile plot that illustrates the significant two-way interactions between load and speed across postures is provided in **Figure 3-8**.

3.4.7 Peak L4/L5 Posterior Shear Loading

A significant main effect of load ($p < 0.0001$) and a significant two-way interaction between speed and posture ($p = 0.0384$) was revealed in peak measures of peak L4/L5 posterior shear loading. Subsequent analysis of simple effects revealed that there was significantly greater peak posterior shear measured in symmetrical, fast lifts ($p = 0.0002$; $d = 0.48$; average difference = 128.7 N) compared to asymmetrical fast lifts. Tukey's *post hoc* test revealed significantly greater magnitudes of peak posterior shear for lifts performed with 24.7 kg of external load ($d = 0.96$; average difference = 268 N). A summary of peak posterior shear at L4/L5 across all experimental conditions is provided in **Figure 3-9**. A profile plot that illustrates the significant two-way interaction between speed and posture is provided in **Figure 3-10**.

Table 3-1: Summary of average lift time (seconds) for ascending portion of the movement across experimental conditions.

Hand Load (kg)	Speed	Load Placement	Mean (s)	Standard Deviation
9.3	Controlled	Symmetrical	0.825	0.136
9.3	Controlled	Symmetrical	0.844	0.118
9.3	Fast	Symmetrical	0.497	0.119
9.3	Fast	Symmetrical	0.535	0.069
24.7	Controlled	Asymmetrical	0.796	0.166
24.7	Controlled	Asymmetrical	0.926	0.208
24.7	Fast	Asymmetrical	0.595	0.180
24.7	Fast	Asymmetrical	0.696	0.142

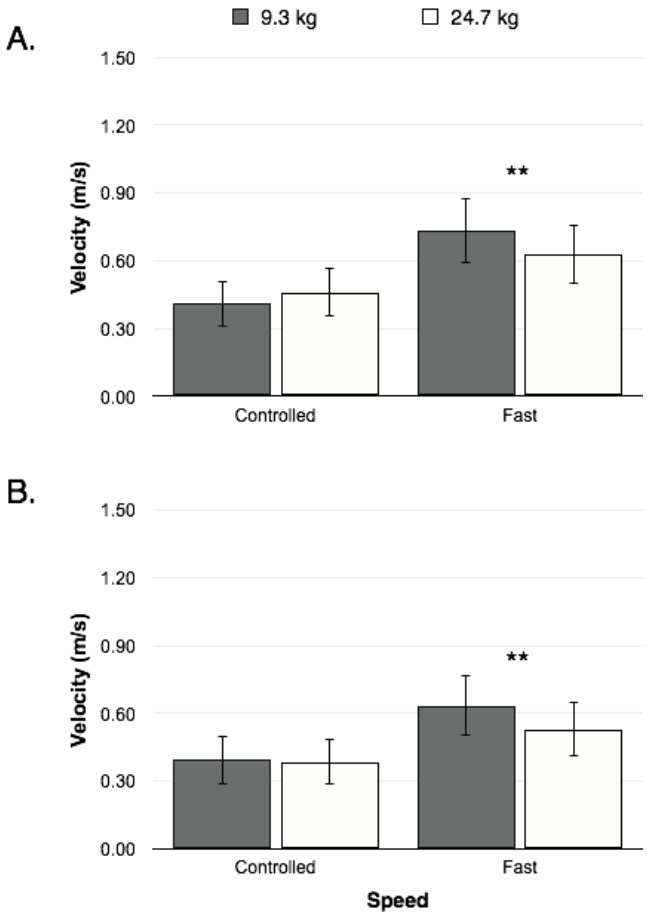

Figure 3-2: Summary of average link-segment model centre of mass vertical velocity across (A) symmetrical and (B) asymmetrical lifting trials. **Significant ($p < 0.0001$)

Table 3-2: Summary of common gain factor used with EMG-assisted model across experimental conditions.

Hand Load (kg)	Speed	Load Placement	Mean (G)	Standard Deviation
9.3	Controlled	Symmetrical	1.437	0.554
9.3	Controlled	Asymmetrical	1.117	0.412
9.3	Fast	Symmetrical	1.289	0.417
9.3	Fast	Asymmetrical	1.023	0.359
24.7	Controlled	Symmetrical	1.636	0.519
24.7	Controlled	Asymmetrical	1.361	0.466
24.7	Fast	Symmetrical	1.519	0.434
24.7	Fast	Asymmetrical	1.178	0.381

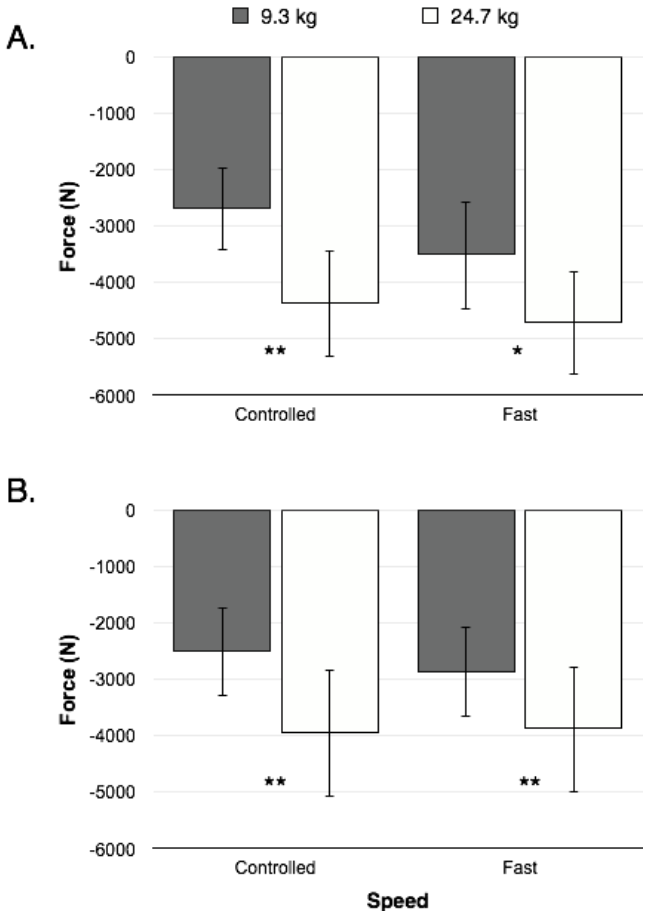

Figure 3-3: Summary of L4/L5 peak compressive joint loading across (A) symmetrical and (B) asymmetrical lifting trials. **Significant ($p < 0.0001$) *Significant ($p < 0.05$)

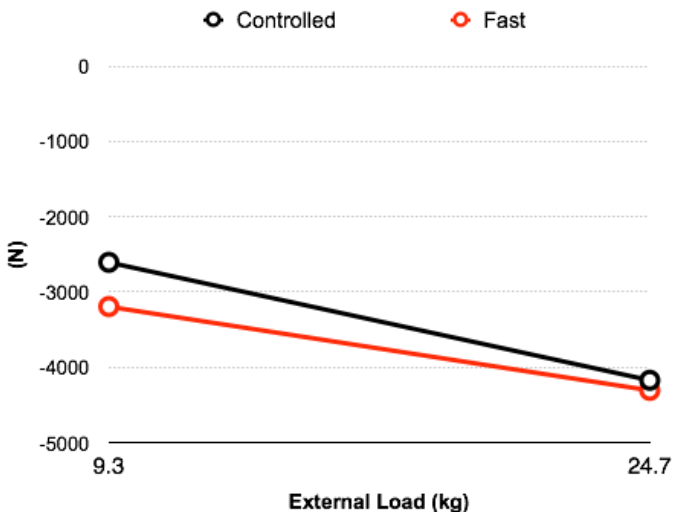

Figure 3-4: Profile plot of collapsed peak L4/L5 compression data across load and speed.

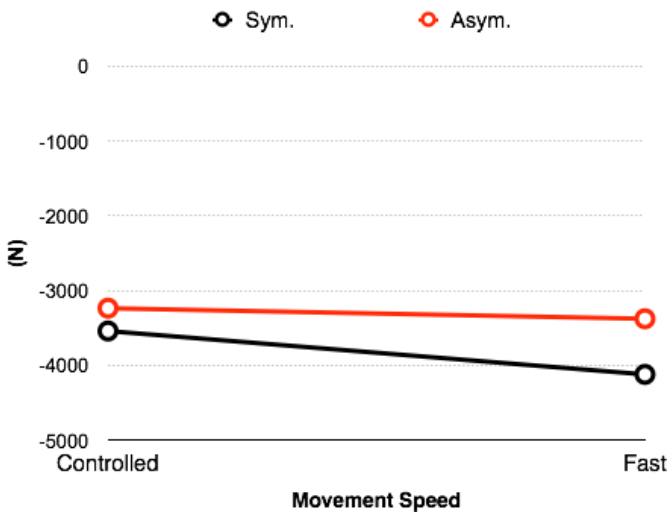

Figure 3-5: Profile plot of collapsed peak L4/L5 compression data across speed and posture.

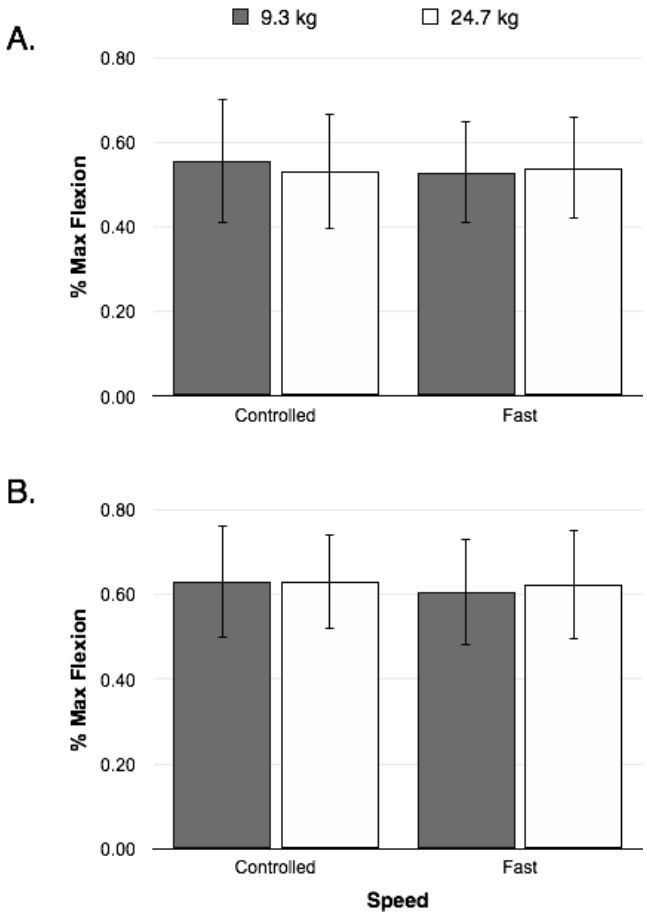

Figure 3-6: Summary of normalized lumbar flexion angle (% max) at the time of peak L4/L5 compressive loading across (A) symmetrical and (B) asymmetrical lifting trials.

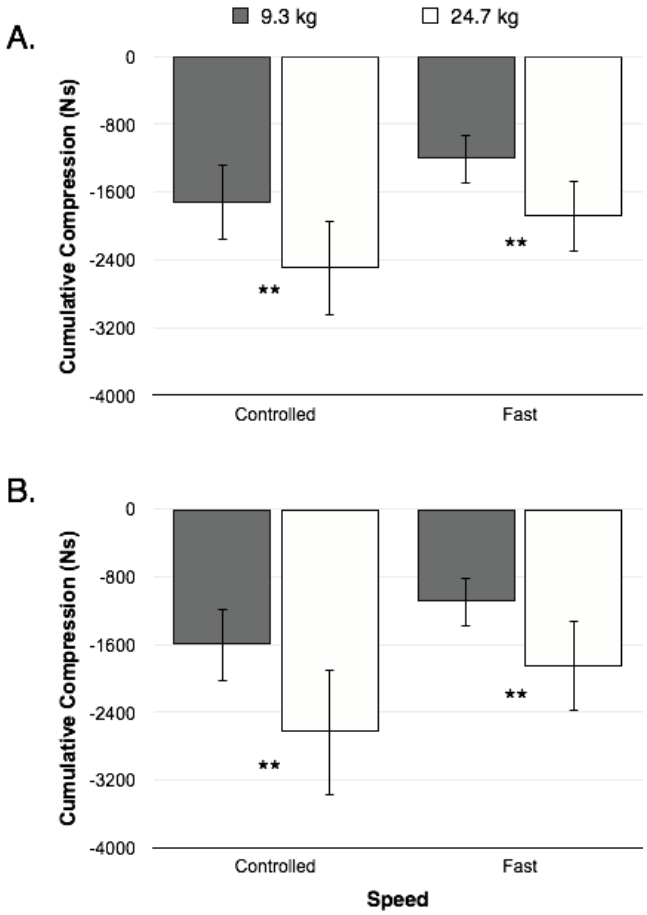

Figure 3-7: Summary of cumulative L4/L5 compressive force (per lift) across (A) symmetrical and (B) asymmetrical lifting trials. **Significant ($p < 0.0001$)

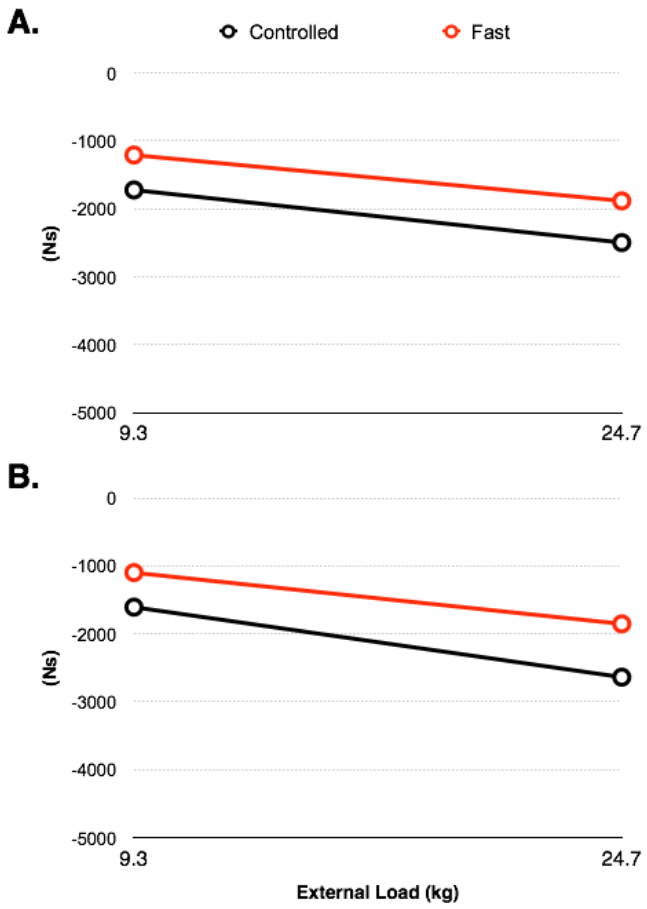

Figure 3-8: Profile plot of collapsed cumulative L4/L5 compression data across load and speed for: (A) symmetrical load placement and (B) asymmetrical load placement.

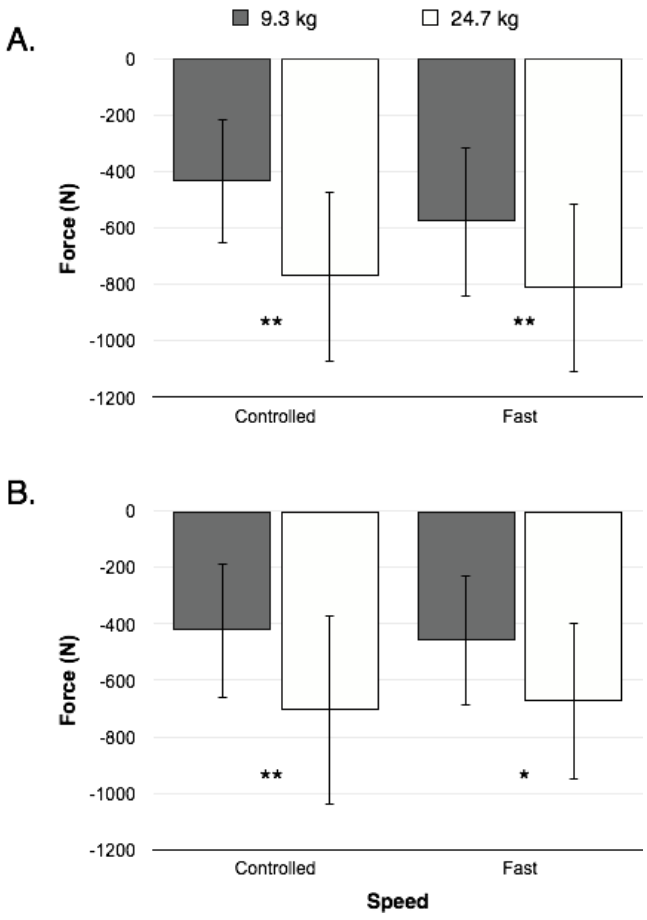

Figure 3-9: Summary of peak posterior shear at L4/L5 across (A) symmetrical and (B) asymmetrical lifting trials. **Significant ($p < 0.0001$) *Significant ($p < 0.05$)

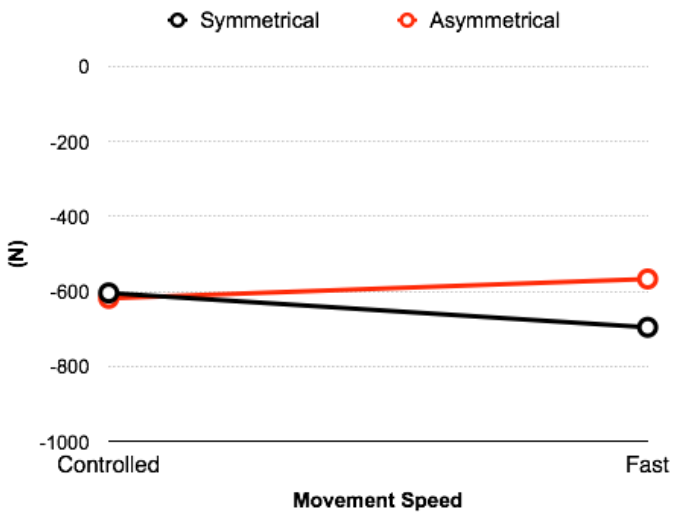

Figure 3-10: Profile plot of collapsed peak L4/L5 posterior shear data across speed and posture.

3.5 Discussion

The results from this study provide strong evidence that known mechanical risk factors for low back injury should not be viewed in isolation when designing/modifying occupational lifting tasks. Consistent with our hypothesis, significant interactions between the magnitude of the external load, movement speed and symmetry of initial load placement (i.e. posture) were revealed in all dependent measures that were used to characterize the time-varying estimates of *in vivo* joint loading. However, lifting trials with asymmetrical load placement were not associated with significantly greater magnitudes of AP joint shear at L4/L5. A significant contribution from this work is the assessment of lumbar spine loads across three different external task demands linked to low back injury using an EMG-driven musculoskeletal modeling approach, sensitive to both intra- and inter- individual movement patterns and muscle activation profiles, across a large sample of participants with manual materials handling experience.

Findings from this study are in agreement with previous literature. For example, research by Lavender et al. (2003) showed that a significant three-way interaction between magnitude of the load, lifting speed and initial lifting height governed peak L5/S1 moments at the lumbar spine. Although not reported herein, the peak L5/S1 moments reported by Lavender et al. (2003) for a 300 N fast-speed lift from floor to waist height closely matched those observed in our high-load (24.7 kg), high-speed trials (peak flexion moments of approximately 200 Nm). However, the lifting speeds reported by Lavender et al. (2003) are much greater than what is presented in the present work. This is likely due to the fact that lifting speed in the Lavender et al. (2003) paper was calculated using the trajectory of the hand marker, whereas in the present study it was based on the vertical displacement of the link-segment model centre of mass. The velocity of the high-speed lifting trials included in this study were similar to that reported by Greenland et al. (2013), who examined the influence of movement speed and type on peak and cumulative low back compressive force. Results from their study demonstrated that peak low back compressive force was significantly different between slow and fast lifting speeds, with approximately 20% greater peak loads observed during the fast trials (Greenland et al., 2013).

Based on survey data from 547 industrial lifting tasks published by Dempsey (2003), the low load (9.3 kg) lifting exposure included in this study was similar to the 50th percentile external load observed in industry. In comparison, the high-load (24.7 kg; upper limit for the NIOSH recommended weight of lift limit) was above the 90th percentile. The asymmetry of initial load placement (45 degrees) examined in the present study reflects approximately the 90th percentile (i.e. approaching the worst case scenario) observed in Dempsey's sample (Dempsey, 2003). In comparing the average magnitudes of peak compressive loading observed in this study to the NIOSH guidelines (Waters et al., 1993), it is noted that both the symmetrical (2697 N) and asymmetrical (2516 N) low-load, low-speed lifting conditions are well below the NIOSH action limit (3400 N); however, with the exception of the low-load, high-speed asymmetrical condition (2872 N), the remaining conditions all exceeded this threshold. A similar trend emerges when the average magnitudes of L4/L5 peak posterior shear are compared to the University of Waterloo's recommended limit (500 N) (McGill & Callaghan, 1999), with only the symmetrical low-load, low-speed (436 N) and asymmetrical, low-load, low-speed (425 N) and low-load, high-speed (460 N) below this limit.

It is interesting that lifting trials performed with asymmetrical load placement were not associated with increased AP shear loading, as shown in previous research (Gallagher et al., 1994). Moreover, there was no significant difference between peak and/or cumulative measures of L4/L5 joint compression between symmetrical and asymmetrical load placement lifting trials. One possible explanation for the differences observed in the present study compared to previous research (e.g. Marras & Mirka, 1992) is that the participants were recruited from industry and possessed an average of 9 years of MMH experience and maintained similar muscular activation (i.e. bracing) across experimental conditions. However, it is possible that our decision to calculate separate (individual specific) common gain factors for the musculoskeletal model of the lumbar spine employed to estimate the resultant L4/L5 joint loading across experimental conditions may have attenuated the expected differences. In-line with this hypothesis, significant main effects of load, speed and posture emerged in the average common gain that was applied to the model across experimental conditions. Although a significantly higher gain factor for the high load (24.7 kg) lifting trials was not entirely unexpected due to the increased physical demands of the lifting task, it was surprising that both the symmetrical and low-speed lifting conditions

followed the same trend. However, considering that the moment balance was performed across all three axes of motion (i.e. the calibration method was sensitive to asymmetrical movements), it was not possible to isolate a single physiological rationale for these findings. Nonetheless, it is important to note that the subject-specific common gain factors applied in this study were similar in magnitude to previous research conducted by our group. For example, Beach (2011) reported an average (SD) common gain factor of 1.60 (0.09) using the same musculoskeletal model with ten male participants for a unilateral 12.7 kg lift from the floor to waist height. Marras et al. (1999) also found that high-load, preferred lifting speed and symmetrical lifting trials were associated with, on average, higher gain factors for an EMG-assisted model, from which the authors concluded that high demand exertions (e.g. heavy load or asymmetric posture) involve the cooperative effort of more muscles (Marras et al., 1999). When more muscles are recruited to support the same external moment a lower gain (i.e. adjustment) of the force producing capacity of the muscles is required (Marras et al., 1999).

It is also noteworthy that the fast speed lifting trials were associated with significantly lower cumulative compression with both symmetrical and asymmetrical load placement. However, it would be interesting to see if this trends still holds if the time-varying magnitudes of compressive force at L4/L5 were weighted according to methods that weight the relative force to the predicted ultimate compressive tolerance of the intervertebral joint in the lumbar spine to account for the fact that higher load magnitudes will result in an increased risk of injury (Parkinson & Callaghan, 2007a). Considering that fast movement speed trials in the present study were approximately 68% of the length of those from the controlled speed condition (with similar magnitudes of peak compressive force) it is hypothesized that overall higher joint forces were applied over a shorter duration of time. Previous research conducted by Howarth et al. (2010) has demonstrated that the application of a weighting factor increased estimates of cumulative compression for both male and female participants during simulated occupational lifting; however, since the males loaded their spines to a relatively higher percentage of their predicted compressive strength when lifting/lowering. The effects of weighting instantaneous compressive loads had a greater influence on the resultant (weighted) cumulative load magnitude in males, particularly when a dynamic modeling approach was employed.

A limitation of the present work is that participants' relative position with respect to the load (i.e. horizontal reach), a factor known to significantly influence the magnitude of the external moment of force applied to lumbar spine was not measured (Faber, Kingma & van Dieën, 2011). However, participants were required to keep their feet on both force plates and the load was repositioned to the same position, in one of two locations (i.e. in front of the body or rotated to the side) after every trial. In addition, no efforts were made to scale the anatomical description in the musculoskeletal model to account for inter-individual differences in muscle size (i.e. physiological cross-sectional area), moment arms, or lines-of-action of the 118 muscle fascicles included in the model employed for our analysis. It is also important to acknowledge that the estimates of low back loading presented in this paper are dependent on the amount of adjustment made to the EMG-based force estimates that were used to drive the 118 fascicles included in the musculoskeletal model through the establishment of a common gain factor. It was decided *a priori* that subject-specific average common gain factors would be established for each experimental condition based on the minimization of the total sum of squared differences between instantaneous estimated of the net L4/L5 joint moment derived from the linked-segment model (M_{LSM}) and the equivalent quantity predicted by the EMG-driven musculoskeletal model (M_{EMG}) across all three trials. The rationale for this decision was that a fixed, constant gain across all experimental conditions would diminish the true effect of the three independent factors under investigation. Moreover, the biological fidelity of estimates of low back joint loading from a musculoskeletal model where the net internal forces (i.e. muscular and passive tissue components) do not balance the linked-segment model should be questioned.

3.6 Conclusion

In summary, results from this investigation provide strong evidence that known mechanical low back injury risk factors should not be viewed in isolation. Rather, injury prevention efforts need to consider the complex interactions that exist between external task demands and their combined influence on internal joint loading. Stated differently, the influence of external demands on *in* vivo estimates of joint loading was not additive. Future research efforts should explore whether the trends observed in the present study, where muscle fatigue was minimized, are similar for prolonged, repetitive lifting exposures.

Chapter 4

Study II: Exploring the combined effects of force, repetition and posture on injury pathways in isolated functional spinal units from sub-acute-failure magnitudes of cyclic compressive loading.

4.1 Overview

Study Design: *In vitro* mechanical testing of porcine cervical functional spinal units (FSUs) paired with histological analysis of excised annulus fibrosus (AF) tissue to characterize interactions between known risk factors linked to injury in the lumbar spine.

Background: Previous research suggests that when the magnitude of peak compressive force applied during cyclic loading exceeds 30% of a functional spinal unit's (FSU) estimated ultimate compressive tolerance (UCT), endplate fracture will occur before intervertebral disc (IVD) herniation. However, the amount of tissue damage imposed to the IVD of "survivor" specimens from these investigations remains unknown, as this threshold has been established through the detection of fatigue injury or using radiographic measures used to track the nucleus pulposus through layers of the AF.

Objectives: The primary objective of this study was to explore interactions between: (i) the magnitude of the applied compressive force, (ii) cycle rate and (iii) degree of postural deviation on known fatigue injury pathways in FSUs at sub-acute-failure magnitudes of peak compressive force. The secondary purpose was to characterize the micro-structural damage imposed to the AF in "survivor" specimens using histological staining methods.

Methods: A total of 126 FSUs were initially included in the study. Three levels of peak compressive force (10, 20 and 40% of specimens' UCT), three cycle rates (5, 10 and 30 cycles per minute) and two dynamic postural conditions (100 and 300% neutral zone range; NZ) were examined using a full-factorial design. Cyclic compressive force was applied using a modified material testing apparatus, using a time-varying waveform with synchronous flexion/extension rotation that was based on *in vivo* estimates of lumbar compression and spine posture during an occupation lifting task. All FSUs were cyclically loaded for 5000 cycles or until fatigue failure occurred. AF tissue from 36 "survivor" FSUs was excised for histological analysis across experimental conditions. Three tissue samples,

consisting of the outermost 10 lamellae, were obtained from the anterior and posterior-lateral regions of the IVD from each specimen. To characterize the micro-structural damage in the AF, frozen tissue samples mounted in OCT compound were serially sectioned using a cryostat microtome, H&E stained and visualized with a brightfield microscope linked to a digital camera. Characteristic images of the micro-structural damage were captures at 10X.

Results: Of the 123 specimens that were considered for analysis, 99 (80%) survived 5000 cycles of cyclic compressive loading. Twenty-four FSUs experienced a fatigue related injury, which could be classified into three primary injury pathways: (i) endplate fracture, (ii) avulsion of the superior endplate and (iii) fracture of the pars interarticularis. A marked difference of the magnitude of peak compressive force was noted in the Kaplan-Meier survival function of experimental conditions that induced fatigue injury in less than 5000 cycles, with a higher probability of survival at 20% UCT. Overall, in the 40% UCT load condition, the probability of survival was less than 67%. When considering the representative images across each of the 10 and 20% UCT experimental conditions, it is noteworthy that a qualitative depiction of emerging interactions could be detected. The micro-structural damage detected in excised samples of AF tissue consisted of clefts and fissures within the intra-lamellar matrix, as well as delamination within the inter-lamellar matrix. There was no consistent trend in the amount of damage that was observed between 10% and 20% UCT loading conditions. However, a moderate effect of posture was noted, with increased disruption observed in tissue samples exposed to 300% NZ postural deviation.

Conclusions: Consistent with previous research, our findings support a threshold of peak compressive force of 30% UCT, where cyclic loading above this level is likely to lead to fatigue injury of the cartilaginous endplate in less than 5000 cycles of *in vitro* mechanical loading. However, findings from our histological analyses demonstrate that considerable IVD disruption occurred in specimens that “survived” 5000 cycles of cyclic loading at 10 and 20% UCT. Therefore, it is strongly recommended that future efforts in injury prevention consider more than just the magnitude of the applied load when evaluating risk of low back injury.

Keywords: injury, fatigue, intervertebral disc, survival, histology

4.2 Introduction

Previous epidemiological studies have identified a link between cumulative exposure to mechanical load and the reporting of low back pain and injury (Coenen et al., 2013; Kumar, 1990; Norman et al., 1998; Seidler, 2001; ,2003). As such, numerous *in vitro* studies have been conducted to explore injury pathways in the lumbar spine to cyclic loading (Adams & Hutton, 1983; Brinckmann, Biggemann & Hilweg, 1988; Brinckmann M & Hilweg, 1989; Callaghan & McGill, 2001; Gallagher, Marras, Litsky & Burr, 2005; Hansson, Keller & Spengler, 1987; Howarth & Callaghan, 2013; Liu, Njus, Buckwalter & Wakano, 1983; Parkinson & Callaghan, 2007a; 2008, Gooyers, McMillan, Howarth, & Callaghan, 2012). In particular, since cumulative mechanical exposure is influenced by several factors, including: (i) the magnitude of the applied force, (ii) frequency of repetition (i.e. cycle rate), (iii) duration of the exposure cycle, and (iv) joint posture, each of these factors have been closely studied to examine their influence on injury mechanisms in the musculoskeletal tissue that surround the spine (e.g. vertebrae, intervertebral disc, cartilaginous endplate, ligaments, joint capsule, etc.).

Depending on the loading profile that is adopted for testing, common injury mechanisms linked to cyclic loading in the lumbar spine include: vertebral fracture (Brinckmann et al., 1988; Brinckmann M & Hilweg, 1989; Hansson et al., 1987; Liu et al., 1983), failure of the cartilaginous endplate (Brinckmann M & Hilweg, 1989; Gallagher et al., 2005; Gregory & Callaghan, 2011; Parkinson & Callaghan, 2007a), intervertebral disc (IVD) disruption (e.g. herniation) (Callaghan & McGill, 2001; Tampier et al., 2007) and fracture of the pars interarticularis (Howarth & Callaghan, 2013). Research conducted by Parkinson and Callaghan (2009) has identified that when the magnitude of peak compressive force applied during cyclic loading exceeds 30% of a functional spinal unit's (FSU) estimated ultimate compressive tolerance (UCT), endplate fracture will occur before IVD herniation, as long as the range of dynamic flexion/extension does not exceed the normal physiologic range of the joint. This is consistent with earlier research conducted by Brinckmann et al. (1988), which found that most FSUs could tolerate 5000 cycles of cyclic compressive at loads below 30% UCT. Specifically, the probability of fracture after 5000 cycles for loads between 30 and 40% UCT was approximately 36% (Brinckmann et al., 1988). However, the amount of tissue damage imposed to the IVD of "survivor" specimens from these

investigations remains unknown, as this threshold is limited by the gross radiographic measures that were applied to track the migration of the nucleus pulposus in the IVD (Parkinson & Callaghan, 2009) or sudden changes in specimen displacement during a loading cycle (Brinckmann et al., 1988). This was followed by subsequent analysis of macroscopic damage by cutting through the IVD and inspecting each vertebrae.

Previous investigations (Chan, Ferguson, Wuertz & Gantenbein-Ritter, 2011; Iatridis, MaClean & Ryan, 2005; Kuga & Kawabuchi, 2001; Tampier et al., 2007) have applied histological staining techniques to characterize the magnitude of intervertebral disc disruption from cyclic mechanical loading. For example, research conducted by our own group (Tampier et al., 2007) has shown that hematoxylin and eosin (H&E) was an effective method for characterizing micro-structural damage imposed to the annulus fibrosus (AF) from a repetitive flexion/extension loading protocol that has previously been used to induce herniation (Callaghan & McGill, 2001). Results from this study indicate that the damage imposed to the AF was characterized by the formation of pockets between adjacent lamellae filled with nucleus pulposus material, which resulted in the formation of clefts between collagen fiber bundles within the intralamellar matrix, as well as delamination between adjacent lamellae. However, to the best of the author's knowledge, no study has examined the combined effects of known mechanical risk factors linked to injury (e.g. force, repetition and posture) on the pattern of intervertebral disc disruption using histological techniques paired with *in vitro* mechanical testing of intact FSUs.

Therefore, the primary objective of this study was to explore the combined effects of: (i) the magnitude of the peak compressive force, (ii) cycle rate and (iii) degree of postural deviation on known injury pathways in isolated FSUs at sub-acute-failure magnitudes of peak compressive force (i.e. below 50% estimated UCT). A secondary objective was to characterize the micro-structural damage imposed to IVD in "survivor" specimens using histological methods. In-line with these objectives, it was hypothesized that:

i. the mechanism of injury in isolated FSUs would be different across levels of peak compressive force, cycle rate, and postural deviation;

ii. micro-structural damage would be detected in the AF of specimens that “survived” all 5000 loading cycles; and
iii. differences in the extent of micro-structural tissue damage would be observed across loading conditions (e.g. low repetition, low force vs. high repetition, high force).

4.3 Materials & Methods

4.3.1 Study Design

In vitro mechanical testing of FSUs was conducted and paired with histological analyses of excised annulus AF tissue to characterize interactions between external task demands on known injury pathways in the lumbar spine. Three independent variables, used to simulate a repetitive occupational lifting task were examined, including: (i) magnitude of peak compressive force, (ii) cycle rate and, (iii) degree of postural deviation.

4.3.2 Specimen Preparation

The cervical spines of 63 porcine specimens (mean age = 6 months, weight = 85 kg) were obtained following death and stored at -20°C. Each cervical spine was separated into two FSUs for *in vitro* mechanical testing, which included two vertebrae and the IVD at the c34 and c56 level; resulting in a total of 126 FSUs. This sample size was determined *a priori* ($\alpha = 0.05$, Power = 0.8; N = 126, minimum per group = 7) using the mean and standard deviation in the number of cycles to failure that was observed in the 10 and 30% UCT loading groups using a similar experimental design (Parkinson & Callaghan, 2009). Therefore, 7 FSUs were tested in each of the 18 experimental conditions that were included in the study. Porcine cervical FSUs were used as surrogates for the human lumbar spine due to their anatomical and functional similarities (Oxland et al., 1991; Yingling et al., 1999); providing superior control over potential confounding factors (e.g. age, nutrition, physical activity) that can impact the mechanical integrity of the tissues surrounding the intervertebral joint.

The inclusion criteria required that FSUs met a non-degenerated disc quality (grade 1) as outlined by Galante (Galante, 1967). Before testing, frozen specimens were thawed at

room temperature for a minimum of 12 hours. Dissection of the cervical spine involved isolating the two FSUs of interest (i.e. c34, c56) and carefully removing the surrounding musculature leaving only the osteoligamentous structures intact, except for the portion of the anterior longitudinal ligament that attached to the anterior surface of the AF, which was removed to exposed the IVD for surface measurements (presented in Chapter 5). Once the dissection protocol was complete, width (W) and depth (D) measurements of the two exposed endplates (superior and inferior) were recorded using digital calipers. These measurements were used to estimate the endplate surface area of the intact intervertebral joint using the equation of an ellipse (**Equation 4-1**), which was then used to predict each FSU's UCT (± 11% error) without destructive testing (**Equation 4-2**) (Parkinson, Durkin & Callaghan, 2005). This method enabled normalization of peak compressive loading across specimens.

Equation 4-1

$$A = \frac{\pi}{4} \times \mathrm{W} \times \mathrm{D}$$

where:

A	=	*estimate of intervertebral joint surface area (mm^2)*
W	=	*average width of superior and inferior exposed endplates (mm)*
D	=	*average depth of superior and inferior exposed endplates (mm)*

Equation 4-2

$$CS = 0.65470 + (0.01361 \times A)$$

where:

CS	=	*estimated compressive strength of FSU (kN)*
A	=	*estimate of intervertebral joint surface area (mm^2)*

Before mounting each FSU for testing, the anterior processes and exposed facets (on the superior and inferior aspect of the FSU) were trimmed to ensure the exposed cartilaginous endplates were responsible for load carriage at the interfaces with the testing system. Next, the FSU was fixed within custom-machined aluminum cups using a combination of wood screws (fixed approximately 1 cm into the centre of the exposed endplates) and non-exothermic dental plaster (Denstone; Miles, Southbend, IN, USA). To prevent specimen dehydration throughout the dissection and potting procedures, all FSUs were misted with a saline solution (0.9 % weight per volume) approximately every 15 minutes.

4.3.3 Procedure

The potted specimens were then mounted in a servo-hydraulic materials testing system (Model 8872; Instron, Canton, MA, USA) that has been modified to apply flexion/extension rotations to FSUs under compressive load. The testing jig was designed to allow the centre of rotation to be aligned (vertically and horizontally) with the geometric centre of the IVD (Callaghan & McGill, 2001). Each specimen was free to translate in the anterior-posterior and medial-lateral direction (via a bearing tray), which enabled the centre of rotation to translate within the joint during loading. To minimize dehydration during mechanical testing, FSUs were wrapped in saline soaked gauze.

Each FSU initially received 15 minutes of static compressive force (300 N) to counter any postmortem swelling that occurred within the IVD (Callaghan & McGill, 2001). This load has previously been identified to equilibrate specimen height, without inducing excessive creep over a period of 15 minutes (Callaghan & McGill, 2001). During this preload test, an independent brushless servomotor (AKM23D; Kollmorgen/Danaher Motion, Radford, VA, USA) connected in-series with a torque cell (T120-106-1K; SensorData Technologies Inc., Sterling heights, MI, USA) was used to establish the angular position of minimal stiffness (Nm/degree) about the flexion/extension axis. Following the preload test, three cycles of passive flexion-extension (PFE) joint rotations were applied (0.5° per second) to identify the limits of each FSU's flexion/extension neutral zone. Using custom software, interfaced with an ISA bus motion controller (Model DMC18x0, Galil Motion Control, Rocklin, CA USA), the

applied moment (Nm) and angular displacement (degrees) were sampled at 25 Hz. The flexion and extension limits of the neutral zone were identified using methods described by Thompson et al. (2003); whereby the first-derivative of a fourth-order polynomial fit to moment-angle data from the last two loading cycles was used to detect the angular displacement where this function deviates from linear. These neutral zone limits were used to establish the dynamic range of flexion/extension rotation that was applied during cyclic testing (**Figure 4-1**).

Upon completion of both the preload and PFE tests, specimens were randomly assigned to 1 of 18 experimental conditions (7 FSUs per group) to examine the combined effects of: (i) the magnitude of the applied compressive force, (ii) cycle rate, and the (iii) magnitude of postural deviation on injury pathways in isolated FSUs. Three levels of peak compressive force (10, 20 and 40% of specimens' ultimate compressive tolerance; UCT), three cycle rates (5, 10 and 30 cycles per minute) and two dynamic postural conditions, including: (i) 100% neutral zone range; average (SD) of 6.79° (2.23) and (ii) 300% neutral zone range; 20.52° (4.41), were examined using a full-factorial design. The 100% neutral zone postural condition was intended to represent a lifting technique with sound mechanics (i.e. minimal spine motion), whereas the 300% condition was designed to bring the isolated joint to the end of its natural physiological range (i.e. where the passive rotational stiffness begins to deviate from linear). Compressive force was applied in accordance with a biofidelic, time-varying waveform (two-seconds duration) that was based on the *in vivo* estimate of compressive loading in the lumbar spine during an occupation lifting task using a dynamic EMG-assisted musculoskeletal model (similar to Chapter 4). The applied compressive force was scaled to run from a minimum of -0.001 N to the desired peak load (i.e. 10, 20, and 40% of each FSU's predicted UCT). Similar to research conducted by Parkinson and Callaghan (2009), dynamic flexion/extension was synchronously applied during each loading cycle using a motion profile recorded from the lumbar spine during the same floor to waist height lift, and was scaled for each posture condition to 100 and 300% of the specimens' neutral zone range (**Figure 4-2**). However, it is important to note that the applied compressive force is not the load that is experienced across the intact vertebral

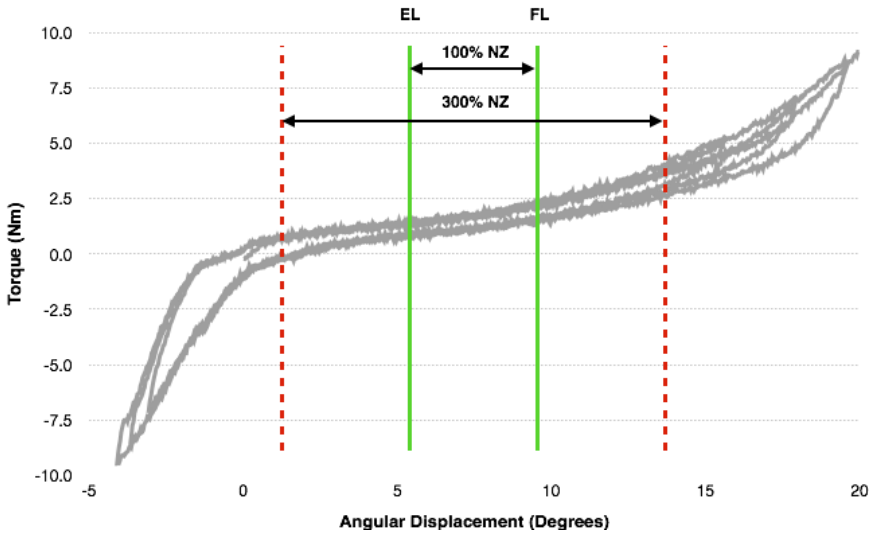

Figure 4-1: Sample passive flexion/extension test.

Note: NZ = neutral zone; FL = Flexion Limit; EL = Extension Limit

joint, except in a neutral posture (i.e. 0°); as this force is partitioned into compressive and shear components through the testing jig.

All FSUs were cyclically loaded for 5000 cycles or until failure occurred, which was identified by specimen height loss greater than 9 mm (Parkinson & Callaghan, 2009). Throughout testing, measurements of the applied compressive force (kN) and vertical position (mm) of the Instron actuator were sampled at 32 Hz using a 16-bit analog-to-digital conversion board (National Instruments, Austin, TX, USA), which enabled post-test determination of the exact loading cycle in cases of where endplate/bone failure occurred. The exact fracture cycle was identified by a change in average cycle compressive stiffness (kN/mm), calculated using single cycle displacement measures at the instance of peak loading (Parkinson & Callaghan, 2007a), as well as a precipitous drop in specimen height (Brinckmann M & Hilweg, 1989; Hansson et al., 1987; Parkinson & Callaghan, 2007) and concomitant change in the applied sagittal-plane torque (**Figure 4-3**).

Upon completion of the mechanical testing protocol, AF tissue from 36 randomly selected “survivor” FSUs (18 c34, 18 c56; two per experimental condition) was excised for histological analysis. Three tissue samples (4 x 4 mm), consisting of the outermost 10 lamellae (approximately 2 mm thick) were obtained from both the anterior and posterior-lateral regions of the IVD (6 total) from each specimen. Each sample was embedded in

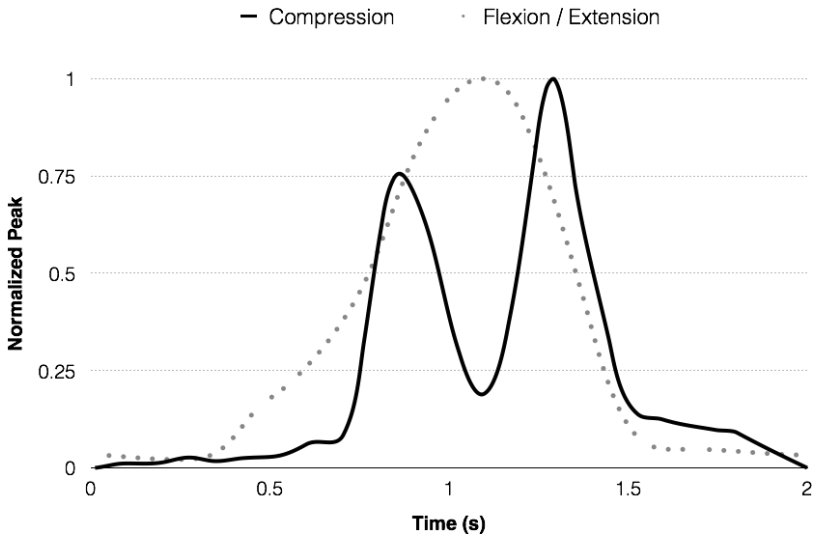

Figure 4-2: Time-varying compression waveform with synchronous flexion/extension that was used for cyclic testing.

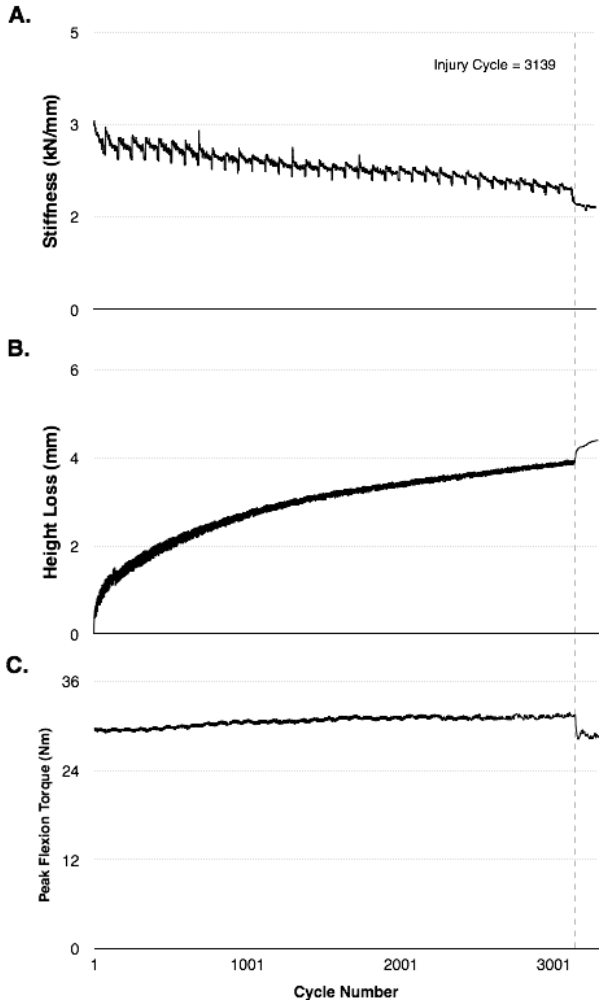

Figure 4-3: Fatigue failure of the cartilaginous endplate identified from single cycle measurements of: (A) compressive stiffness, (B) specimen height loss and (C) peak sagittal-plane torque.

Tissue-Tek OCT (Optimum Cutting Temperature; Sakura Finetek, Torrance, CA, USA) compound and then rapidly frozen in liquid nitrogen and stored at -80°C until sectioning.

4.3.4 Histological Analyses

To characterize the micro-structural damage in the AF, frozen tissue samples mounted in OCT compound were serially sectioned in the frontal and transverse planes using a cryostat microtome. A total of 54 tissue sections from each specimen, obtained from the anterior and posterior-lateral regions of the IVD (in each plane) were mounted onto Vectabond coated (Vector Laboratories, Burlingame, CA, USA) glass microscope slides and air dried for five minutes. Eighteen 10 μm sections were cut from the superficial (9 anterior, 9 posterior-lateral) and deep layers (9 anterior, 9 posterior-lateral). An additional 18 sections were cut in the transverse plane across all layers of the sample (9 anterior, 9 posterior-lateral). The sections were then stained with hemaetoxylin and eosin (H&E) and visualized using a brightfield microscope (Nikon Instruments Inc., Melville, NY, USA) linked to a digital camera (PixeLink, Ottawa, ON, Canada).

The H&E staining protocol consisted of: (i) immersing each tissue section in hemaetoxylin for 60 seconds, (ii) rinsing the glass microscope slide in tap water (10x, repeated 1-second submersion), (iii) counter-staining with eosin for 90 seconds, (iv) 5x, 1-second submersion in 70% ethanol, (vi) 5x, 1-second submersion in 95% ethanol, (vii) 5x, 1-second submersion in 100% ethanol (viii) 5x, 1-second submersion in Xylene. Lastly, the tissue sections were air-dried and mounted in Permount (Fischer Scientific Co., Fair Lawn, NJ, USA) with a #2 coverslip. Characteristic images from each specimen were captured at 10X magnification (2048 x 1536 RGB image resolution) using Image-Pro Plus analysis software (Media Cybernetics, Silver Spring, USA).

A full-factorial qualitative analysis of micro-structural damage was assessed across: (i) magnitude of peak compressive force (10% UCT, 20% UCT), (ii) cycle rate (5, 10 and 30 cycles per minute), (iii) degree of postural deviation (100% vs. 300% NZ range) and (iv) radial location on the IVD (anterior vs. posterior-lateral). Since the cyclic loading protocol was not immediately stopped when an endplate fracture occurred, it was not possible to

conduct controlled histological comparisons of the disruption imposed to the IVD across specimens assigned to the 40% UCT loading conditions since they were exposed to a different number of loading cycles and cumulative compression. Unfortunately, evidence of non-physiological freezer damage emerged in some stained tissue sections, potentially due to post-mortem freezing and/or flash freezing in OCT compound with liquid nitrogen. This damage was characterized by a circular pattern of disruption in the intra-lamellar matrix and if present the specimen was excluded from our analysis. Tissue samples from three specimens were excluded, including: (i) c34, 10% UCT, 5 cycles per min., 300% neutral zone, (ii) c34, 10% UCT, 30 cycles per min., 300% neutral zone, and (iii) c34, 20% UCT, 10 cycles per min., 100% neutral zone.

4.3.5 Statistical Analyses

All statistical analyses were computed using SAS software (version 9.2, SAS Institute Inc., Cary, NC) with a significance level (α) of 0.05 set *a priori*. Specimen randomization was assessed using a three-way (force, cycle rate and postural deviation) general linear model (GLM) to test for group differences in the estimated endplate area (mm^2) of the intact joint or neutral zone range (degrees) across experimental conditions. The Kaplan-Meier estimator was used to estimate the survival function for each experimental condition (Kaplan & Meier, 1958).

4.4 Results

4.4.1 Specimen Randomization

Successful randomization across experimental conditions was achieved, as no significant main effects of force, cycle rate or postural deviation were revealed in estimates of endplate area ($p > 0.3104$) or neutral zone range ($p > 0.6744$). Interestingly, there were also no significant differences in estimates of endplate area or neutral zone range between failed specimens compared with those that survived the cyclic mechanical exposure (endplate area: $p = 0.3065$; neutral zone range: $p = 0.6525$). Due to technical difficulties in synchronizing the cyclic compressive load with the flexion/extension axes, three FSUs were excluded from the analyses presented, resulting in a total of 123 specimens.

4.4.2 Fatigue Injury

Of the 123 specimens that were considered for analysis, 99 (80%) survived 5000 cycles of cyclic compressive loading. Twenty-four FSUs experienced a fatigue-related injury, which could be classified into three primary injury pathways: (i) endplate fracture (**Figure 4-4A**), (ii) avulsion of the superior cartilaginous endplate on the anterior border of the vertebrae (**Figure 4-4B**) and (iii) fracture of the pars interarticularis (**Figure 4-4C**). A summary of the distribution of all 24 specimens across each injury mechanism is provided in **Table 4-2**. Interestingly, 23/24 (96%) of the fatigue related injuries occurred in the 40% UCT experimental conditions. There were no fatigue injuries observed in the 10% UCT group and only one FSU (c56; 10 cycles per minute, 300% neutral zone range) underwent a fracture of the pars interarticularis in the 20% UCT condition. Half of all fatigue-related injuries (12/24) were endplate fractures, of which 11 occurred in the superior vertebrae. Although there were 8 avulsions of the superior endplate, this mechanism of failure only occurred in the 300% neutral zone range conditions. When analyzed by cycle rate, it is noteworthy that half (12/24) of all fatigue injuries were observed in the 5 cycles per minute condition, compared to only 4 (17%) when the cycle rate was 30 repetitions per minute.

4.4.3 Survival Analysis

A marked difference in the magnitude of peak compressive force was noted in the survival function between experimental conditions that induced fatigue injury in less than 5000 cycles, with a higher survivorship at 20% UCT (**Figure 4-5)**. However, within the 40% UCT group there were no detectable differences across cycle rate and posture conditions - depicted by several intersections in the survival functions. It is noteworthy that across all 40% UCT loading groups, the probability that specimens will survive 5000 cycles of cyclic compressive loading is below 67% (highest for 10 cycles per minute at 100% neutral zone range: 67% and lowest for 5 cycles per minute at 100% neutral zone range: 0%).

4.4.4 Histological Analyses

The micro-structural damage observed in excised samples of AF tissue consisted of clefts and fissures within the intra-lamellar matrix, as well as delamination within the inter-lamellar matrix. Representative images (captured at 10x) of the disruption observed in the intra-lamellar matrix from the anterior and posterior-lateral regions of the IVD are presented in **Figures 4-6** and **4-7** respectively. Damage observed between layers in the AF (i.e. inter-lamellar matrix; sectioned in the transverse plane) is depicted in **Figure 4-8**. There was no consistent trend in the amount of damage that was observed between 10% and 20% UCT loading conditions. However, a noticeable effect of posture was observed across some conditions, with increased damage in tissue samples from the 300% NZ range condition. Tissue samples excised from the posterior-lateral region were also found to have more disruption (i.e. clefts, fissures, etc.), in comparison to those excised from the anterior region of the IVD. Similarly, more disruption was observed in sections that were obtained from deeper layers of the IVD, compared to those obtained from the superficial portion of the AF.

When considering the representative images across each of the 10 and 20% UCT experimental conditions, it is noteworthy that a qualitative depiction of emerging interactions could be detected. For example, in the representative images from tissue samples harvested from the anterior region of the IVD, comparable micro-structural damage can be seen in superficial layers from specimens assigned to the 20% UCT force condition at 5 cycles per minute (300% neutral zone) to those in the 10% UCT force condition at 30 cycles per minute (300% neutral zone). Moreover, in the representative images from tissue samples harvested from the posterior-lateral region of the IVD, comparable micro-structural damage can be seen in superficial layers from specimens assigned to the 10% UCT force condition at 5 cycles per minute (300% neutral zone) to those in same 10% UCT force condition but applied at 30 cycles per minute (100% neutral zone). Lastly, when examining differences in the amount of the damage imposed to the inter-lamellar matrix (i.e. between layers), it is interesting that comparable damage is observed in tissue samples excised from the posterior-lateral region in samples assigned to the 20% UCT force group at 5 cycles per

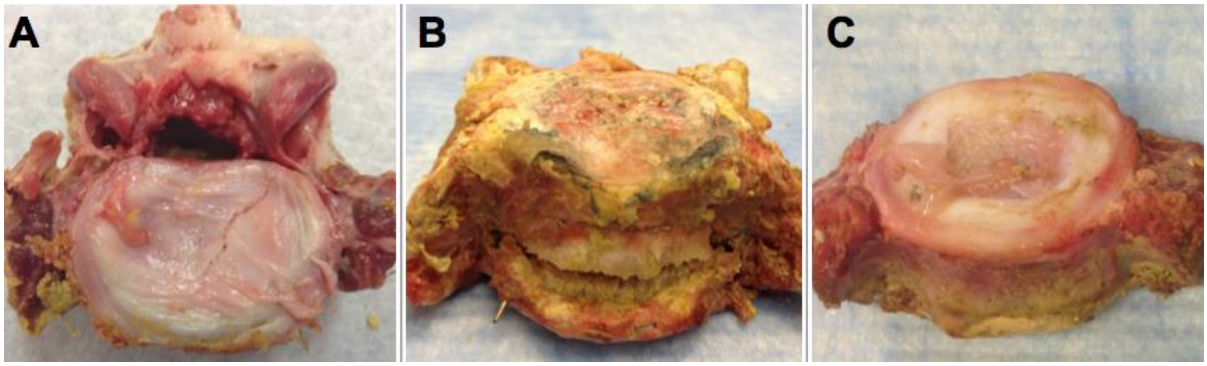

Figure 4-4: Classification of fatigue failure injury mechanisms: (A) Cartilaginous endplate fracture, (B) Avulsion of the superior endplate, (C) Fracture of pars interaticularis (posterior elements removed).

Table 4-1: Distribution of functional spinal units (FSUs) across experimental conditions, with group average endplate area and neutral zone (NZ) range of motion.

Force	Cycle Rate (per min.)	Postural Deviation (%NZ)	Endplate Area (mm^2)		Neutral Zone Range (degrees)		Number of FSUs		
			Mean	SD	Mean	SD	C34	C56	N =
10	5	100	754.78	88.70	6.58	2.46	3	3	6
10	5	300	727.19	55.44	7.07	1.64	4	3	7
10	10	100	704.92	76.56	7.00	1.61	4	3	7
10	10	300	729.94	36.46	7.07	1.48	3	4	7
10	30	100	713.90	35.85	5.57	1.64	3	4	7
10	30	300	708.43	42.92	6.50	1.44	4	3	7
20	5	100	733.82	52.80	7.29	3.77	4	3	7
20	5	300	725.08	62.49	7.00	1.04	3	4	7
20	10	100	720.80	60.07	6.29	0.70	3	4	7
20	10	300	734.00	34.57	6.43	1.17	3	3	6
20	30	100	758.96	36.46	7.21	2.91	4	3	7
20	30	300	740.83	45.36	7.43	1.74	3	4	7
40	5	100	731.04	87.16	6.64	1.25	3	4	7
40	5	300	750.76	27.18	7.07	1.17	4	3	7
40	10	100	722.97	38.46	7.00	2.68	3	3	6
40	10	300	751.90	77.57	7.07	1.88	3	4	7
40	30	100	666.53	61.86	7.14	1.25	3	4	7
40	30	300	744.70	50.75	6.21	1.52	4	3	7
Total							61	62	123

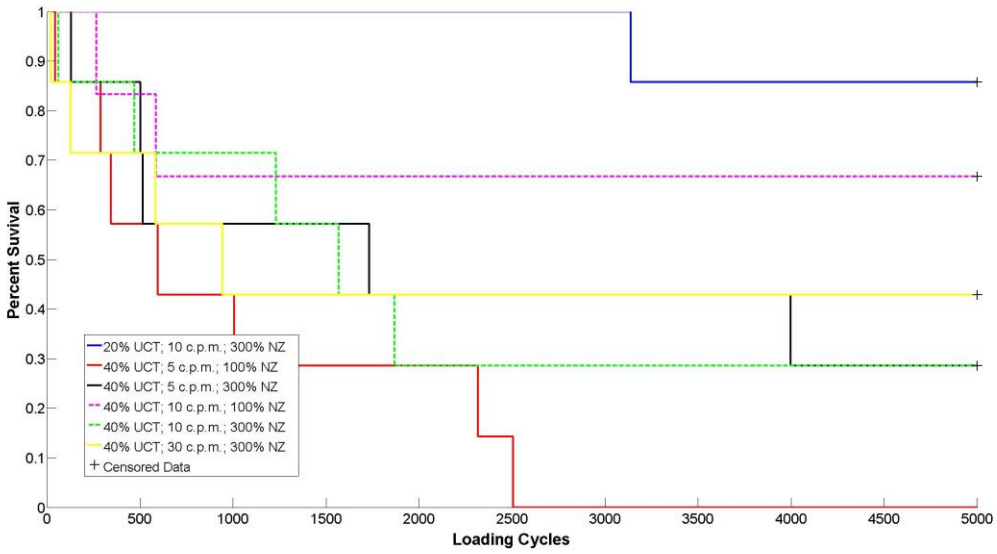

Figure 4-5: Kaplan-Meier survival analysis across cyclic loading conditions that induced fatigue injury. Note that the survival function of all other experimental conditions (not shown on the graph) would be a horizontal line with a y-intercept equal to 1.

Table 4-2: Distribution of fatigue injury across experimental conditions.

Force (%UCT)	**Repetition** (Cycles / min.)	**Posture** (% NZ)	**Injury Frequency**				**Total**
			EF	EA	PF	M	
20	10	300			1		1
40	5	100	7			7	7
40	5	300		3			5
40	10	100	2			2	2
40	10	300	2	2	1	2	5
40	30	100					0
40	30	300	1	3		1	4
	Total		12	8	2	12	24

Note: EF = Endplate Fracture EA = Endplate Avulsion PF = Pars Fracture M = Mixed; combination of EF & EA

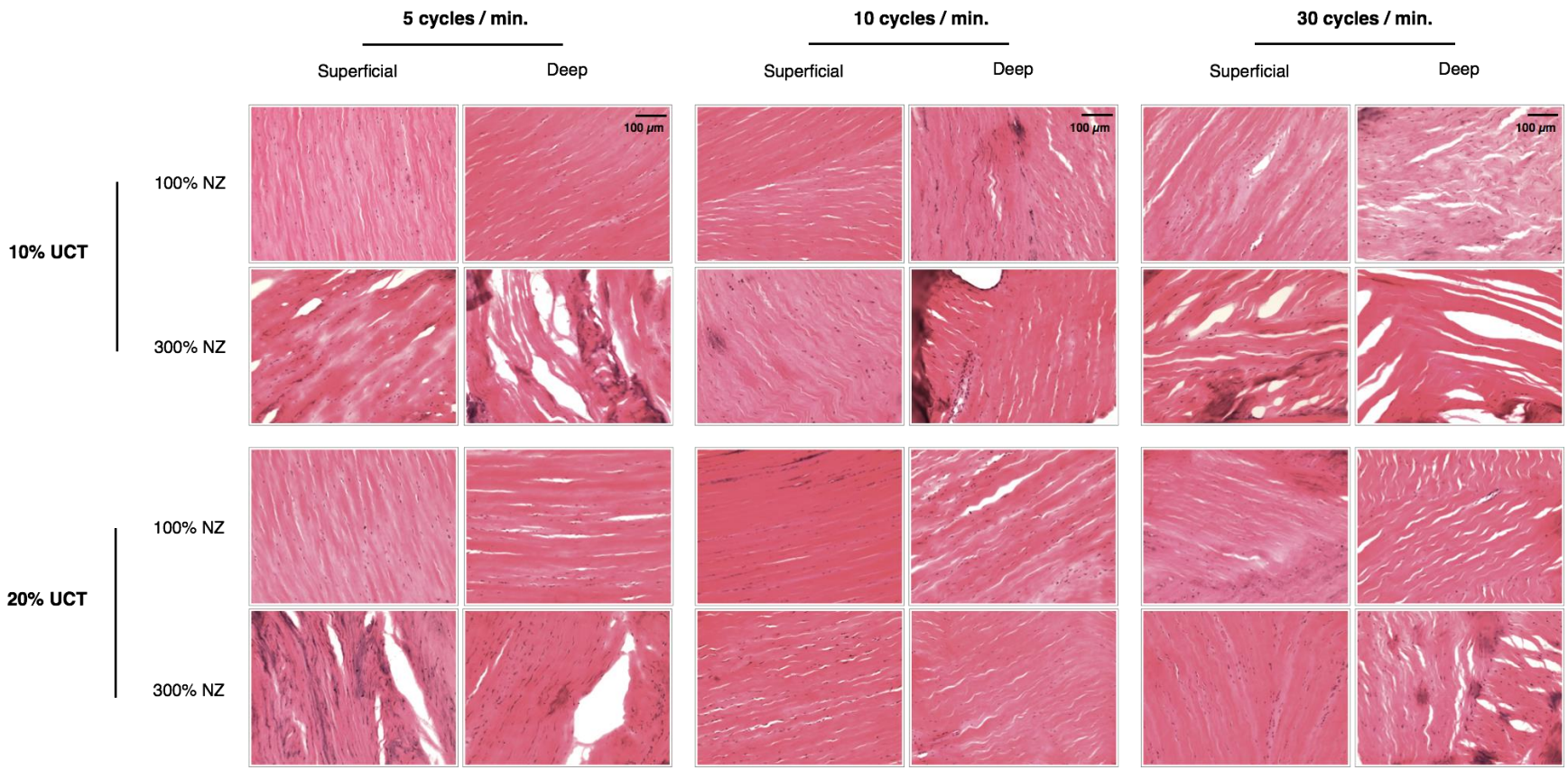

Figure 4-6: Representative images of micro-structural damage in excised samples of annulus fibrosus tissue from the anterior region of the intervertebral disc (sectioned in the frontal plane) across experimental conditions.

Note: UCT = ultimate compressive tolerance NZ = neutral zone

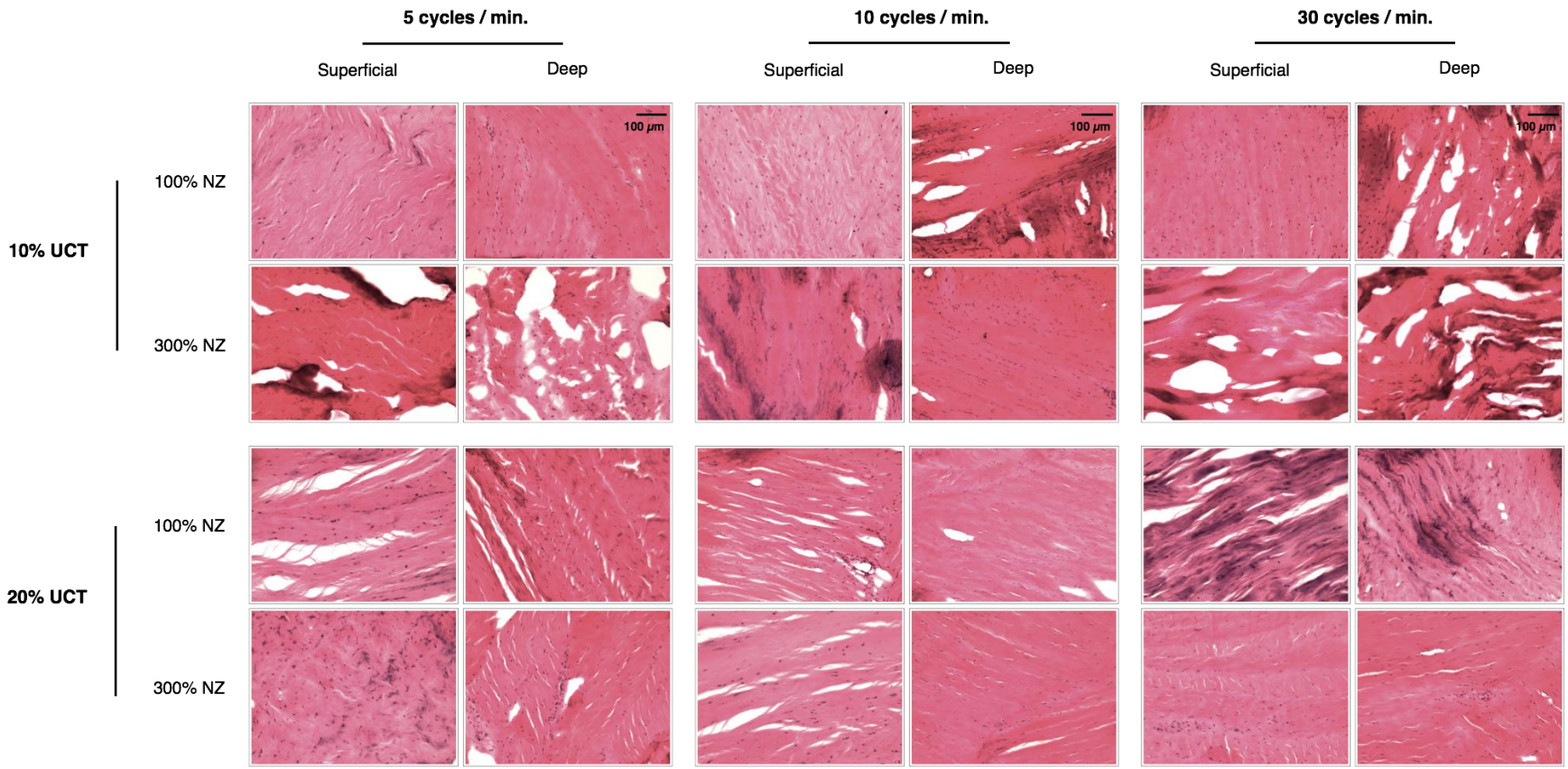

Figure 4-7: Representative images of micro-structural damage in excised samples of annulus fibrosus tissue from the posterior-lateral region of the intervertebral disc (sectioned in the frontal plane) across experimental conditions.

Note: UCT = ultimate compressive tolerance NZ = neutral zone

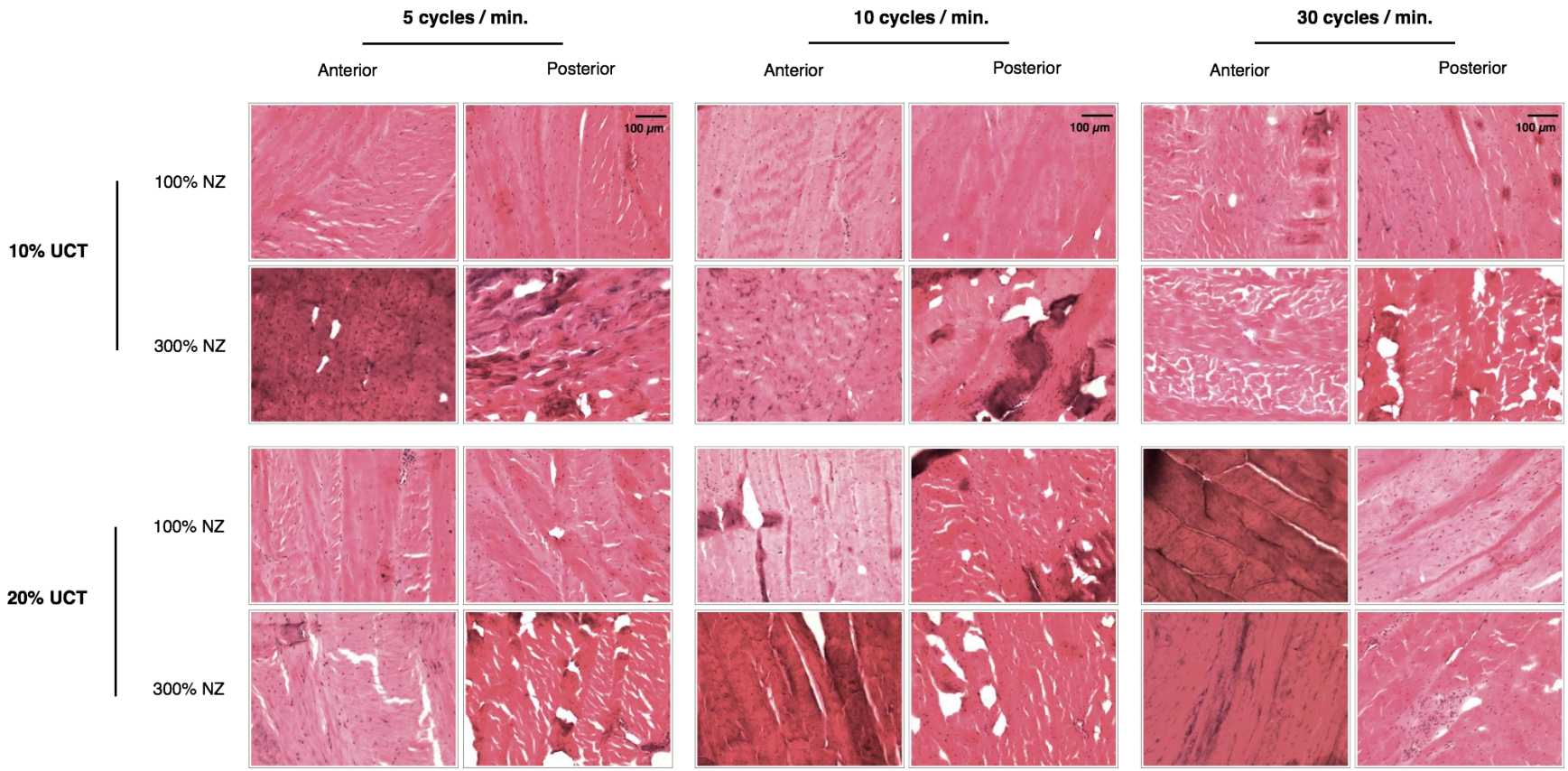

Figure 4-8: Representative images of micro-structural damage in excised samples of annulus fibrosus tissue of the intervertebral disc (sectioned in the transverse plane) across experimental conditions.

Note: UCT = ultimate compressive tolerance NZ = neutral zone

minute (300% neutral zone) to those assigned to the 10% UCT force group at 30 cycles per minute (300% neutral zone).

4.5 Discussion

Consistent with our hypothesis, the mode of specimen failure was different across levels of peak compressive force, cycle rate, and postural deviation (e.g. specimens assigned to 300% neutral zone condition experienced either endplate avulsion or pars fracture before endplate fracture). Despite the fact that 99/123 specimens "survived" 5000 cycles of cyclic compressive loading, synchronously paired with dynamic flexion/extension", there was considerable micro-structural damage observed in the AF. Interestingly, the magnitude of postural deviation was found to have the greatest influence on the amount of disruption imposed to the annulus fibrosus. Findings from this work underscore the need for future injury prevention efforts to consider more than just the magnitude of the applied load (i.e. force) when evaluating potential risk of injury.

Considering some of the practical applications of this work, it is interesting to note that the only biomechanical consideration in the revised NISOH lifting equation (Waters et al., 1993) is at low cycle rates, where the recommended weight limit (RWL) of 23 kg was intended to limit the magnitude of lumbosacral stress below a threshold of 3400 N (i.e. NIOSH action limit). However, the frequency multiplier (used to discount the RWL) at higher cycle rates was predominantly based on the synthesis of psychophysical (up to 4 lifts per minute; Snook & Ciriello, 1991) and physiological literature (e.g. energy expenditure prediction equations developed by Garg & Banaag, 1988). Unfortunately, there is currently no consideration for the effect of improper lifting mechanics (e.g. if worker adopts a flexed lumbar spine) and the accumulation of micro-damage that can occur in the IVD with repetitive loading. Previous research (Dempsey, McGorry & Maynard, 2005) has shown that the revised NIOSH lifting equation is an analysis tool that is widely adopted by Certified Professional Ergonomists, with approximately 83% of respondents having reported using the tool and almost 28% of those users at a frequency of once per month. However, earlier research published by the same author (Dempsey, 2003) reporting on a sample of 547 industrial lifting tasks has shown that the 50th and 90th percentile lifting frequency was 1 and 8 lifts per minute, respectively. In other words, there is minimal consideration for any

biomechanical criterion for the upper 50% of all repetitive lifting tasks in industry. Nonetheless, findings from this work suggest that consideration for lifting technique (i.e. maintaining a neutral spine posture) may be more effective in preventing low back injury for repetitive lifting tasks, since our histological data show that considerable IVD disruption was observed at low magnitudes of compressive loading with cyclic deviated posture.

It should also be noted that to isolate differences in the magnitude of the applied load, while keeping cycle rates consistent and maintaining the same cumulative load within each force group, it was necessary to alter the rates of loading and unloading during each two-second loading cycle. The largest difference in loading rate was between the 40% and 10% UCT experimental conditions, with the 40% loading rate being four times greater. However, previous research published by Yingling et al. (1997) has demonstrated that differences in the UCT of porcine cervical FSUs between these conditions was rather small. Although, a notable change in stiffness and total displacement to failure was observed in the Yingling et al. (1997) study, with significantly greater stiffness and reduced displacement at failure in the 4000 N/s condition (i.e. 40% UCT). Moreover, differences in movement speed occurred between the 100 and 300% NZ posture conditions.

The frequency of macroscopic fatigue injury observed across each of the different experimental conditions is consistent with previous research. As an example, using a similar loading protocol Parkinson and Callaghan (2009) showed that when the magnitude of peak compressive force exceeded 30% of a FSU's estimated UCT, endplate fracture will occur before IVD herniation. Although specimens included in this study were exposed to a maximum of 21,600 cycles (cycle length = 2 seconds, applied at 0.5 Hz for a maximum of 24 hours) with a baseline 300 N of static compressive force, the average (SD) injury cycle for the 10% and 30% UCT groups were 14,400 (6859) and 5031 (3944), respectively; with no significant differences in the cumulative compression to failure. This is in agreement with the results from the present study with only one fatigue injury documented in the 20% UCT group (after 4303 cycles). Moreover, our findings support previous recommendations that at loads below 30% UCT, most specimens will tolerate 5000 load cycles without fracture (Brinckmann M & Hilweg, 1989). In 2005, Gallagher et al. performed an *in vitro* biomechanics study to simulate the lifting of a 9-kg load initiated at three torso flexion angles

and characterize its effect on the fatigue failure response of lumbosacral motion segments loaded at a cycle rate of 0.33 Hz for 10,200 cycles (Gallagher et al., 2005). Results from this study demonstrated the dramatic impact of spinal posture on the fatigue life of FSUs. In particular, specimens that were loaded in the 0 degree condition averaged 8,253 cycles to failure, whereas those assigned to the 22.5 and 45 degrees flexion conditions, failed at 3,257 and 263 cycles, respectively (Gallagher et al., 2005).

Previous research has demonstrated the AF is effective at resisting failure because its laminate structure is robust to crack propagation and requires multiple cracks and micro-failure to accumulate before ultimate failure occurs (Iatridis & Gwynn, 2004). Failure mechanisms in a single layer of a composite structure include fiber failure and propagation of fiber failure with fiber pullout from longitudinal tension, matrix cracking from transverse tension, and fiber buckling from longitudinal compression (Iatridis & Gwynn, 2004). Multiple failure mechanisms may be present within a layer, depending on the history of stresses applied and number of loading cycles. On the laminate level (i.e. multiple layers), these micro- mechanisms result in transverse cracks in planes parallel to the fibers, fiber dominated failures in planes perpendicular to the fibers, and delamination between layers of the laminate (Iatridis & Gwynn, 2004).

When considering the distribution and type of injuries that were documented in this study, a significant effect of postural deviation was found. Specifically, specimens exposed to dynamic flexion/extension to a range of 300% of their neutral zone experienced either a fracture of the pars interarticularis of the superior vertebrae or avulsion of the superior endplate (i.e. separation of the endplate from the vertebral body). A known mechanism for fatigue fracture of the pars interarticularis (i.e. neural arch) is repetitive hyperextension (Standaert & Herring, 2000). Similarly, avulsion of the cartilaginous endplate at the anterior border of the vertebrae has been linked to forceful hyperextension (Denis & Burkus, 1992). However, it should be acknowledged that the porcine FSUs included in the study were skeletally immature (mean age = 6 months) and that previous research using the same porcine animal model has noted endplate avulsion injuries with cyclic compressive loading (Tampier et al., 2007). Yingling et al. (1999) also noted a similar mechanism of injury with compression loading at high load rates, which was attributed to weak bony attachment of

the annulus to the vertebral body compared to the strength of the collagenous fibers of the annulus, which ultimately lead to rupture of the annulus-bone interface (Yingling et al., 1997). Therefore, since it is likely that the cartilaginous endplate has not yet fully fused to the vertebral bodies it is possible that the specimens tested may have been at an increased risk for this injury, although this mechanism of failure was only observed in the 300% neutral zone range posture conditions with peak compressive loads of 40% UCT.

Consistent with previous research (Tampier et al., 2007), increased intervertebral disc disruption was noted in AF tissue samples excised from the posterior-lateral region of the IVD compared to those from the anterior region. Similarly, samples obtained from the deeper layers of the annulus fibrosus were found to have increased damage compared to those that were dissected more superficially. Clefts and fissures within the intra-lamellar matrix and the delamination between adjacent lamellae were characteristic of this damage. A qualitative depiction of emerging interactions between the magnitude of the applied load, cycle rate and postural deviation could be observed among the representative images from specimens that were assigned to each experimental condition. Interestingly, our histological findings closely match the mechanism of damage that was presented by Pezowicz et al. (2006) who employed excessive intradiscal pressure to induce disruption to the annular wall. However, recent work conducted by our group (Noguchi, 2013) has provided evidence that excessive intradiscal pressure is likely not the sole mechanism for AF failure, as we observed, on average, a 62% decrease in intradiscal pressure with a 45% decrease in height using a similar bore-screw insertion technique after one hour of cyclic loading. However, it is interesting to note that the rate that maximum and minimum pressure decrease were different, resulting in an increase in the range of intradiscal pressure occurring within a loading cycle (Noguchi, 2013).

To the authors' knowledge, this investigation represents one of the first efforts to pair *in vitro* biomechanical testing with histological staining methods to characterize the combined influence of various exposure variables that have previously been linked to low back injury (i.e. force, repetition and posture). However, there are a several potential limitations that should be addressed. First, it should be acknowledged that the application of the findings from this study are limited by the choice of using porcine cervical FSUs,

combined with the absence of any physiological repair mechanisms, as seen *in vivo*. However, previous research has confirmed anatomical and functional similarities (Oxland et al., 1991; Yingling et al., 1999) between the porcine cervical spine and the human lumbar spine; providing superior control over potential confounding factors (e.g. age, nutrition, physical activity) for *in vitro* biomechanics studies. Although the repair processes initiated by micro-damage in living tissues cannot be simulated in an *in vitro* experiment, previous *in vitro* research has contended that the 5000 loading cycles included in our study may easily accumulate *in vivo* within two weeks of manual work or industrial exposure (Brinckmann et al., 1988). Moreover, Lotz et al. (1998) have demonstrated that murine intervertebral discs exposed to one week of static compression failed to fully recover one month after the loading protocol was ceased. This suggests that the accumulation of damage would exceed the rate of repair in both the IVD and cartilaginous endplate for the accelerated loading protocol that was examined in the present study. The results presented in this study are also limited by the non-destructive method (average error = 11%) that was used to approximate the UCT of FSUs included in the study, which is based on approximating the intact intervertebral joint surface area using the equation of an ellipse to estimate failure force (Parkinson et al., 2005). This approach may not be suitable for human specimens, where a wide range of bone mineral density in the lumber vertebrae would be expected.

4.6 Conclusion

Consistent with previous research, our findings support a threshold of peak compressive force of 40% UCT, where cyclic loading above this level will likely lead to fatigue injury of the cartilaginous endplate in less than 5000 cycles of *in vitro* mechanical loading. However, results from our histological analyses show that considerable IVD disruption occurred in specimens that “survived” 5000 cycles of cyclic loading at 10 and 20% UCT. Current efforts are underway to quantify differences in the amount of micro-structural damage across experimental conditions (e.g. size of clefts, density of disruption, etc.). Collectively, our findings suggest that future injury prevention should consider more than just the magnitude of the applied force when evaluating risk of low back injury (i.e. the technique employed for lifting should also be considered).

Chapter 5

Study III: Exploring interactions between force, repetition and posture on intervertebral disc height loss and bulging in isolated functional spinal units from sub-maximal cyclic compressive loading.

5.1 Overview

Study Design: *In vitro* mechanical testing of FSUs paired with pre/post surface profile scans of the anterior surface of the IVD using a 3D laser scanner to characterize changes in IVD height loss bulging of the AF across loading conditions.

Background: Most *in vitro* studies are limited in the ability to partition intervertebral disc (IVD) height loss from total specimen height loss since the net changes in the actuator position of the materials testing system used for testing simply reflect net changes to the entire osteoligamentous system of FSUs used for testing. Moreover, previous research conducted to characterize changes in IVD bulging has been limited to static compressive loading for 15 minutes or less.

Objectives: To explore interactions between: (i) the magnitude of the applied compressive force, (ii) cycle rate and (ii) degree of postural deviation on IVD height loss, as well as pre/post changes in annulus fibrosus (AF) bulging in order to better understand the structural changes that occur in the IVD under cyclic loading conditions.

Methods: A total of 99 porcine cervical FSUs were included in the study. Three levels of peak compressive force (10, 20 and 40% UCT), three cycle rates (5, 10 and 30 cycles per minute) and two dynamic postural conditions (100% and 300% of specimens' neutral zone range) were examined using a full-factorial design. Compressive force was applied using a time-varying waveform based on estimates of *in vivo* loading using a dynamic EMG-assisted model of the lumbar spine during a floor to waist height lift, which was synchronous paired with dynamic flexion/extension. All FSUs were cyclically loaded for 5000 cycles or until fatigue failure occurred. Surface scans from the anterior aspect of the IVD were recorded in a both a neutral and flexed posture before and after the cyclic loading protocol using a 3D laser scanning device. The peak anterior bulge of the AF at the midline of the IVD in the frontal plane was computed from the 3D surface profiles, pre/post testing. To facilitate the comparison of AF bulging measurements between specimens and improve the anatomical

interpretation of this measure, the maximum anterior bulge perpendicular to a vector defined by the endpoints of the superior and inferior endplates has been reported.

Results: A significant three-way interaction (p = 0.0092) between the magnitude of peak compressive force, cycle rate and degree of postural deviation was observed in cycle-varying specimen height loss data. However, a significant main effect of peak compressive force (p=0.0003) was observed in IVD height loss obtained from the 3D surface profiles, pre/post testing. A wide range of Pearson product-moment correlation between total specimen height loss and IVD height loss (r = -0.54 to 0.95) was observed across experimental conditions, with the relative contribution of IVD height loss to total specimen height loss, ranging from 19 to 58%. Significant main effects of postural deviation (p=0.0016) and time (p=0.0423) were observed in peak measures of AF bulging. A wide range of Pearson product-moment correlation was also observed (r = -0.44 to 0.78) between IVD height loss and IVD bulging across experimental conditions.

Conclusions: This investigation provides evidence that total specimen height loss is not an accurate depiction of cycle-varying changes in the IVD across a range of *in vivo* scenarios that were replicated during *in-vitro* testing of FSUs. The magnitude of the applied compressive load was the only exposure variable that significantly influenced IVD height loss, as measured from the 3D surface profiles. Interestingly, postural deviation was the only factor that significantly affected the magnitude of peak AF anterior bulge, pre/post testing.

Keywords: intervertebral disc, height loss, bulge, laser scanner

5.2 Introduction

Specimen height loss is a dependent measure that is commonly examined in *in vitro* spine biomechanics studies. Previous research conducted by van der Veen et al. (2008) has demonstrated that deformation in the intervertebral disc (IVD), cartilaginous endplates and vertebrae all contribute to the total height loss of a functional spinal unit (FSU) mechanically loaded in compression. Unfortunately, most *in vitro* studies are limited in the ability to partition this height loss across each of these anatomical structures since the net differences in the actuator position of the materials testing system used for testing simply reflects overall changes to the entire osteoligamentous system of FSUs and mounting interfaces used for testing. Of clinical importance, exaggerated height loss has been linked to IVD bulging, which is a known mechanism for low back pain due to compression of the spinal cord in the spinal canal or impingement of the nerve roots in the neural foramina (Brinckmann M & Hilweg, 1989; Cuchanski, Cook, Whiting & Cheng, 2011; Stokes, 1988; Wenger & Schlegel, 1997).

One of the first investigations to characterize the IVD bulge from an intact human intervertebral joint under mechanical load was conducted by Hirsch and Nachemson (1954), who demonstrated that a 100 kg compressive load imposed, on average, 1.5 mm of specimen height loss and 0.75 mm of anterior disc bulge in healthy functional spinal units (FSUs), compared to 1.9 mm of height loss and 1.0 mm bulge in those with degenerated IVDs. Using a similar measurement technique, Reuber et al. (1982) later reported posterior IVD bulge across various loading scenarios. In a neutral posture, 400 N of static compressive force imposed, on average, 0.40 mm of IVD bulge across all specimens, which was further increased to 0.56 mm when the magnitude of the compressive load was doubled (800 N) (Reuber et al., 1982). When 400 N of compressive force was simultaneously applied with a 7.9 Nm flexion moment (inducing less than 5 degrees of rotation) the posterior-lateral region of the IVD experienced, on average, a slight inward displacement of -0.40 mm compared to the initial 400 N baseline measure in a neutral posture (Reuber et al., 1982). Interestingly, the opposite trend was observed when a 9.8 Nm extension moment was applied, as an additional posterior bulge of 0.10 mm occurred in the IVD (Reuber et al., 1982). However, the results from these studies are limited by the use of a measurement

device that physically contacts the outer edge of the IVD, which may interfere with the true deformation the AF.

Research conducted by Stokes (1988) represents some of the first efforts to quantify IVD bulging in human lumbar FSUs with mechanical loading using a non-contact measurement technique, which consisted of adhering small photographic targets for optical tracking to the surface of the outer surface of the AF with a thin layer of petroleum jelly. Based on stereo photographs the average IVD bulge with 2.15 kN of compressive force was 0.82 and 0.58 mm on the anterior and posterior regions of the disc, respectively (Stokes, 1988). Interestingly, the amount of vertical compression/deformation of the IVD (measured photographically) was reported to be less than the amount of ram displacement of the materials testing system by a factor of more than two times (Stokes, 1988). Conflicting results were presented by Wenger and Schlegel (1997) using an axial photogrammetric method, which demonstrated that the AF bulge was greatest in the posterior-lateral region (average bulge = 0.93 mm) and smallest anteriorly (average bulge = 0.37 mm) in human lumbar motion segments with the posterior structures removed (statically loaded with 2.5 kN of compression in a neutral posture).

More recently, Heuer et al. (2007) investigated the time-varying changes in human IVD bulging under static compressive force using a custom non-contact laser-scanning device. With the posterior structures removed, human lumbar FSUs were statically loaded (500 N) in a neutral posture for 15 minutes, which resulted in an immediate IVD height loss of 1.14 mm that later progressed to a net change of 1.30 mm in IVD height (Heuer et al., 2007). Interestingly, the largest changes in IVD bulging were observed in the anterior and posterior-lateral regions after 15 minutes (Heuer, Schmitt, Schmidt, Claes & Wilke, 2007). The median bulge recorded in the anterior and posterior-lateral regions of the IVD were 0.86 mm (range 0.46 – 1.34 mm) and 0.45 mm (range = 0.24 – 0.90 mm), respectively (Heuer et al., 2007). Later work conducted by the same group was performed to characterize the effect of posture on IVD bulging (Heuer et al., 2008b). Results from this investigation revealed that the median IVD bulge was 0.86 and 0.33 mm in the anterior and posterior-lateral regions, respectively, which changed to 1.90 mm (anterior) and -1.44 mm (posterior;

inward bulge) when a 7.5 Nm flexion moment was applied. However, to the best of the author's knowledge the combined effects of the magnitude of the compressive load, postural deviation and cycle rate have on IVD height loss and transverse bulging have yet to be investigated with prolonged, cyclic loading.

Therefore, the primary objective of this study was to explore interactions between: (i) the magnitude of the applied compressive force, (ii) frequency of loading (i.e. cycle rate) and (iii) degree of postural deviation on IVD height loss in isolated FSUs subjected to sub-maximal cyclic compressive loading. A secondary objective was to quantify the amount of pre/post AF bulging across loading conditions to better understand the structural changes that occur in the IVD of intact FSUs under cyclic loading conditions. In-line with these objectives, the following hypotheses were formulated:

i. significant interactions between the magnitude of peak compressive force, cycle rate and postural deviation would emerge in: (a) time-varying measures of specimen height loss, as calculated from the actuator position of the mechanical testing system, and (b) intervertebral height loss, as computed from pre/post scans of the anterior surface of the FSU;
ii. significant interactions between the magnitude of peak compressive force, cycle rate and postural deviation would emerge in quantitative measures of AF bulging from the anterior surface of the IVD;
iii. total specimen height loss would be significantly correlated to IVD height loss across experimental conditions; however, the net change in actuator height of the Instron would be significantly greater than the overall change in displacement between the cartilaginous endplates; and
iv. IVD height loss would be significantly correlated with the magnitude of AF bulging across experimental conditions.

5.3 Materials & Methods

5.3.1 Study Design

In vitro mechanical testing of FSUs paired with pre/post surface scans of the anterior profile of the IVD using a 3D laser scanner to characterize changes in IVD height loss and AF bulging across loading conditions. Three independent variables used to simulate repetitive occupational lifting task exposures were examined in this study, including: (i) magnitude of peak compressive force, (ii) cycle rate and (iii) and degree of postural deviation.

5.3.2 Specimen Preparation

The cervical spines of 63 porcine specimens (mean age = 6 months, weight = 85 kg) were obtained following death and stored frozen at -20°C. The cervical spine was separated into two FSUs for testing, which included two adjacent vertebral bodies and the IVD at the level of c34 and c56; resulting in a total of 126 FSUs that were initially included in the study. Porcine cervical FSUs were used as surrogates for the human lumbar spine due to their anatomical and functional similarities (Oxland et al., 1991; Yingling et al., 1999), providing superior control over potential confounding factors (e.g. age, diet, physical activity) that can impact the mechanical integrity of the tissues surrounding the intervertebral joint.

The inclusion criteria for specimens included in this investigation required that FSUs met a non-degenerated disc quality (grade 1) as outlined by Galante (1967). Before testing, frozen specimens were thawed at room temperature for a minimum of 12 hours. Dissection of the cervical spine involved isolating the two FSUs of interest (i.e. c34, c56) and carefully removing the surrounding musculature, leaving only the osteoligamentous structures intact, except for the portion of the anterior longitudinal ligament that attached directly to the anterior surface of the AF, which was removed to expose the IVD for surface profile scanning. Once the dissection protocol was complete, width and depth measurements of the two exposed endplates (upper-superior and lower-inferior) were recorded using digital calipers. These measurements were used to estimate an average intervertebral joint endplate surface area using the equation of an ellipse (**Equation 4-1**; see Chapter 4).

Estimates of endplate surface area were then used as input for a regression equation (average error ± 11%) to approximate each FSU's UCT without destructive testing (Parkinson et al., 2005). This allowed for normalization of peak compressive loading across specimens.

Before mounting the FSUs for testing, the anterior processes and exposed facets (on the superior and inferior aspect of the FSU) were trimmed to ensure that the exposed cartilaginous endplates were responsible for load carriage across the joint. Next, the locations of the cartilaginous endplates on the anterior surface of the FSU (i.e. above and below the IVD) were marked with three steel pins (0.5 mm diameter; a total of 6 per specimen). One pin was placed at the centre of the IVD and two on the anterolateral sides (**Figure 5-1**). This was done to facilitate pre/post registration of the resultant 3D surface profiles obtained from the anterior surface of the IVD from each FSU. The superior and inferior vertebrae of the FSU were then fixed within custom-machined aluminum cups using a combination of wood screws (fixed 1 cm into the exposed endplates) and non-exothermic dental plaster (Denstone; Miles, Southbend, IN, USA). To prevent specimen dehydration throughout the dissection and potting procedures, all FSUs were kept hydrated with a saline mist (0.9 % weight per volume solution) that was applied approximately every 15 minutes.

5.3.3 Procedure

Potted specimens were mounted in a servo-hydraulic materials testing system (Model 8872; Instron, Canton, MA, USA), modified to apply flexion/extension motion to FSU while under compressive load. This testing jig was designed to allow the centre of rotation to be aligned (vertically and horizontally) with the geometric centre of the IVD (Callaghan & McGill, 2001). Each specimen was free to translate in the anterior-posterior direction (via bearing tray), which enabled the centre of rotation to translate within the joint during the cyclic loading protocol. To minimize dehydration during the prolonged mechanical exposure, all specimens were wrapped in saline soak gauze (0.9% weight per volume solution). Each FSU initially received 15 minutes of static compressive force (300 N) to counter any postmortem swelling (mean height loss = 0.95 mm; SD = 0.20) that occurred

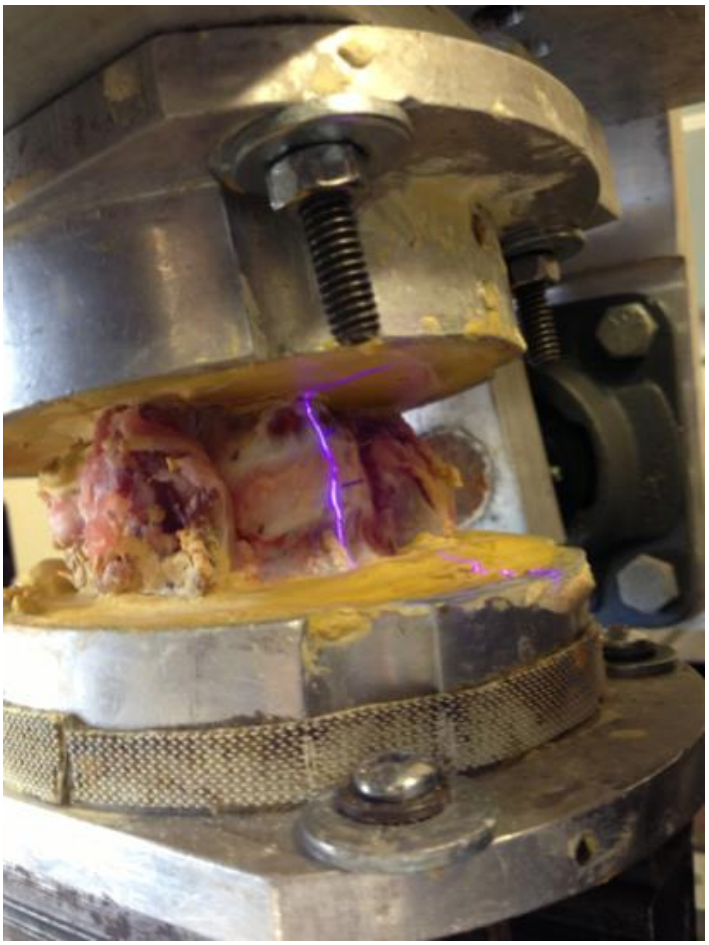

Figure 5-1: Functional spinal unit potted in custom machined aluminum cups with non-exothermic dental plaster (yellow) and mounted in a modified materials testing system. Three stainless steel pins (0.5 mm diameter) were inserted into the superior and inferior cartilaginous endplates (6 total) to facilitate pre/post registration of the 3D surface profile and identify the superior and inferior boundaries of the IVD. The visible (blue) laser on the anterior surface of the FSU was translated across the specimen to construct individual surface profiles.

within the specimen (Callaghan & McGill, 2001). This load has been identified in previous work to equilibrate specimen height, without inducing excessive creep over duration of 15 minutes (Callaghan & McGill, 2001). During this preload test, an independent brushless servomotor (AKM23D; Kollmorgen/Danaher Motion, Radford, VA, USA) connected in-series with a torque cell (T120-106-1K; SensorData Technologies Inc., Sterling heights, MI, USA) was used to establish the angular position of minimal stiffness passive (Nm/degree) about the flexion/extension axis. Following the preload test, three cycles of passive flexion-extension (PFE) joint rotations test were applied (rate = 0.5° per second) to identify the limits of each FSU's neutral zone in the sagittal plane. Using custom software, interfaced with an ISA bus motion controller (Model DMC18x0, Galil Motion Control, Rocklin, CA USA), the applied moment (Nm) and angular displacement (degree) were continuously sampled at 25 Hz. The flexion and extension limits of the neutral zone were identified using methods described by Thompson et al. (2003); whereby the first-derivative of a fourth-order polynomial fit to moment-angle data from the last two loading cycles was used to detect the angular displacement where this curve deviates from linear. These endpoints were used to define the dynamic flexion/extension posture that was applied during testing.

Upon completion of both the preload and PFE tests, specimens were randomly assigned to 1 of 18 experimental conditions (7 FSUs per group) to examine interactions between: (i) the magnitude of the applied compressive force, (ii) cycle rate and (iii) the degree of postural deviation on the joint mechanics of each FSU. Three levels of peak compressive force (10, 20 and 40% of specimens' ultimate compressive tolerance; UCT), three cycle rates (5, 10 and 30 cycles per minute), and two dynamic postural conditions, including: (i) 100% neutral zone range; average (SD) of 6.79° (2.23) and (ii) 300% neutral zone range; 20.52° (4.41) were examined using a full-factorial design. Compressive force was applied using a time-varying waveform (normalized over two-seconds; see Chapter 4) based on estimates of *in vivo* loading using a dynamic EMG-assisted model of the lumbar spine (Parkinson & Callaghan, 2009). The applied compressive force was scaled to run from a minimum of -0.001 N (nominal compressive load to prevent the Instron from lifting the specimen off the bearing tray) to the desired peak load (i.e. 10, 20, and 40% of each FSU's UCT). Dynamic flexion/extension was synchronously applied to FSUs during each loading cycle using a motion profile recorded from the lumbar spine during the same floor to waist

height lift (Parkinson & Callaghan, 2009), and was scaled for each posture condition to 100 and 300% of the specimens' neutral zone range. The 100% neutral zone postural condition was intended to represent a lifting technique with sound mechanics (i.e. minimal spine motion), whereas the 300% condition was designed to bring the isolated joint to the end of its natural physiological range (i.e. where the passive rotational stiffness begins to deviate from linear).

All FSUs were cyclically loaded for 5000 cycles or until fatigue failure occurred, which was identified by specimen height loss greater than 9 mm (Parkinson & Callaghan, 2009). Throughout testing, measurements of the applied compressive force (kN) and vertical position (mm) of the Instron actuator were continuously sampled at 32 Hz using a 16-bit analog-to-digital conversion board (National Instruments, Austin, TX, USA). In addition, a high-speed, 2D laser displacement sensor (LJ-V7080, Keyence Corporation, Osaka, Japan; accuracy of 46 µm in the transverse direction and resolution of 20 µm in the vertical direction) was used to characterize the anterior surface profile of the IVD. The 2D laser displacement sensor (**Figure 5-2**) was mounted on a 48 cm linear guide (NSK Ltd., Tokyo, Japan) and interfaced with a glass scale incremental encoder (LS 328-C, Heidenhain, Schaumburg, IL, USA; accuracy 10 µm) to obtain a 3D cross-sectional scan of the anterior surface of the FSU every 40 µm in the frontal plane. Surface scans were recorded in both a neutral and flexed posture that was defined by the flexion limit from the passive flexion/extension test with 300 N of applied compressive force. Each scan was recorded in less than two-seconds, which considering previous research it was assumed that the resultant surface profile was not significantly affected by viscoelastic changes in the IVD while the scans were captured (Heuer et al., 2008b).

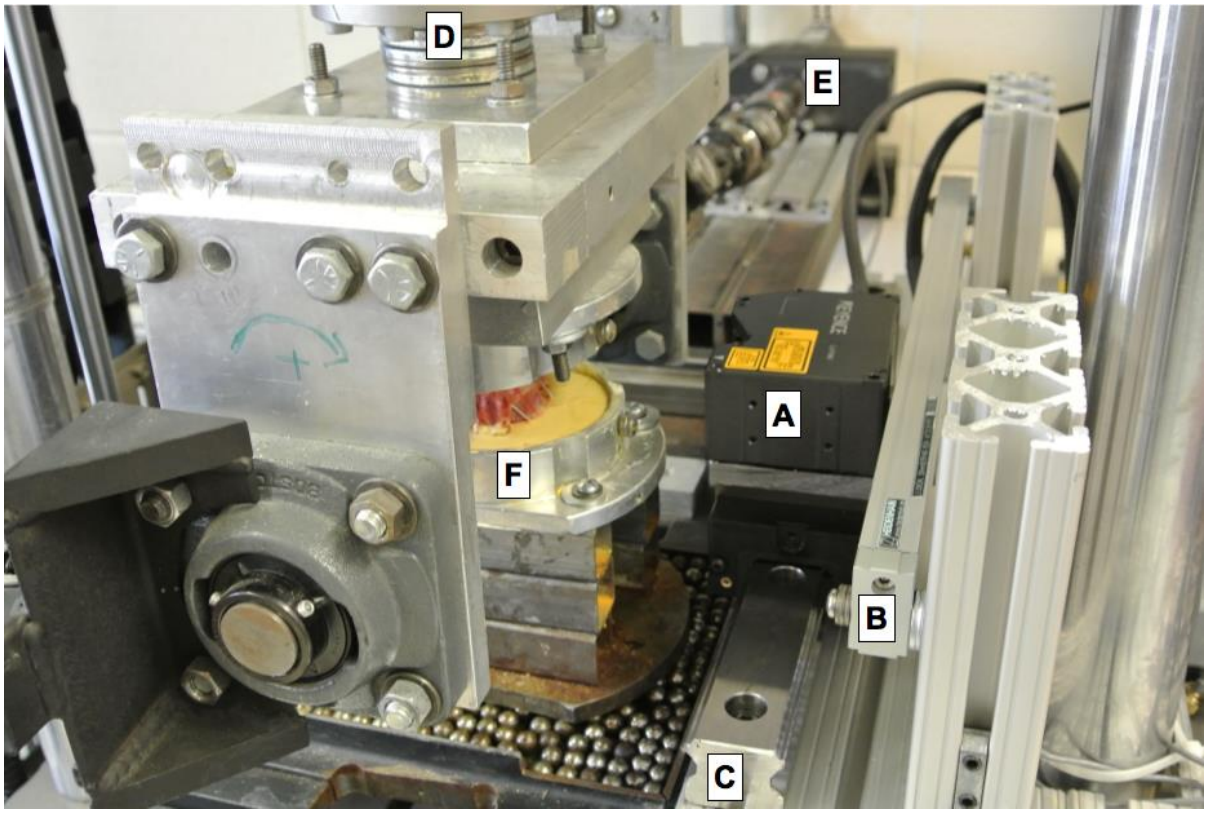

Figure 5-2: Modified materials testing apparatus with 3D laser scanner. (A) 2D laser head, (B) linear encoder, (C) linear guide, (D) 20 kN load cell in-line with Instron actuator, (E) flexion/extension torque motor, (F) functional spinal unit potted in custom machined aluminum cups with non-exothermic dental plaster.

5.3.4 Data Processing

Due to technical difficulties in synchronizing the cyclic compressive load with the flexion/extension axes, three FSUs were excluded from the analyses presented in this paper, resulting in a total of 123 specimens that were considered for the study. In addition, since the cyclic loading protocol was terminated early (i.e. before 5000 cycles were complete) in specimens that experience fatigue failure to protect materials testing system, an additional 24 FSUs from the 40% UCT force condition were also excluded, leaving a sample size of 99 “survivor” specimens that were considered for the present study.

5.3.4.1 Time-Series Mechanical Waveforms

All cycle-varying mechanical waveforms (e.g. compressive force, actuator position, angular position of specimen, applied flexion/extension moment) were processed in MATLAB (version R2013b, Mathworks, Natick, MA). Each signal was dual-pass filtered with a 2nd order low-pass digital Butterworth filter, with an effective cutoff frequency of 10 Hz. Individual loading cycles were identified using the compressive force waveform with a threshold of 100 N to determine the initiation and termination of each loading cycle.

5.3.4.2 Laser Scanner Data

All laser scanner data were processed in MATLAB (version R2013b, Mathworks, Natick, MA). Each 2D scan (i.e. 800 data points; equally spaced every 20 μm in the vertical direction) captured every 40 μm along the anterior surface of the FSU (a total of M scans in the frontal plane) was “stitched together” to create an M x 800 data matrix, which was digitally filtered using a 2D median spatial filter to reduce noise and preserve edges (e.g. location of the steel pins). Sufficient data was captured surrounding the perimeter of the IVD to ensure that any distortion introduced by the median filter did not affect the resultant 3D surface profile.

5.3.5 Dependent Measures

Peak specimen height loss (mm), as measured by the axial position of the Instron actuator was calculated after 1, 10, 100, 1000, 2000 and 5000 cycles. Intervertebral disc height loss; calculated as the vertical distance between the superior and inferior endplates (marked using the steel pins) was computed from pre/post 3D anterior surface profiles that were rendered for each specimen in a neutral posture. Similarly, the peak AF bulging at the midline of the IVD in the frontal plane was computed from the 3D surface profiles captured in a flexed posture, pre/post testing. To facilitate the comparison of AF bulge measurements between specimens and improve the anatomical interpretation of this measure, the maximum anterior bulge perpendicular to a vector defined by the endpoints of the superior and inferior endplates has been reported (**Figure 5-3**).

5.3.6 Statistical Analyses

All statistical analyses were computed using SAS software (version 9.2, SAS Institute Inc., Cary, NC) with a significance level (α) of 0.05 determined *a priori*. To examine interactions between the magnitude of peak compressive force, cycle rate and degree of postural deviation on cycle-varying specimen height loss, a four-factor (cycle number, force magnitude, cycle rate, postural deviation) mixed general linear model was applied, with cycle number as a repeated measure. Simple effects were used to analyze all significant interactions (e.g. influence of postural deviation on force x cycle rate interaction). Effect sizes for all significant comparisons were evaluated using Cohen's *d*, using a pooled estimate of the population standard deviation from both groups (Cohen, 1988).

5.4 Results

5.4.1 Specimen Randomization

Successful randomization of FSUs across experimental conditions was achieved, as there were no significant main effects of force, cycle rate or postural deviation revealed in estimates of endplate area (p = 0.7197, 0.7316 and 0.4382, respectively) or neutral zone range, as determined by the passive flexion-extension tests (p = 0.7812, 0.5998 and 0.6010 respectively).

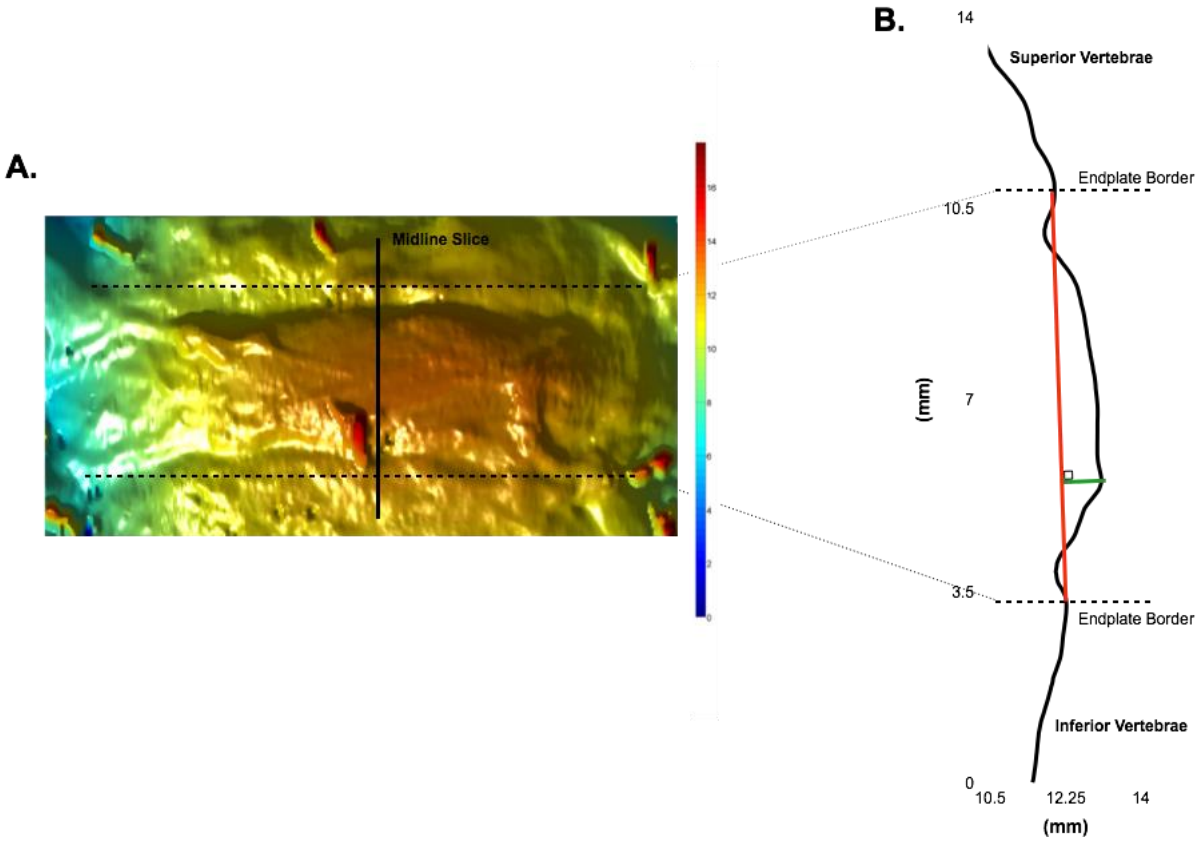

Figure 5-3: (A) Resultant 3D profile of the anterior surface of the intervertebral disc, (B) Convention used to report bulging measurements (mm) of the annulus fibrosus in a flexed posture.

5.4.2 Specimen Height Loss

A significant three-way interaction ($p = 0.0092$) between the magnitude of peak compressive force, cycle rate and degree of postural deviation was observed in cycle-varying specimen height loss data (**Figure 5-4**), as calculated using the axial position of the Instron actuator. Subsequent analysis of the interaction between cycle rate and postural deviation at each magnitude of compressive load revealed that significant main effects of cycle number ($p < 0.0001$), cycle rate ($p < 0.0001$) and postural deviation ($p < 0.0001$) emerged in specimens assigned to the 10% UCT group. Specifically, FSUs assigned to the 10% UCT group that were cyclically loaded at a rate of 10 cycles per minute experienced significantly greater height loss compared to the 5 cycles ($p < 0.001$; $d = 0.37$; mean difference = 0.22 mm) and 30 cycles per minute ($p = 0.0020$; $d = 0.12$; mean difference = 0.07 mm) conditions. Moreover, specimens in the 10% UCT group that were cyclically loaded at 30 cycles per minute experienced significantly greater height loss compared to those in the 5 cycles per minute conditions ($p = 0.0057$; $d = 0.24$; mean difference = 0.14 mm). There was no significant difference ($p > 0.4420$) in the magnitude of specimen height loss in the first 100 loading cycles; however, significant differences ($p < 0.0020$; $d > 0.71$) were noted in all comparisons after 1000 cycles. When considering the effect of postural deviation at 10% UCT, specimens that were flexed/extended to 300% of their neutral zone range experienced significantly greater height loss ($p < 0.0001$, $d = 0.47$; average difference = 0.28 mm) compared to the 100% condition.

A significant two-way interaction ($p = 0.0054$) between cycle rate and postural deviation was observed in specimens that were cyclically loaded at 20% UCT. There was no significant difference ($p = 0.7876$) in the magnitude height loss that was observed between the 100% and 300% neutral zone range postural deviations at a rate of 30 cycles per minute; despite the significant increase that was observed in the 300% neutral zone range condition at a rate of 5 ($p < 0.0001$, $d = 0.66$; mean difference = 0.60 mm) and 10 cycles per minute ($p = 0.0211$, $d = 0.34$; mean difference = 0.34 mm). A significant main effect of cycle number ($p < 0.0001$) was also noted; however, there were no significant differences in the magnitude of height loss in the first 10 loading cycles ($p = 0.3784$). All other comparisons at 100, 1000, 2000 and 5000 cycles were significantly different ($p < 0.0330$, $d > 0.70$), with greater height loss measured with increasingly more loading cycles.

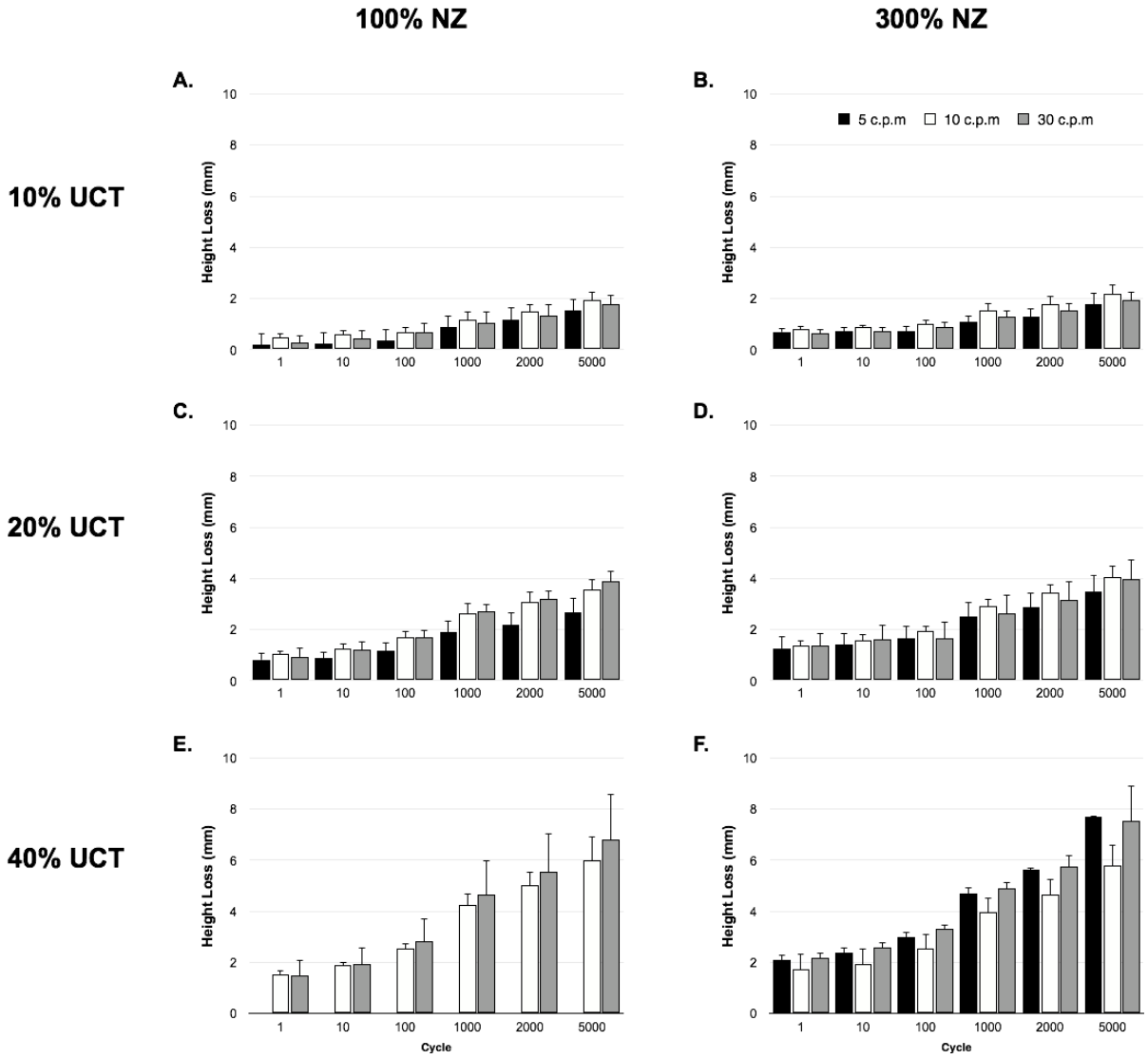

Figure 5-4: Cycle-varying specimen height loss across: (A) 10% ultimate compressive tolerance (UCT) @ 100 % neutral zone (NZ); (B) 10% UCT @ 300 % NZ; (C) 20% UCT @ 100 % NZ; (D) 20% UCT @ 300 % NZ; (E) 40% UCT @ 100 % neutral zone (NZ); (F) 40% UCT @ 300 % NZ.

Significant main effects of cycle rate ($p = 0.0082$) and cycle number ($p < 0.001$) were noted in specimens that were cyclically loaded at 40% UCT. Tukey's *post hoc* test revealed that specimens assigned to both the 5 and 30 cycles per minute conditions experienced significantly greater height loss ($p < 0.05$, $d > 0.27$) compared to the 10 cycles per minute condition. No difference was observed between the 5 and 30 cycles per minute conditions. There were no significant differences in the magnitude of height loss in the first 10 loading cycles; however, all other comparisons at 100, 1000, 2000 and 5000 cycles were significantly different ($p < 0.05$, $d > 0.88$), with greater height loss occurring with increasingly more loading cycles.

5.4.3 Intervertebral Disc Height Loss

A significant main effect of peak compressive force magnitude ($p = 0.0003$) was observed in IVD height loss data, as calculated from the 3D surface profiles of each FSU captured in a neutral posture, pre/post testing. Main effects of cycle rate and degree of postural deviation were not significant ($p = 0.54$ and 0.95, respectively). Overall, a peak compressive force of 40% UCT was associated with significantly greater IVD height loss compared to the 10% ($p < 0.05$, d = 1.38) and 20% ($p < 0.05$, d = 1.11) conditions. A summary of IVD height loss across experimental conditions is provided in **Figure 5-5**.

The average relative contribution of IVD height loss to total specimen height loss varied across experimental conditions, ranging from 19 to 58% (**Table 5-1**)**.** Scatter plots illustrating linear regression analyses between IVD height loss and specimen height loss across all experimental conditions for the 10 and 20% UCT force conditions is provided in **Figure 5-6**. Specimens from the 40% UCT force level were excluded since there was only one condition that had more than three surviving specimens (100% neutral zone range @ 30 cycles per minute). Overall, total specimen height loss was a poor description of IVD height loss. A wide range of Pearson product-moment correlations were observed (-0.54 to 0.95) across experimental conditions.

Table 5-1: Average relative contribution of intervertebral disc height loss compared to total specimen height loss.

Force	Repetition	Posture	Average Relative Contribution*	Standard Deviation
10	5	100	0.49	0.34
10	5	300	0.19	0.10
10	10	100	0.38	0.15
10	10	300	0.27	0.18
10	30	100	0.58	0.14
10	30	300	0.49	0.21
20	5	100	0.34	0.18
20	5	300	0.35	0.30
20	10	100	0.33	0.22
20	10	300	0.26	0.16
20	30	100	0.26	0.13
20	30	300	0.21	0.14

Note: *Relative contribution = IVD height loss (mm) / specimen height loss (mm)

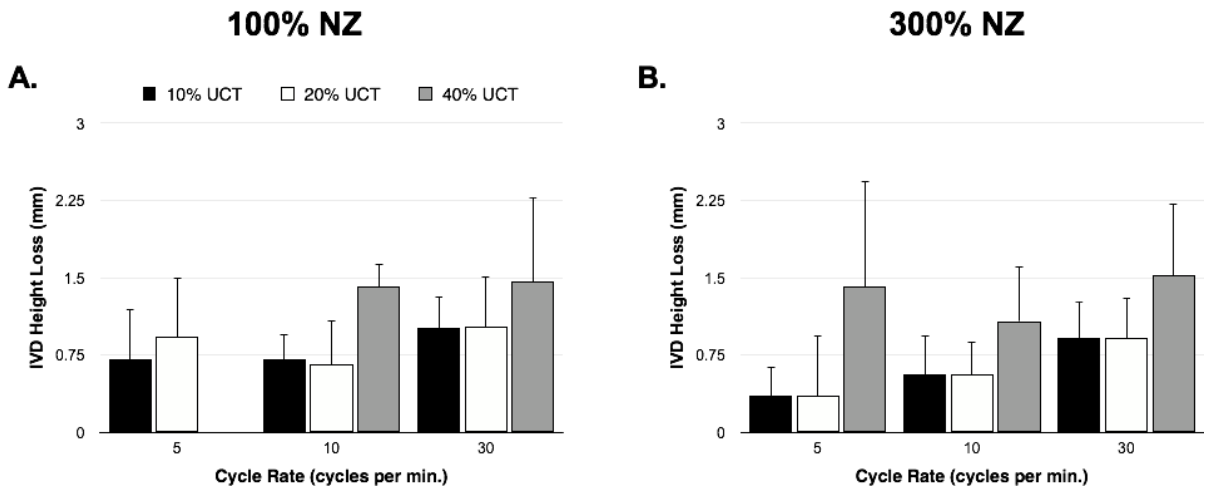

Figure 5-5: Intervertebral height loss as calculated from the 3D surface profile of the anterior aspect of the IVD, separated by (A) 100% and (B) 300% neutral zone postural deviation.

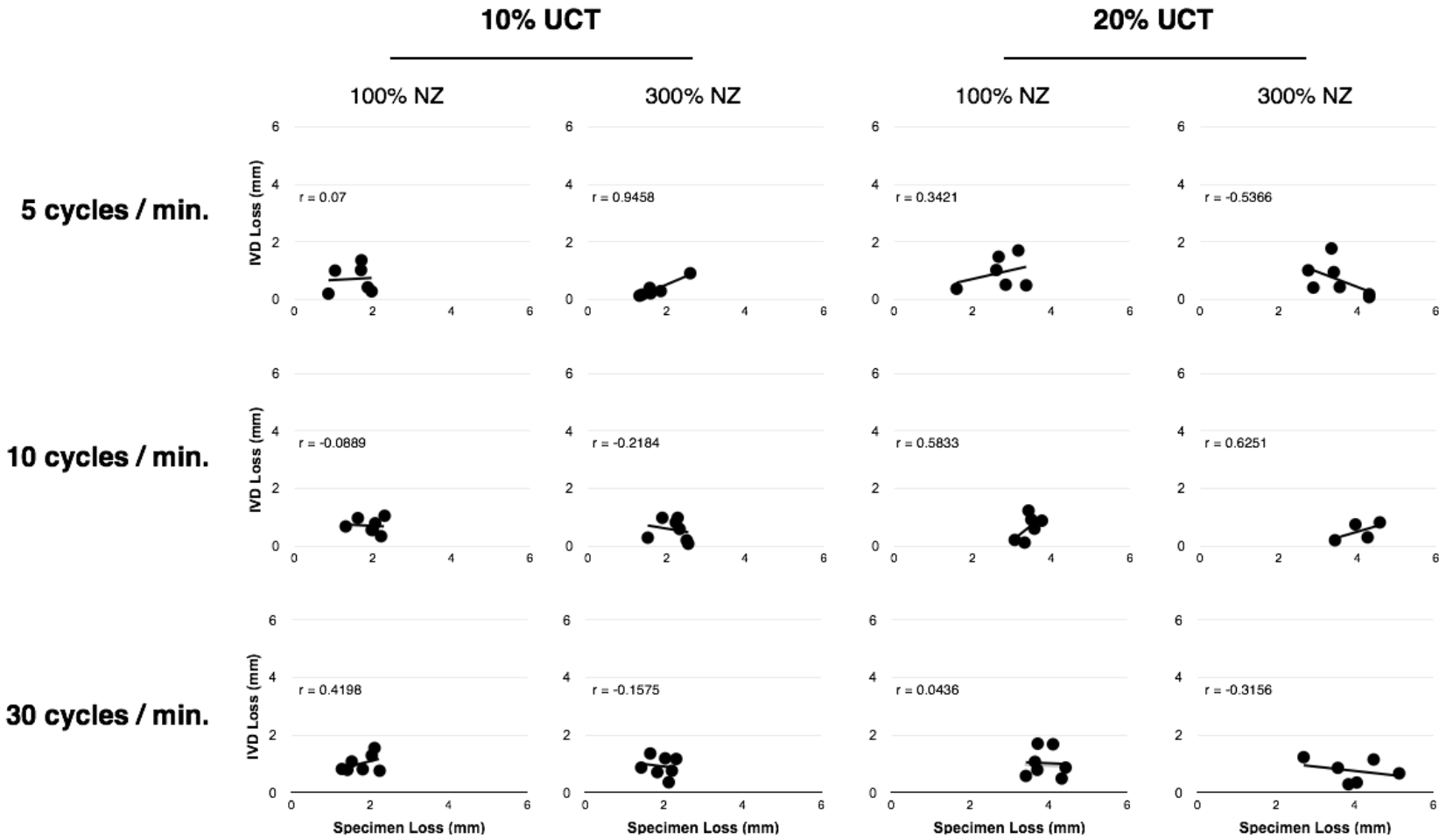

Figure 5-6: Scatter plots illustrating linear regression analyses that were performed between intervertebral height loss and specimen height loss data across experimental conditions in both the 10% and 20% ultimate compressive tolerance loading conditions.

5.4.4 Annulus Fibrosus Bulging

Significant main effects of postural deviation ($p = 0.0016$) and time ($p = 0.0423$) were observed in peak AF bulge measurements. *Post hoc* analyses revealed that specimens that were exposed to repetitive postural deviation to 100% NZ range exhibited significantly greater anterior bulge ($p < 0.05$, $d = 0.42$, mean difference = 0.23 mm) compared to those assigned to the 300% condition. Moreover, the anterior bulging of the AF in a flexed posture was found to be significantly greater ($p < 0.05$, $d = 0.03$, mean difference = 0.17 mm) in 3D scans captured prior to the cyclic mechanical exposure. A summary of the average AF bulge measurements recorded at the midline of the IVD across experimental conditions is provided in **Figure 5-7.** Sample AF disc bulge profiles Pre/Post testing in both a neutral and flexed posture are provided in **Figure 5-8.**

Scatter plots illustrating linear regression analyses between IVD height loss and IVD bulging across all experimental conditions for the 10 and 20% UCT force conditions is provided in **Figure 5-9**. Specimens from the 40% UCT force level were excluded since there was only one condition that had more than three surviving specimens (100% neutral zone range @ 30 cycles per minute). Overall, a wide range of Pearson product-moment correlations were observed (-0.44 to 0.78) between IVD height loss and IVD bulging across experimental conditions.

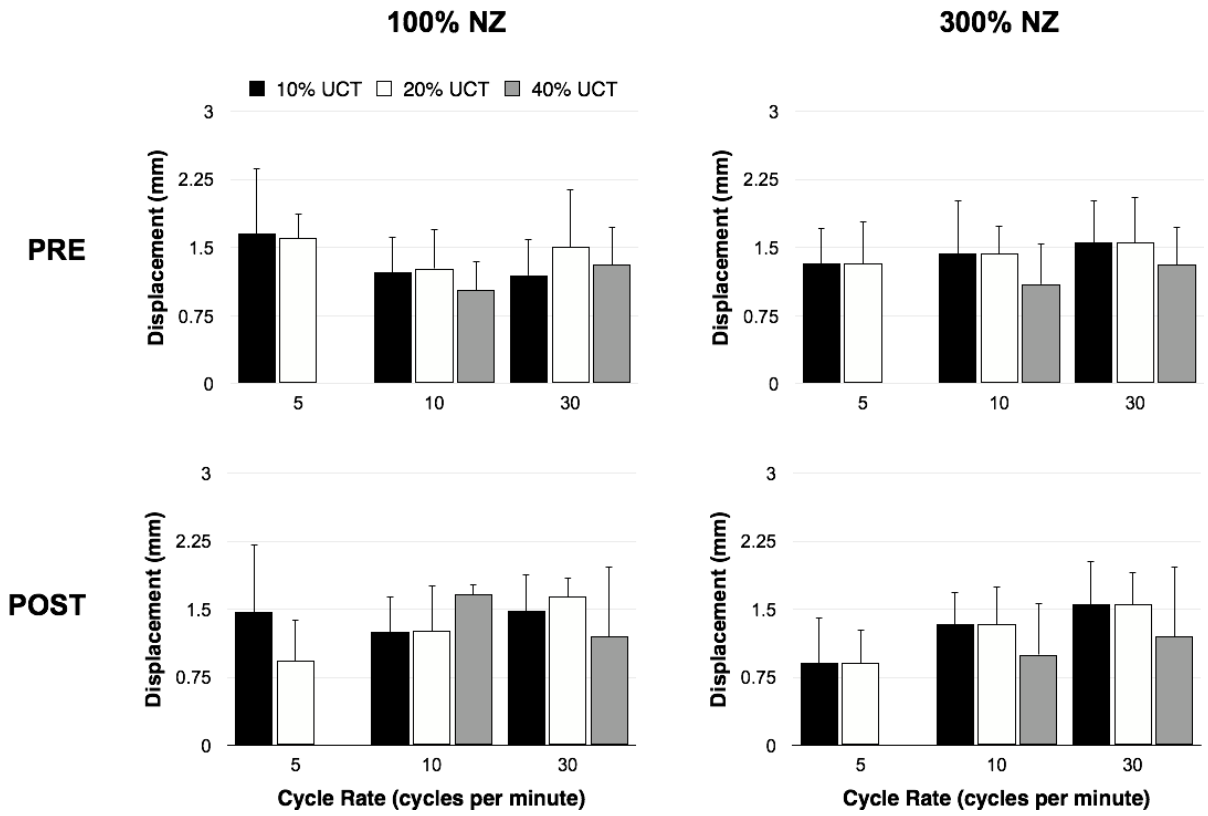

Figure 5-7: Average pre- and post-test peak AF bulge of the intervertebral disc measured at the midline of the joint across experimental conditions.

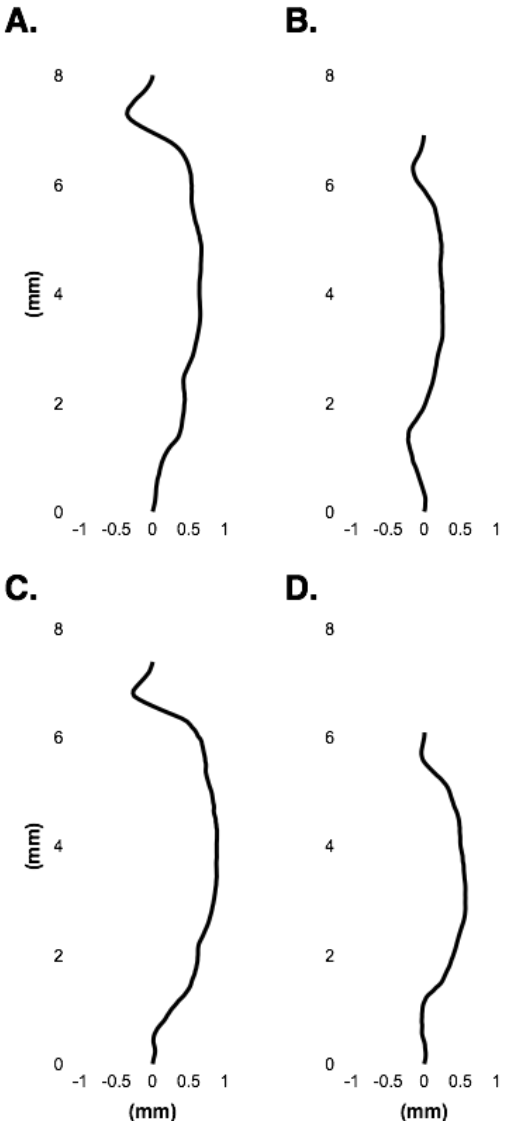

Figure 5-8: Example AF disc bulge profiles (sagittal view) normalized relative to a vector that was defined by superior and inferior endplate border. (A) pre-neutral, (B) post-neutral, (C) pre-flexed, (D) post-flexed (S176; c56, 20% UCT, 30 cycles per minute, 300% neutral zone).

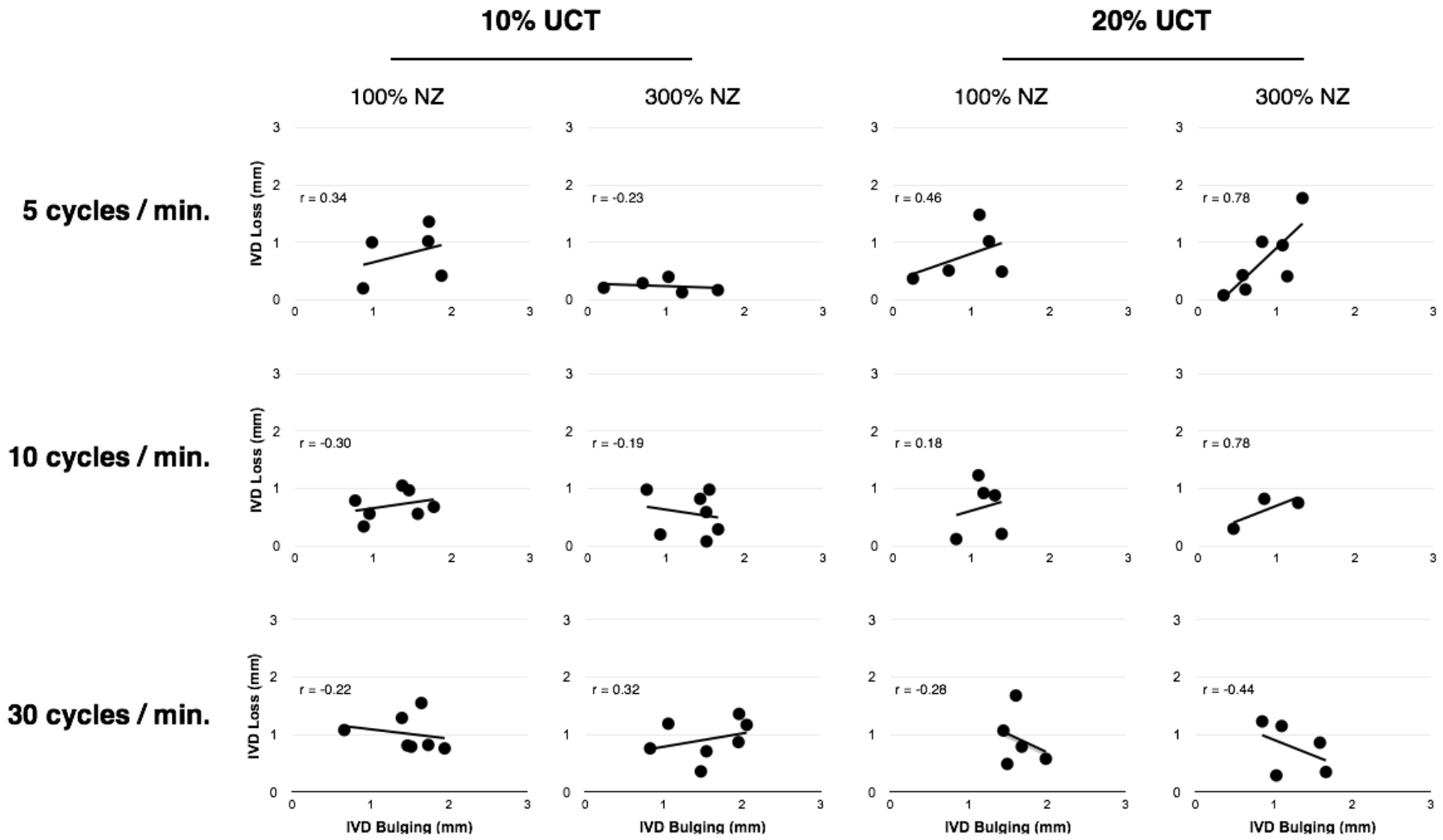

Figure 5-9: Scatter plots illustrating linear regression analyses that were performed between intervertebral height loss and post-testing intervertebral disc bulging across experimental conditions in both the 10% and 20% ultimate compressive tolerance loading conditions.

5.5 Discussion

Consistent with our hypothesis, a significant three-way interaction emerged in cycle-varying measures of specimen height loss; however, it is interesting that the magnitude of the applied load was the only exposure found to significantly impact IVD height loss (as measured from the 3D surface profiles of the IVD). This suggests that the interaction observed in specimen height loss may have been driven by time-varying changes in either the cartilaginous endplates or vertebral bodies. The relative contribution of IVD height loss to total specimen height loss was shown to vary across experimental conditions (ranging from 19 to 58%) with the greatest relative proportion observed in the 10% UCT loading group (average relative contribution = 40%). Overall, total specimen height loss was a poor descriptor of pre/post changes in the IVD. Moreover, our hypothesis that the combined effects of the magnitude of the applied force, cycle rate and postural deviation would significantly impact quantitative measures of AF bulge in the IVD was rejected. Based on the results presented in this study, the magnitude of postural deviation (i.e. 100 vs. 300% neutral zone range) was the only exposure variable that significantly affected the magnitude of AF bulging.

Although this is one of the first studies to investigate the impact of cyclic loading on IVD bulging using non-contact methods, there are some aspects of our study that can be compared to previous work. For example, a recent study conducted by Heuer et al. (2008a;, 2008b) characterized the effect of posture on the AF bulge of the IVD after a 15 minute preload with 500 N of static compressive force, which is similar to the loading protocol that was applied before the pre-test scans were captured in the present study. Results from the Heuer investigation revealed that the median IVD bulge was 1.90 mm (anterior) and -1.44 mm (posterior; inward bulge) when a 7.5 Nm flexion moment was applied (Heuer et al., 2008b). Interestingly, across all specimens that were included in the present study, the average (SD) pre-test AF bulge of the IVD measured at the midline of the anterior region of the IVD in a flexed posture was 1.35 mm (SD = 0.48), which is less than what has been reported by Heuer and colleagues (2008b). However, an important difference between our work is that the posterior structures remained intact in the present study, which Heuer et al. (2008b) later showed that the median IVD bulge measured at the anterior region of the IVD in a flexed posture increased by approximately 1.4x when the anterior longitudinal ligament

and vertebral arches were removed (median bulge = 2.14 mm) compared to intact specimens (median bulge = 1.56 mm). These differences may also be attributable to the use of porcine cervical FSUs, which are approximately 50% of the size of human lumbar motion segments (Yingling et al., 1999).

It is interesting that the magnitude of AF bulging in a flexed posture was significantly greater in the 3D surface profiles that were captured prior to the cyclic mechanical exposure, as well as those specimens that were constrained to 100% of their NZ range (compared to the 300% NZ condition). This is consistent with recent findings in our lab that repetitive flexion/extension was associated with a decrease in intradiscal pressure after one hour of cyclic loading (Noguchi, 2013). Based on these results, our initial hypothesis that an increase in IVD height loss would result in significantly greater magnitudes of AF bulge was rejected. Moreover, a wide range of Pearson product moment correlation (from r = -0.44 to 0.78) was observed between IVD height loss and magnitude of IVD bulging across experimental conditions. These findings conflict with some of the earlier data published by Heuer et al. (2007), which showed that IVD bulging was time-dependent, with the largest changes in AF bulge observed in the posterior and posterior-lateral regions (maximum difference = 0.1 mm). However, an important difference between this study and the work of Heuer et al. (2007) that may explain this difference is that our pre-test 3D profile scans were captured after 15 minutes of static compressive (i.e. preload) that imposed, on average, 0.95 mm of specimen creep, which was then followed by three cycles of passive flexion-extension adding an additional 15 minutes of testing duration. Therefore, since AF bulging and axial deflection of the cartilaginous endplate into the underlying trabecular bone have been shown to play an important role during the early phases of FSU creep deformation due to compressive load (Brinckmann & Horst, 1985; Heuer et al., 2008b; Heuer et al., 2007; Hirsch & Nachemson, 1954; MacLean, Owen & Iatridis, 2007; Pei et al., 2014; Reuber et al., 1982) it is possible that most of the structural changes that occurred to the IVD occurred before the cyclic loading protocol even began (i.e. once the cartilaginous endplates come into contact, the AF bulge of the IVD is constrained). Based on the histological analyses presented in the previous chapter (Chapter 4), which show increased disruption in the AF for specimens assigned to the 300% NZ postural condition, it is possible that the inner layers of

the IVD may have actually folded inwards resulting in less anterior displacement (i.e. bulging), as shown previously in human lumbar FSUs and in cadaver assessment of IVD tissue (Adams, Freeman, Morrison, Nelson & Dolan, 2000; Yasuma et al., 1993; Yasuma et al., 1990).

When comparing the magnitude of total specimen height loss to a similar investigation previously conducted by our group, Parkinson and Callaghan (2009) reported an average (SD) height loss of 3.3 (0.4) and 4.7 (1.3) mm for specimens that were loaded to 10% and 30% of their UCT (respectively), which is greater than what was observed in the present study. However, specimens included in this earlier work were cyclically loaded up to a maximum of 21,600 cycles (12 hours at a rate of 30 cycles per minute) or until failure, which equated to an average (SD) of 14,400 (6859) and 5031 (3944) cycles for the 10% and 30% UCT loading groups respectively (Parkinson & Callaghan, 2009). In addition, a 300 N static compressive load was applied between cycles. However, research conducted by Drake and Callaghan (2009) has demonstrated increased compression on artificial spinal nerve roots placed in porcine cervical FSUs with an average (SD) of 3.5 mm (0.88). The resultant pressure that was recorded on the instrumented nerve roots in this study was approximately 44% of the required force (26.29 mN) that was needed to initiate pain behavior in rats (Hubbard, Chen & Winkelstein, 2008), indicating that both the 20 and 40% UCT loading groups in the present work could contribute to potential pain pathways in the lumbar spine with cyclic compressive loading, since the magnitude of specimen height loss well exceeded 3.5 mm after 5000 cycles.

The application of findings from this study to the human lumbar spine is limited by the use of porcine cervical FSUs, which does not take into account any physiological repair of the tissues or the natural restoration of intervertebral joint height in a healthy spine due to diurnal changes in fluid loss / reabsorption (Adams, Dolan & Hutton, 1987; Zander, Krishnakanth, Bergmann & Rohlmann, 2010). It is also important to note that IVD height loss and AF bulging data are not meant to apply to clinical situations, particularly since the insertion of the anterior longitudinal ligament on the anterior face of the AF was removed to allow scanning of the annulus. Previous research conducted by Heuer et al. (2008b) has

shown that the longitudinal ligaments stabilize the IVD and help prevent it from bulging. It should also be noted that IVD height loss measurements that were calculated from the 3D surface profiles of the IVD are also limited by the fact that all measurements were computed on the anterior region of the IVD with 300 N of compressive force. However, it was not possible to obtain measurements from the posterior-lateral region of the IVD on intact specimens. Heuer et al. (2008b) have previously shown that the peak IVD bulge measured in the posterior-lateral region was approximately 24% of the magnitude measured on the anterior surface (peak AF bulge at posterior-lateral region = 0.42 mm, compared to 1.77 mm on the anterior surface) (Heuer et al., 2008b). Although not reported in their paper, it is possible that these differences may be attributable to the difference in AF wall height between the anterior and posterior-lateral regions of the IVD or attributed to the removal of the posterior elements of the FSU. The results presented in this study are also limited by the non-destructive method (average error = 11%) that was used to approximate the ultimate compressive tolerance of FSUs included in the study, which is based on approximating the intact intervertebral joint surface area using the equation of an ellipse to estimate failure force (Parkinson et al., 2005). This approach may not be suitable for human specimens, where a wide range of bone mineral density in the lumber vertebrae would be expected.

Although the results from this study are not intended to reflect an *in vivo* scenario, it is interesting to note that a 2001 study conducted by Fredericson et al. have shown using MRI that the average (SD) posterior IVD bulge in the morning was 1.92 mm (0.35) in a flexed posture, with a trend of increased bulging observed after 10 hours of normal activity (average = 2.18 mm). These findings are in good agreement with a more recent study conducted by Zou et al. (2009), who also employed MRI to characterize the magnitude of posterior disc bulge in a sample of 513 Chinese patients with back pain. Results from this study demonstrate the magnitude of IVD disc bulge increased by approximately 2x between joints with grade I (approximate posterior bulge = 2 mm) and grade V degeneration (approximate posterior bulge = 4 mm) (Zou et al., 2009).

5.6 Conclusion

This investigation provides evidence that total specimen height loss is not an accurate depiction of IVD changes in all test scenarios that occur *in-vivo* and are replicated during *in-vitro* testing of FSUs. The magnitude of the applied compressive load was the only independent factor that significantly impacted IVD height loss, as measured from the 3D surface profiles that were constructed from the laser scanner data. Interestingly, postural deviation was the only exposure variable that significantly impacted the magnitude of peak AF bulge, pre/post testing. Future research should attempt to pair the 3D laser scanning system with a linear actuator in order to characterize cycle-varying changes in the 3D surface profile of the IVD (i.e. capture surface scans after every cycle).

Chapter 6

Study IV: Exploring interactions between the magnitude of tissue stretch and cycle rate on the mechanical properties of the annulus fibrosus during cyclic, biaxial tensile loading.

6.1 Overview

Study Design: An *in vitro* biomechanics study exposing multilayer samples of isolated annulus fibrosus (AF) tissue to sub-maximal, cyclic biaxial tensile loading.

Background: Previous research has shown that the intervertebral disc (IVD) undergoes multidirectional tensile strain under *in vivo* loading conditions. *In vitro* testing has found that biaxial tensile testing of excised samples of AF tissue results in higher stresses at considerably lower magnitudes of strain compared to uniaxial testing methods. However, the cycle-varying changes in the mechanical properties of the AF have yet to be studied under cyclic biaxial tensile loading conditions.

Objectives: The primary objective of this study was to explore interactions between: (i) the magnitude of peak tissue stretch and (ii) cycle rate on cycle-varying changes in the mechanical properties of the AF tissue during cyclic biaxial tensile loading. A secondary purpose was to examine whether the mechanical response of multilayer AF tissue samples would be different about each axis of loading or across radial locations of the IVD.

Methods: Ninety-six AF tissue samples, consisting of 3-5 lamellae, were excised from two radial locations on the IVD, including: (i) the anterior and (ii) posterior-lateral regions. Each tissue sample was randomly assigned to 1 of 12 experimental conditions to examine interactions between the magnitude of peak tissue stretch and cycle rate on the mechanical properties of isolated multilayer AF tissue samples, during cyclic biaxial tensile loading. Three levels of peak biaxial tissue stretch (circumferential-axial), including: (i) 6-10%, (ii) 9-15% and (iii) 12-20% and two cycle rates (5 and 10 cycles per minute) were examined using a full factorial design. Biaxial tensile load was applied in displacement control using a BioTester tensile loading apparatus in a temperature (29° C ± 1) and humidity (90% ± 5) controlled local testing environment. Top-down digital images of the tissue's surface were captured during both the stretch portion of cycles 1, 10 and 100 using an overhead CCD camera.

Results: A significant three-way interaction between the radial location on the IVD, magnitude of tissue stretch and cycle rate ($p = 0.0053$) and a significant two-way interaction between the axis of loading and magnitude of tissue stretch ($p < 0.0001$) was observed in measures of peak tensile stress. Similarly, significant two-way interactions were observed in the S-S moduli between: (i) magnitude of tissue stretch and cycle rate ($p = 0.0004$), as well as (ii) magnitude of tissue stretch and axis of loading ($p < 0.0001$). Significant two-way interactions between: (i) the magnitude of tissue stretch and axis of tensile loading ($p < 0.0001$), (ii) cycle rate and axis of tensile loading ($p = 0.0174$) and (iii) transverse location of the IVD and cycle rate ($p = 0.0005$) were observed in cycle-varying measures of peak surface strains that were calculated using a virtual gauge region defined on the surface of each tissue sample.

Conclusion: Results from this study emphasize the cycle-varying tensile stress response of the AF, which changed across loading axis and region of the IVD. However, it is interesting that no significant changes were observed in S-S moduli after 100 cycles of cyclic biaxial tensile loading. These findings provide novel insight into the cycle-varying stress-relaxation that occurs in multilayer samples of AF tissue, which may be linked to the known mechanism of IVD tissue failure (i.e. development of fissures and clefts) under chronic loading conditions.

Keywords: intervertebral disc, annulus fibrosus, biaxial tension, stress, strain

6.2 Introduction

The intervertebral disc (IVD) is a complex, heterogeneous structure (Bruehlmann et al., 2002; Hayes et al., 2001; Inoue, 1981) designed to allow movement in the spine and transmit load between adjacent vertebrae. Previous studies have shown that the annulus fibrosus (AF) undergoes multidirectional tensile strain under *in vivo* loading conditions (McNally & Adams, 1992; Stokes, 1987; van Deursen, Snijders, Kingma & van Dieën, 2001), and has recently been examined as such to characterize the material properties of single lamellae (Bruehlmann, Hulme & Duncan, 2004; Gregory & Callaghan, 2010) and multilayer samples of isolated AF tissue (Bass, Ashford, Segal & Lotz, 2004; Gregory, Veldhuis, Horst, Brodland & Callaghan, 2011). Bass and colleagues (2004) were one of the first groups to examine the mechanical properties of human AF tissue subject to biaxial tensile loading, as previous studies had relied solely on uniaxial testing methods (Ebara et al., 1996; Elliott & Setton, 2001; Green et al., 1993; Skaggs et al., 1994). Results from this study showed that biaxial testing resulted in higher stresses at considerably lower magnitudes of strain compared to uniaxial tensile tests, from which the authors concluded that constitutive models derived from uniaxial tests were insufficient to prescribe physiologically relevant materials properties for the tissue samples (Bass et al., 2004). More recent work conducted by Gregory and colleagues (2011) showed similar findings using bilayer samples of isolated AF tissue. In this investigation it was revealed that the maximal stress and stretch-ratio moduli (i.e. stiffness) were significantly higher than those observed in uniaxial tests (increases of 97% and 118% respectively).

However, the mechanical properties of the AF have yet to be studied in cyclic, biaxial tensile loading conditions. Although previous studies have examined the fatigue failure behavior of isolated AF tissue samples in uniaxial tensile loading (Green et al., 1993), it was hypothesized that this mechanical exposure may not replicate the same mechanism of injury that is sustained by the IVD under chronic loading conditions. Therefore, the primary purpose of this study was to explore interactions between the magnitude of peak tissue stretch and frequency of loading (i.e. cycle rate) on cycle-varying changes in the mechanical properties of multilayer samples of AF tissue during cyclic, biaxial tensile loading. A secondary purpose was to examine whether the mechanical response of multilayer AF tissue samples would be different in each axis of loading (i.e. axial, circumferential) and

whether this response would vary across regions of the IVD (i.e. anterior vs. posterior-lateral). In-line with these objectives, it was hypothesized that:

i. a significant interaction between the magnitude of peak tissue stretch and loading cycle rate would emerge in cycle-varying mechanical properties of excised samples of AF tissue;
ii. the mechanical response of AF tissue samples to cyclic, biaxial tensile loading would be significantly different in each orthopedic loading axis; and
iii. there would be no significant differences in mechanical properties in tissue samples excised from different transverse locations on the IVD (e.g. anterior vs. posterior-lateral) regions.

6.3 Materials & Methods

6.3.1 Study Design

An *in vitro* biomechanics study exposing multilayer samples of isolated AF tissue to sub-maximal, cyclic biaxial tensile loading. The combined effects of two independent factors on the material properties of excised AF tissue samples were examined in this investigation, including: (i) the magnitude of peak tissue stretch (to replicate postural variation) and (ii) cycle rate. All tests were performed in displacement control.

6.3.2 Tissue Preparation

Ninety-six (96) AF tissue samples were dissected from the IVD of 48 porcine cervical functional spinal units (24 c34, 24 c56; mean age = 6 months, mean weight = 80 kg), which were obtained immediately following death and stored frozen at -20°C. The inclusion criteria for this investigation required that FSUs meet a non-degenerated disc quality (grade 1) as outlined by Galante (Galante, 1967). Frozen specimens were thawed for a minimum of 12 hours at room temperature. Each tissue sample, composed of 3-5 lamellae, was dissected from the IVD using a stereoscopic zoom microscope (Nikon SMZ 1000, Nikon Instruments Inc., NY, USA) at an intermediate depth (i.e. between layers 3 to 8). Tissue samples were excised from two radial locations on the IVD, including: (i) the anterior and (ii) posterior-lateral regions. Before testing, each tissue sample was reduced to approximately 5 x 5 mm

sections, with an average (SD) area of 30.6 mm^2 (6.7) and a thickness of 0.83 mm (0.11) that was measured using a laser displacement measurement sensor (ZX-LD40L Smart Sensor, Omron Canada Inc., Toronto, ON, Canada). To minimize specimen dehydration throughout the dissection protocol, all AF tissue samples received superficial misting using a 0.9% weight per volume saline solution every few minutes. Next, tiny reflective particles were randomly scattered over the superficial surface of the tissue section to improve surface tracking, as the adhesion forces of the moist tissue secured each particle in place during testing. The mass of each sample (covered in reflective particles) was then recorded using an analytical scale (resolution = 0.001g) before it was mounted in a BioTester loading system (Cellscale, Waterloo, ON, Canada), a mechanical testing apparatus specifically designed to apply biaxial tensile load to thin biological tissues.

6.3.3 Mechanical Testing

Each AF tissue sample was mounted in the BioTester apparatus using four BioRakes, consisting of five sharpened tungsten wires that were rigidly fixed and connected in-line with a linear actuator (tine diameter = 0.25 μm; tine spacing = 0.70 mm), with an approximate apron width of 0.70 mm between the edge of the tissue sample and the location of puncture (Eilaghi, Flanagan, Brodland & Ethier, 2009). All samples were housed in a temperature (29° C ± 1) and humidity (90% ± 5) controlled local testing environment (**Figure 6-1**), which helped to ensure consistent hydration of the tissue samples during testing. Tensile load was applied to AF tissue samples along both the compressive axis (axial), as well as the circumferential axis (perpendicular to the axial direction) using two, stepper-motor linear actuators (resolution = 1 μm) connected in series with two, 2.5 N load cells (accuracy = 0.2% full scale). Force and actuator displacement were continuously sampled at 30 Hz during testing. In addition, top-down digital images of the tissue's surface were captured at 15 Hz during both the stretch and recovery portion of cycles 1, 10 and 100 using an overhead CCD camera with an image resolution of 1280 by 690 pixels (Sony XCD-910, Sony Electronics Inc., Tokyo, Japan).

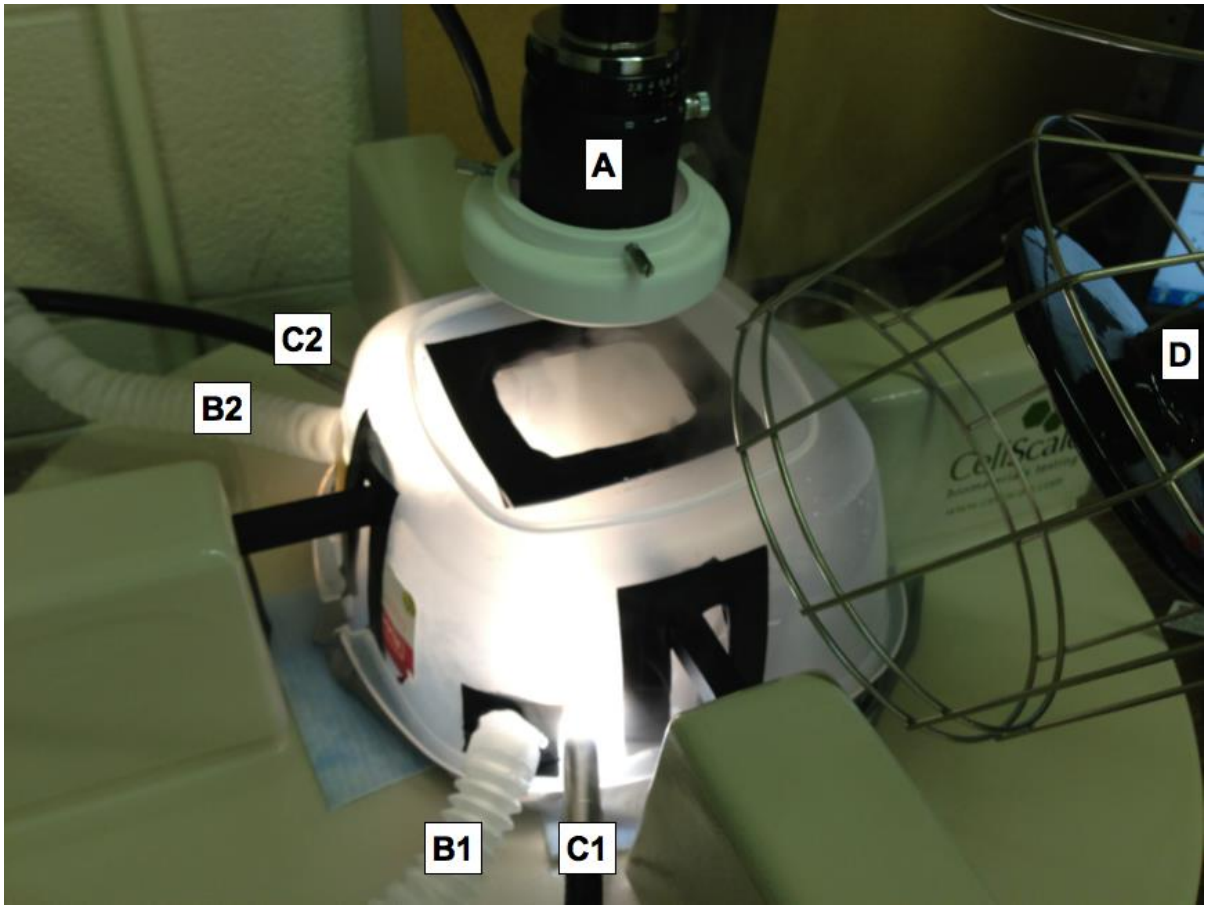

Figure 6-1: Temperature and humidity controlled local testing environment. (A) CCD camera used for optical surface strain tracking, (B1, B2) Humidifying foggers, (C) Indirect gooseneck lighting, (D) Infrared heat source. Not shown in the photograph is a combined humidity and temperature sensor placed inside the local testing environment that was used to control both the humidity and heat sources. Humidifying foggers were turned off during cycles 1, 10 and 100 for surface strain tracking.

Once secured in the BioTester, AF tissue samples were preloaded to 10 mN in each direction, to ensure consistent tensioning across samples before initiating the testing protocol. The preloaded position was considered the sample's resting length (i.e. stretch ratio = 1.0). Next, each sample was preconditioned through three cycles of biaxial tensile stretch (three-seconds duration) and recovery (three-seconds duration), to a stretch ratio of 6-10, 9-15, and 12-20% in circumferential and axial axes respectively using a triangular waveform. Stretch ratios examined in this study were based on a ratio of 1.65 for the maximum axial/circumferential surface strains recorded on the anterior surface of human lumbar motion segments using a 3D laser scanning device (Heuer et al., 2008b), calculated across all experimental conditions that were included in the study (i.e. intact, posterior elements removed, spinal ligaments removed).

Upon completion of the preconditioning loading cycles, AF tissue samples were stratified by radial location (anterior, posterior-lateral) and segment level (c34, c56) and randomized to 1 of 12 experimental conditions (8 samples per condition with equal distribution) to examine the combined effects of the magnitude of peak tissue stretch and cycle rate on the materials properties of isolated multilayer AF tissue samples, during cyclic biaxial tensile loading. Three levels of peak biaxial tissue stretch: (circumferential-axial), including: (i) 6-10%, (ii) 9-15% and (iii) 12-20% and two frequencies of loading (5 and 10 cycles per minute) were examined using a full factorial design. Biaxial tensile load was applied in displacement control using a triangular waveform (1 cycle = six seconds; three seconds stretch and three seconds recovery). However, due to the feasibility of controlling specimen hydration for durations longer than 15 minutes, AF tissue samples were only cyclically loaded to 100 cycles. Post-testing, cross-sectional thickness and mass measurements were recorded to characterize any dehydration that occurred.

6.3.4 Data Reduction

All cycle-varying mechanical waveforms (e.g. tensile force, actuator displacement) were processed in MATLAB (version R2013b, Mathworks, Natick, MA). Each signal was dual-pass filtered with a 2nd order low-pass digital Butterworth filter, with an effective cutoff frequency of 10 Hz. Individual loading cycles were identified using the actuator

displacement waveforms to determine the initiation and termination of each loading cycle. Digital images captured of the tissue's superficial layers (i.e. top-down view) during mechanical testing were processed using LabJoy software (Version 5.8 Waterloo, ON, Canada). For each test, a source image was defined as the first image captured with 10 mN of tension applied about each axis. Next, 8 virtual tracking points were defined (*in silica*) approximately 0.5 mm parallel to locations that each sharpened tungsten wire pierced the tissue sample on the apex of a tiny reflective particle on the surface of the tissue (**Figure 6-2**). These virtual markers were used to define a gauge region for each sample tested. The displacement of all 8 virtual points were tracked on successive images captured during testing (15 Hz) using a template matching algorithm that has been integrated into the LabJoy software package and has been validated previously (Eilaghi et al., 2009). The average change in length of parallel virtual markers on opposite sides of the tissue sample (i.e. 3 sets of points per loading axis) served as a measure of specimen elongation. For each axis of loading, peak surface strain was calculated. Normal engineering stress was calculated using the measured tensile force (about each axis of loading) divided by the cross-sectional area of the tissue sample measured in the plane normal to the applied tensile force, which included approximately 35% of the apron width (Eilaghi et al., 2009). From these data, stress stretch-ratio curves were produced about each axis of loading using displacement measured from the linear actuators.

6.3.5 Dependent Measures

For each axis of loading, cycle-varying changes in: (i) stress stretch-ratio moduli (MPa); calculated as the slope of the linear region of the stress stretch-ratio curve using single cycle measurement, (ii) peak stress (MPa), (iii) peak surface strain; calculated using the virtual gauge region was computed, as well as (iv) pre/post changes in specimen thickness and mass. Typical loading cycles for each direction of loading is provided in **Figure 6-3.**

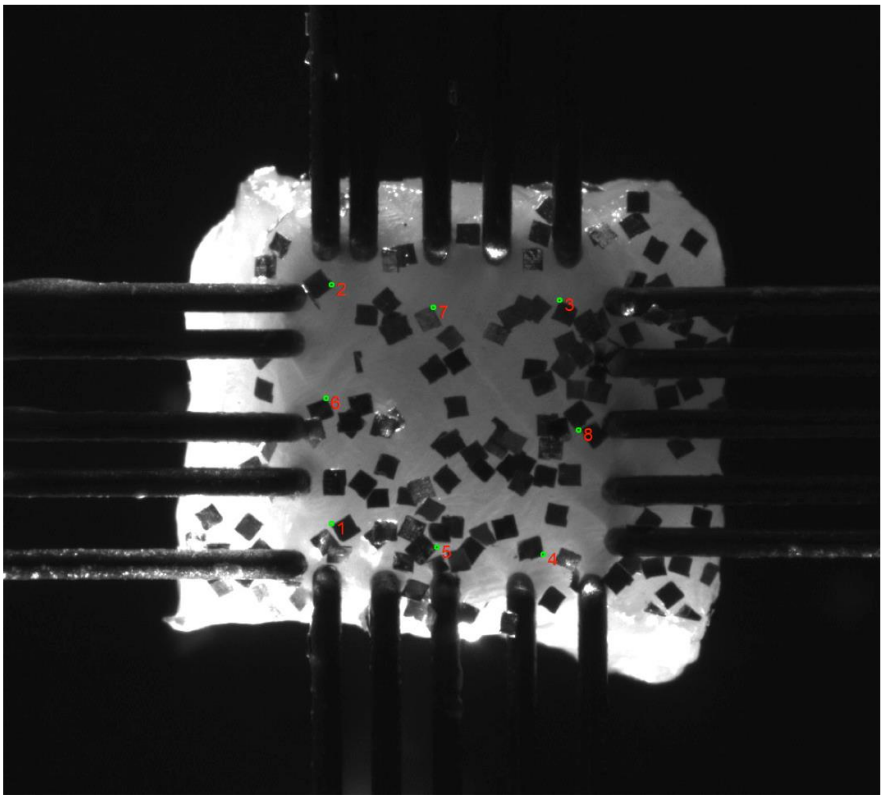

Figure 6-2: Annulus fibrosus tissue sample mounted in the BioTester apparatus using four Biorakes, each consisting of five sharpened tungsten wires. A total of eight virtual tracking markers, positioned at the apex of one of the reflective markers, were used for surface strain tracking.

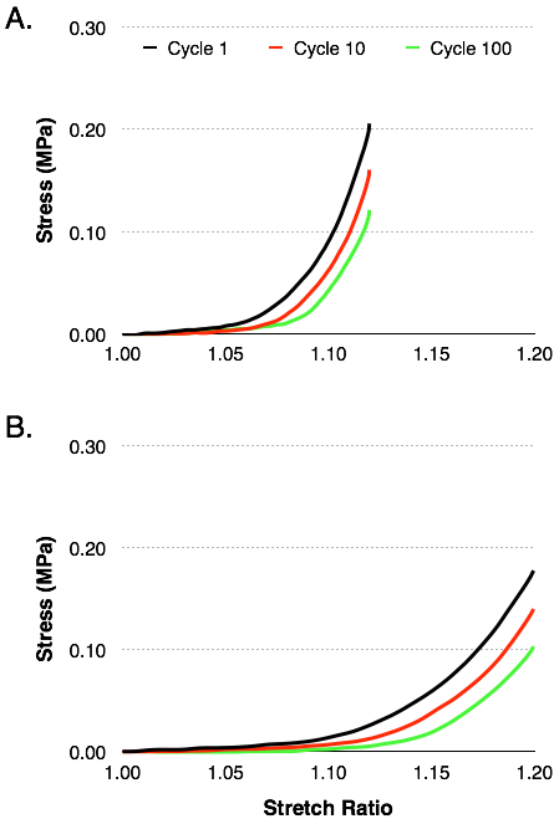

Figure 6-3: Sample cycle-varying changes of stress stretch-ratio loading curves for (A) circumferential and (B) axial loading axes (S7, c34, anterior sample, 10 cycles per minute).

6.3.6 Statistical Analyses

All statistical analyses were computed using SAS software (version 9.2, SAS Institute Inc., Cary, NC), with a significance level (α) of 0.05 determine *a priori*. Since AF tissue samples were reduced to a similar size (5 mm x 5 mm), it was decided *a priori* that all dependent measures would be collapsed across cervical level (i.e. c34, c56). A four-factor (radial location, magnitude of stretch, cycle rate and cycle number) repeated-measures general linear model, with time cycle number as a repeated measure was used examined pre/post changes in specimen thickness and mass. Simple effects were used to analyze all significant interactions (e.g. influence of radial location on peak stretch x cycle rate interaction). Effect sizes for all significant comparisons were evaluated using Cohen's d, using a pooled estimate of the population standard deviation from both groups (Cohen, 1988).

6.4 Results

6.4.1 Pre/Post Changes in Cross-Sectional Thickness and Mass

There was no significant change ($p = 0.5841$) observed in pre/post measurements of specimen cross-sectional thickness. However, a significant reduction in pre/post tissue mass emerged across all experimental conditions ($p = 0.0028$, $d = 0.43$; average difference = 9.3%). A significant interaction between the magnitude of tissue stretch and radial location on the IVD was also observed in pre/post measurements of tissue mass ($p < 0.0001$). Subsequent analysis of simple effects revealed that, on average, anterior AF tissue samples had greater mass than those excised from the posterior-lateral region ($p < 0.038$, $d > 0.77$; mean difference = 0.005 g), except for specimens tested in the 9-12% (circumferential/axial) stretch-ratio conditions ($p = 0.1637$). A summary of pre/post thickness and mass measurements across experimental conditions is summarized in **Table 6-1**.

6.4.2 Peak Tensile Stress

A significant three-way interaction across the radial location on the IVD, magnitude of peak tissue stretch and cycle rate ($p = 0.0053$), and significant two-way interactions between magnitude of tissue stretch and cycle number ($p < 0.0001$) and magnitude of tissue stretch

Table 6-1: Summary of pre/post measurements of specimen thickness and mass.

Rad. Loc.	Stretch Ratio (%)	Cycle Rate	Mass				Thickness			
			PRE		POST		PRE		POST	
			Mean	SD	Mean	SD	Mean	SD	Mean	SD
Anterior	6/10	5	0.040	0.006	0.036	0.006	0.875	0.094	0.866	0.092
Anterior	6/10	10	0.037	0.004	0.032	0.004	0.828	0.053	0.817	0.093
Anterior	9/15	5	0.032	0.008	0.029	0.005	0.768	0.114	0.760	0.117
Anterior	9/15	10	0.033	0.007	0.031	0.004	0.846	0.109	0.832	0.087
Anterior	12/20	5	0.039	0.006	0.035	0.007	0.777	0.089	0.753	0.094
Anterior	12/20	10	0.039	0.006	0.034	0.006	0.932	0.095	0.889	0.071
Posterior	6/10	5	0.031	0.009	0.026	0.009	0.802	0.075	0.788	0.111
Posterior	6/10	10	0.029	0.007	0.030	0.005	0.737	0.115	0.755	0.132
Posterior	9/15	5	0.037	0.009	0.032	0.010	0.872	0.087	0.847	0.106
Posterior	9/15	10	0.037	0.006	0.036	0.006	0.888	0.106	0.883	0.103
Posterior	12/20	5	0.037	0.010	0.034	0.010	0.822	0.112	0.879	0.141
Posterior	12/20	10	0.029	0.004	0.026	0.005	0.793	0.093	0.775	0.070

Note: Mass measurements include the reflective particles that were randomly scattered on the surface of each specimen.

and loading axis ($p < 0.0001$) were observed in measures of peak tensile stress. Subsequent analysis of the interaction between the magnitude of tissue stretch and cycle rate across both anterior and posterior-lateral AF tissue samples revealed that a significant two-way interaction emerged in both radial location ($p = 0.0006$ and $p < 0.0001$, respectively). However, Tukey's *post hoc* test revealed a significant difference in the magnitude of peak stress between cycle rates ($p = 0.01$) in the posterior-lateral region during the first loading cycle. Moreover, a significant difference between first and 100th loading cycle in the posterior-lateral region was also observed at a rate of 10 cycles per minute ($p = 0.0028$). No significant differences ($p = 0.5089$) between orthopedic loading axes were observed at 6-10%; however, significant differences were observed at 9-15% ($p = 0.0465$) and 12-20% stretch ($p < 0.0001$). Moreover, significantly greater peak stress was observed in the first stretch cycle ($p = 0.006$; $d > 0.51$; compared to cycles 10 and 100) at a stretch ratio of 12-20%. No significant cycle-varying changes in peak stress ($p > 0.9101$) were observed in the 6-10% or 9-15% stretch-ratio loading conditions. A summary of peak tensile stress for AF tissue samples excised from the anterior and posterior-lateral regions of the IVD is provided in **Figures 6-4** and **6-5**, respectively. A profile plot that illustrates the significant two-way interactions between peak stretch and cycle rate across radially locations on the IVD is provided in **Figure 6-6**. Moreover profile plots illustrating the significant two-way interactions between magnitude of peak stretch and loading axis, as well as magnitude of peak stretch and cycle number are provided in **Figure 6-7** and **Figure 6-8**.

6.4.3 Stress Stretch-Ratio Moduli

With a coefficient of determination criterion of 0.99 used to define the linear region of the stress stretch-ratio curve (i.e. S-S moduli), there were 25 specimens with no detected linear region; 16 specimens from the 9-10% stretch ratio condition, 8 specimens from 9-15% condition and 1 from the 12-20% condition. However, from the remaining 71 specimens, significant two-way interactions between the magnitude of tissue stretch and the axis of tensile loading ($p < 0.0001$), as well as the magnitude of tissue stretch and cycle rate ($p = 0.0004$) emerged. Subsequent analysis of simple effects revealed significantly greater magnitudes of S-S moduli in the circumferential direction at 12-20% magnitude of peak stretch ($p = 0.0090$; d = 0.84; mean difference = 0.39 MPa); however, no significant

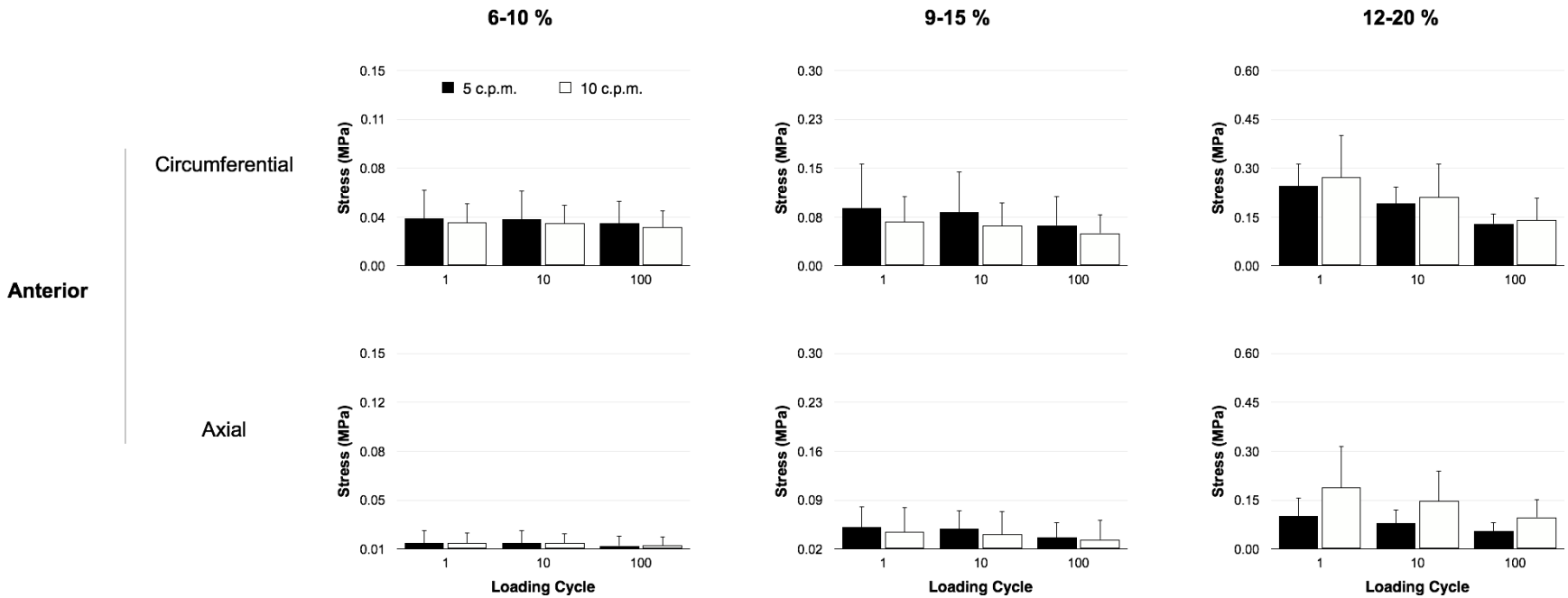

Figure 6-4: Peak tensile stress in annulus fibrosus tissue samples excised from the anterior region of the intervertebral disc, across experimental conditions. ***Note***: y-axis scale doubles when moving left to right.

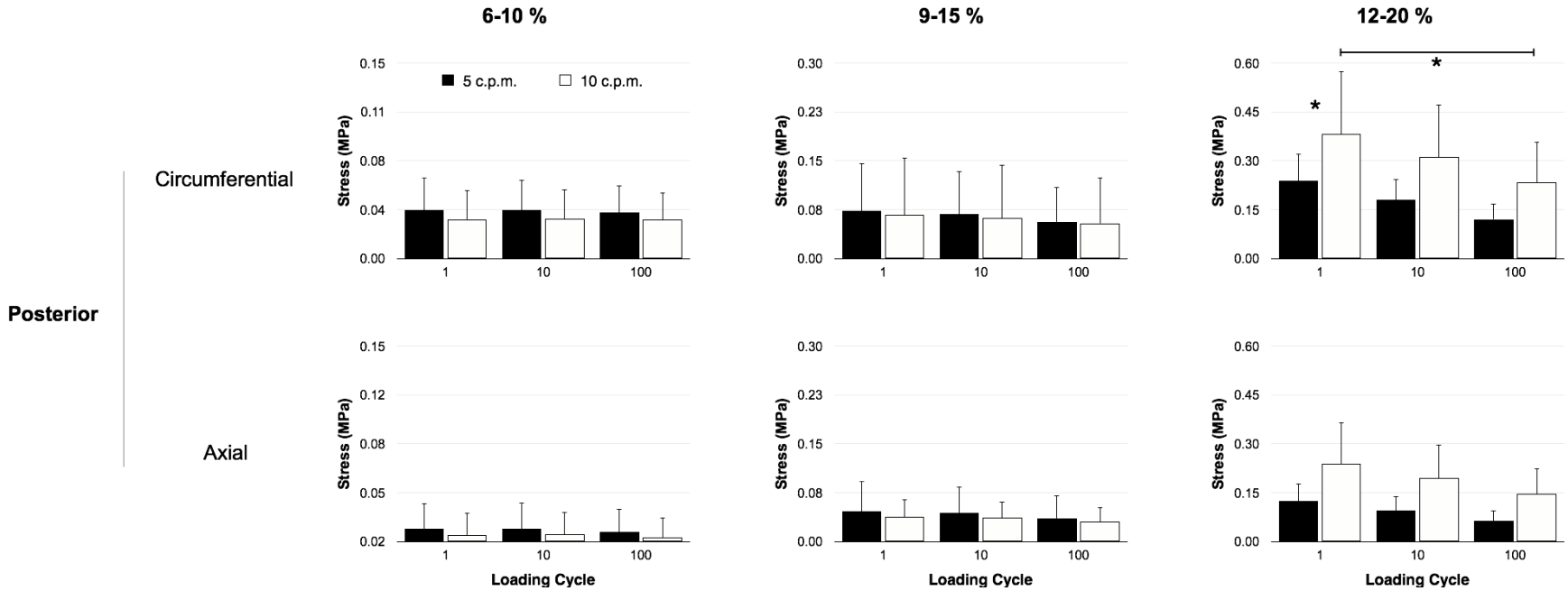

Figure 6-5: Peak tensile stress in annulus fibrosus tissue samples excised from the posterior-lateral region of the intervertebral disc, across experimental conditions. ***Note***: y-axis scale doubles when moving left to right.

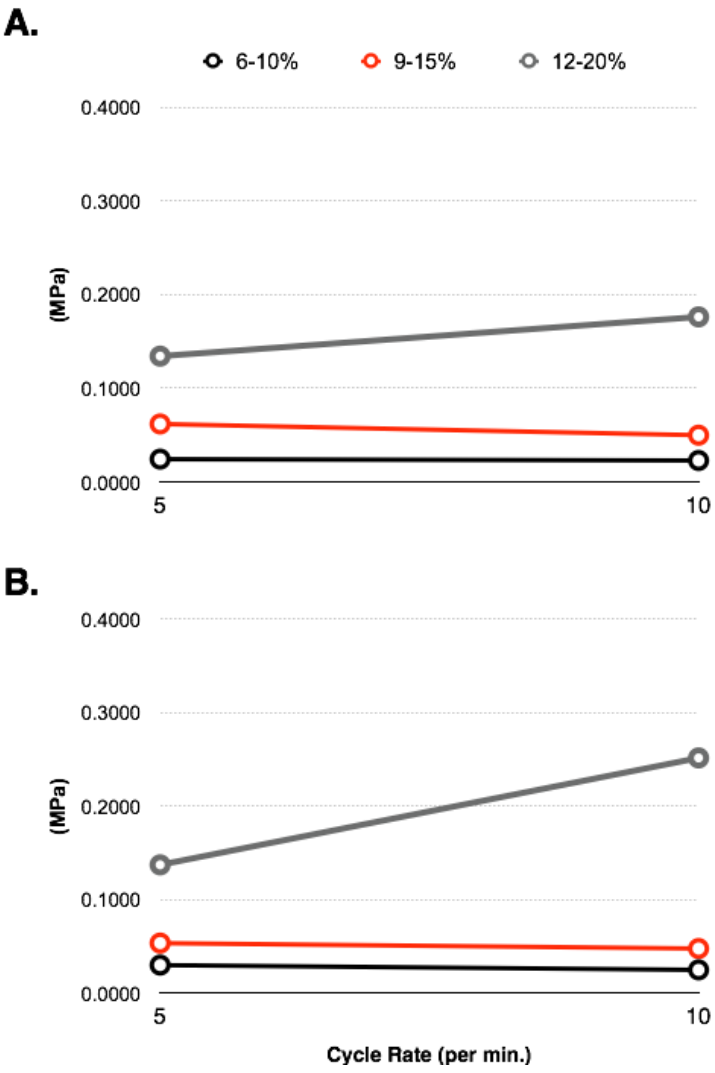

Figure 6-6: Profile plot of collapsed peak stress data across magnitude of peak stretch and cycle rate for: (A) anterior and (B) posterior-lateral regions.

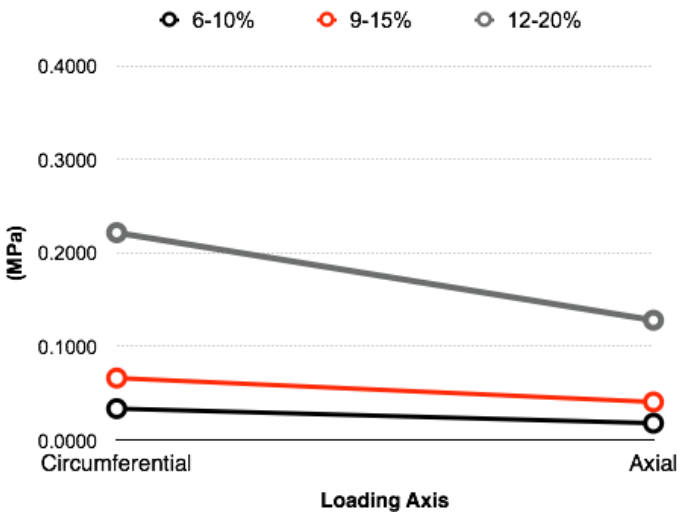

Figure 6-7: Profile plot of collapsed peak stress data across loading axis and magnitude of peak stretch.

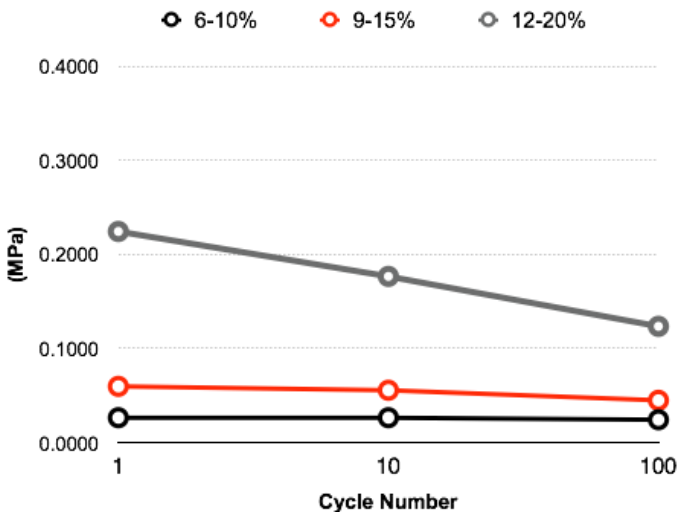

Figure 6-8: Profile plot of collapsed peak stress data across cycle number and magnitude of peak stretch.

differences were observed between the 6-10% and 9-15% tensile loading conditions (p > 0.4904). Moreover, there were no significant differences observed in the S-S moduli between cycle rates for the 6-10% and 9-15% tensile loading conditions (p > 0.9987); however, a significant difference did emerged in the 12-20% condition (p < 0.0001; d = 0.54; mean difference = 1.24 MPa). A summary of stress stretch-ratio moduli measures in AF tissue samples excised from the anterior and posterior-lateral regions of the IVD is provided in **Figures 6-9** and **6-10** respectively. Moreover profile plots illustrating the significant two-way interactions between magnitude of peak stretch and loading axis, as well as magnitude of peak stretch and cycle number are provided in **Figure 6-11** and **Figure 6-12**.

6.4.4 Peak Surface Strain

Significant two-way interactions between: (i) the magnitude of tissue stretch and axis of tensile loading (p < 0.0001), (ii) cycle rate and axis of tensile loading (p = 0.0174) and (iii) radial location on the IVD and cycle rate (p = 0.0005) emerged in cycle-varying measures of peak surface strain that were calculated using a virtual gauge region defined on the surface of each excised AF tissue sample. Subsequent analysis of simple effects revealed significantly greater peak surface strains at 10 cycles per minute in samples excised from the posterior-lateral region, compared to those which were loaded at 5 cycles per minutes (p = 0.0005; d = 0.33; mean difference = 0.01). Moreover, significantly greater peak strains were observed at each cycle rate (p < 0.0001; d = 0.78; mean difference = 0.02) when collapsed across each magnitude of tissue stretch. No significant differences (p = 0.0867) were observed between cycles 1, 10 and 100 in either axis of tensile loading. Summaries of peak surface strains measures in each axis of loading (i.e. axial, circumferential) across experimental conditions are provided in **Figures 6-13** and **6-14**, respectively. Moreover profile plots illustrating the significant two-way interactions between magnitude of peak stretch and loading axis, cycle rate and loading axis and radial location and cycle rate are provided in **Figure 6-15**, **Figure 6-16** and **Figure 6-17**. It is noted that the average peak surface strain about each axis of loading was less than the ascribed displacement for each experimental condition supporting the use of the virtual gauge region to eliminate the edge mounting effects caused by the rake insertions.

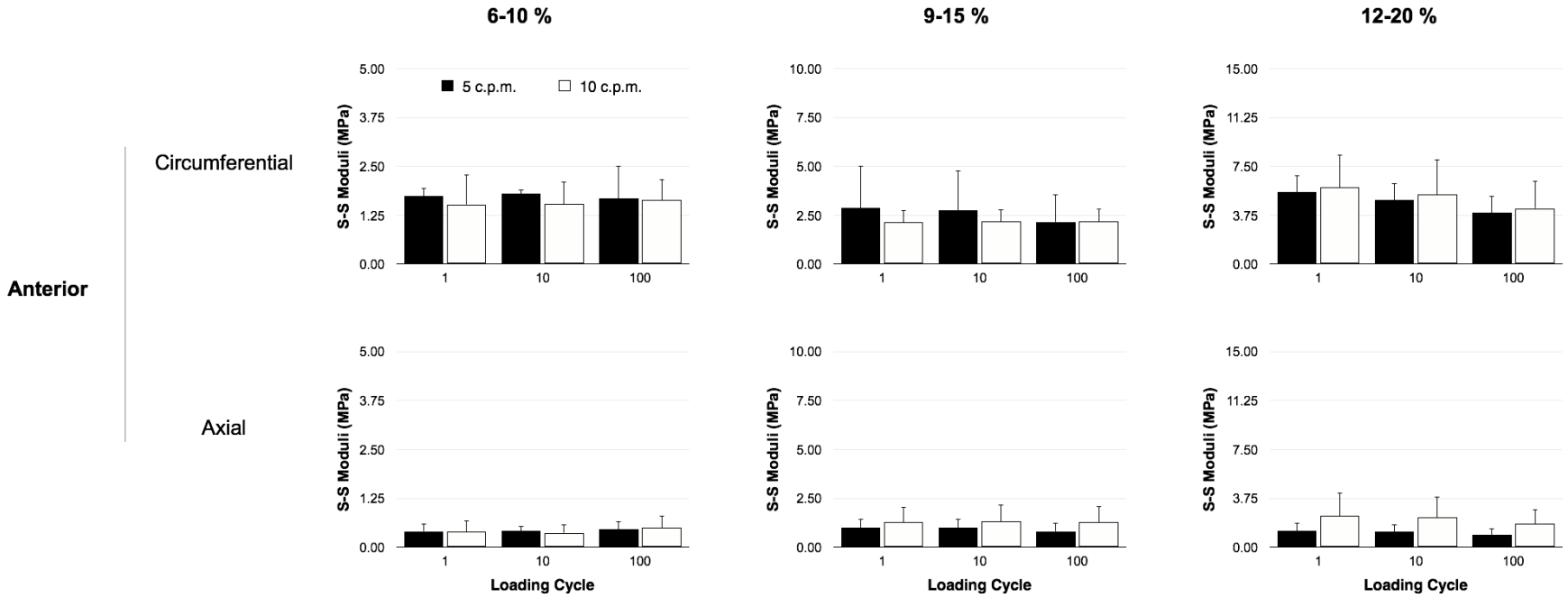

Figure 6-9: Stress stretch-ratio moduli of annulus fibrosus tissue samples excised from the anterior region of the intervertebral disc, across experimental conditions. ***Note***: y-axis scale doubles when moving left to right.

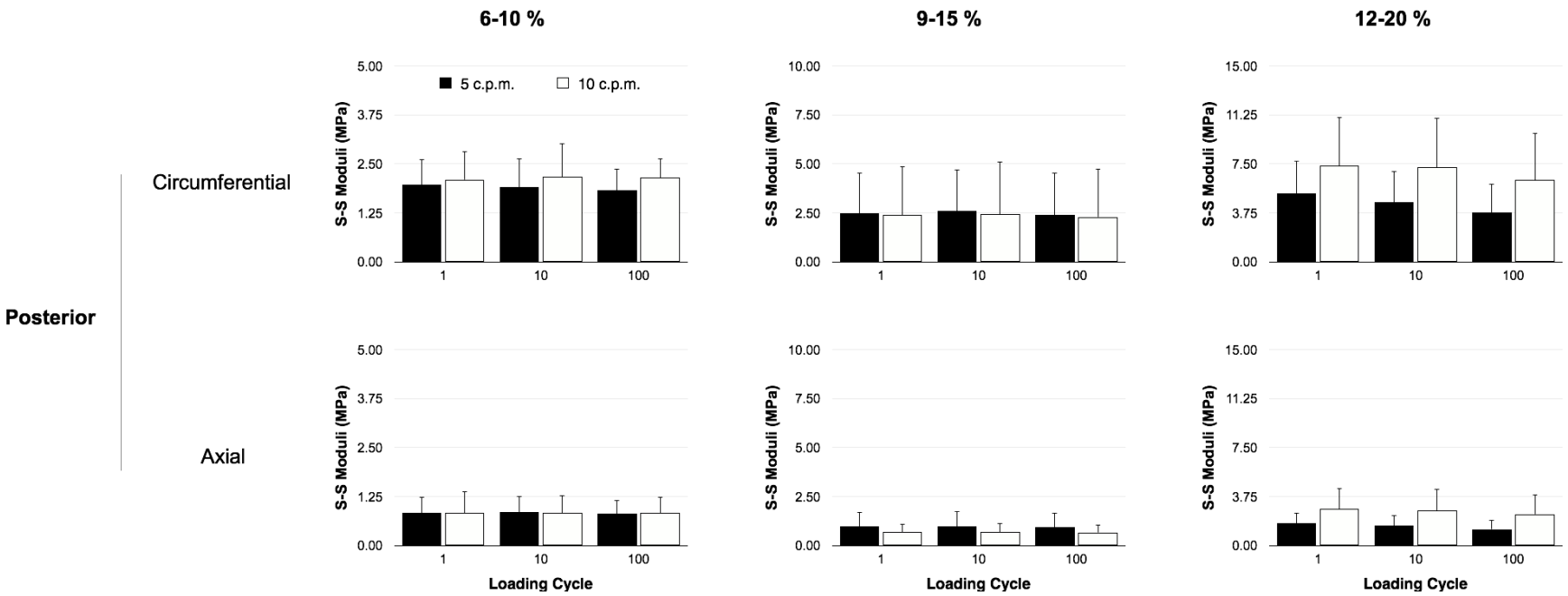

Figure 6-10: Stress stretch-ratio moduli of annulus fibrosus tissue samples excised from the posterior-lateral region of the intervertebral disc, across experimental conditions. ***Note***: y-axis scale doubles when moving left to right.

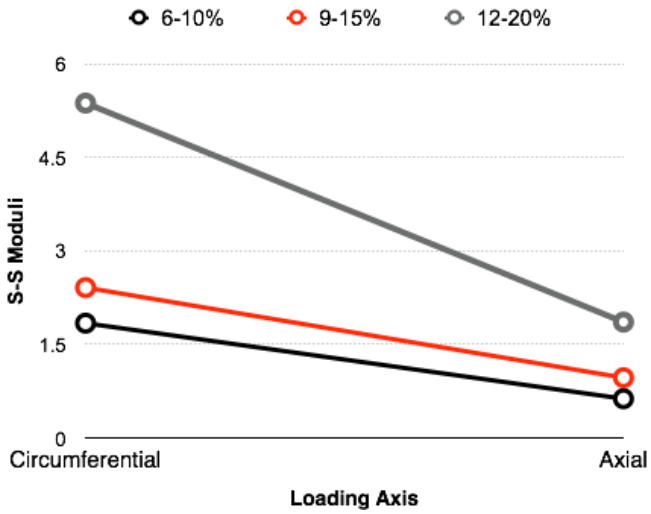

Figure 6-11: Profile plot of collapsed S-S moduli data across magnitude of peak stretch and loading axis.

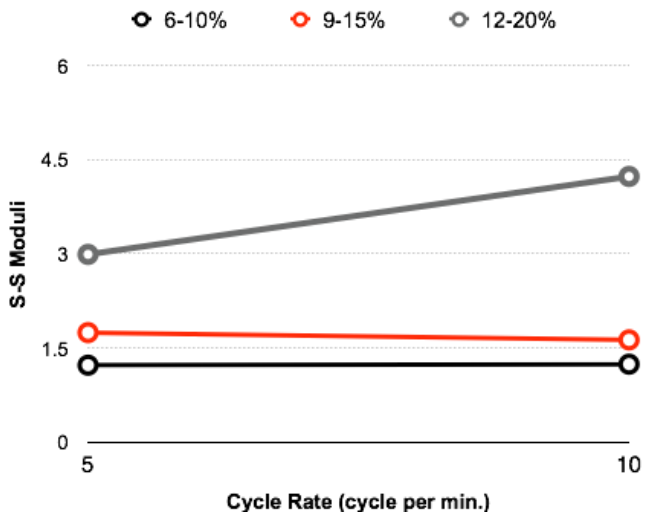

Figure 6-12: Profile plot of collapsed S-S moduli data across magnitude of peak stretch and cycle rate.

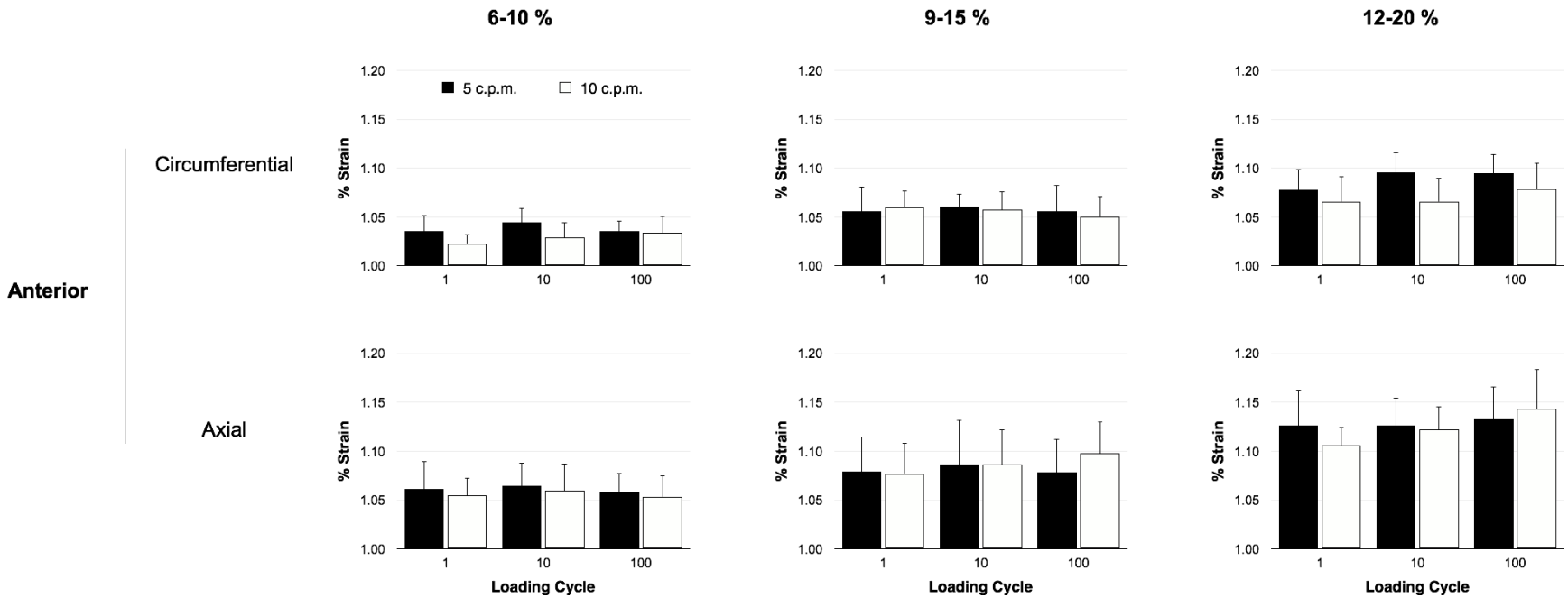

Figure 6-13: Average peak surface strains (%) in tissue samples excised from the anterior region of the intervertebral disc loading across experimental conditions.

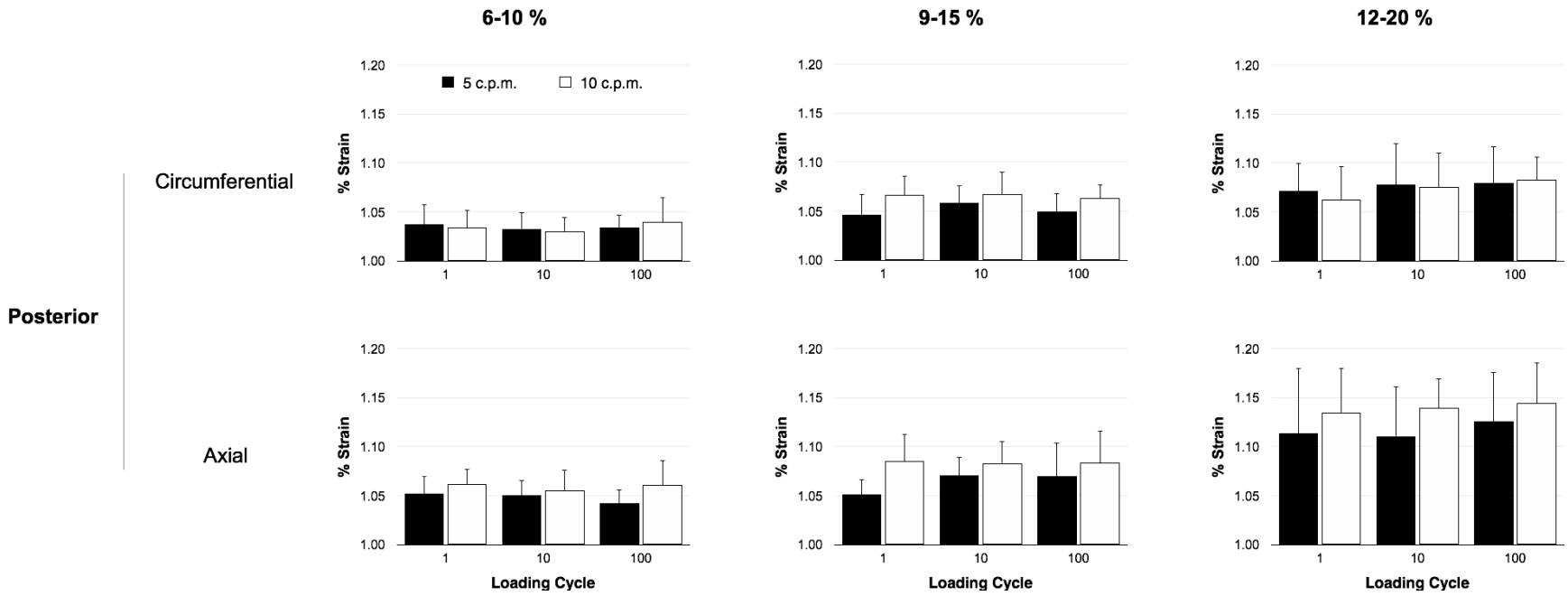

Figure 6-14: Average peak surface strains (%) in tissue samples excised from the posterior-lateral region of the intervertebral disc loading across experimental conditions.

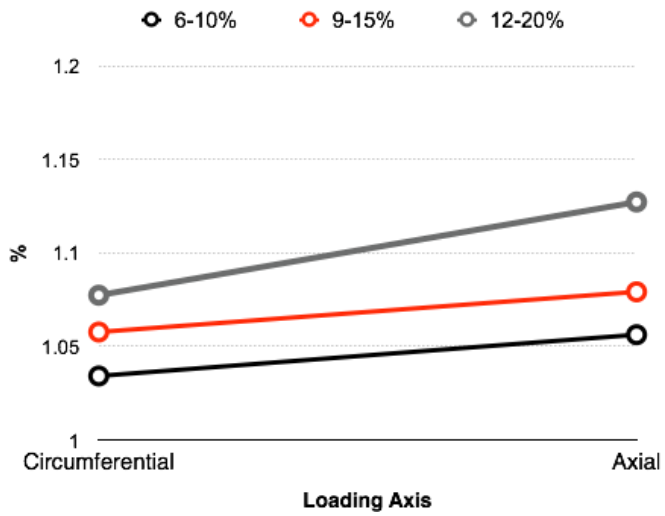

Figure 6-15: Profile plot of collapsed surface strain data across magnitude of peak stretch and loading axis.

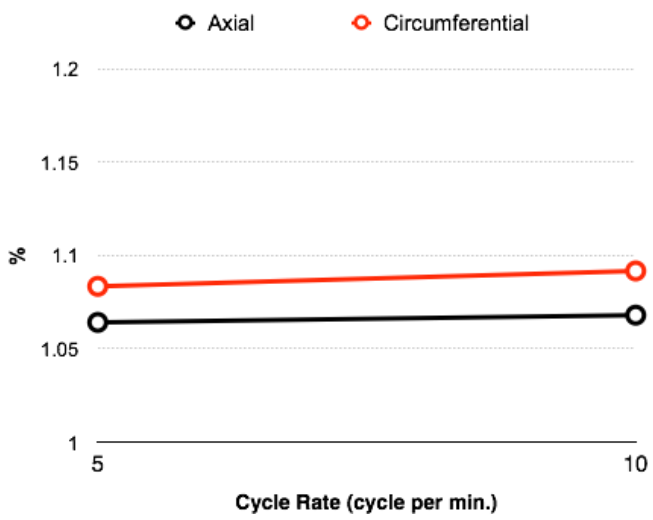

Figure 6-16: Profile plot of collapsed surface strain data across cycle rate and loading axis.

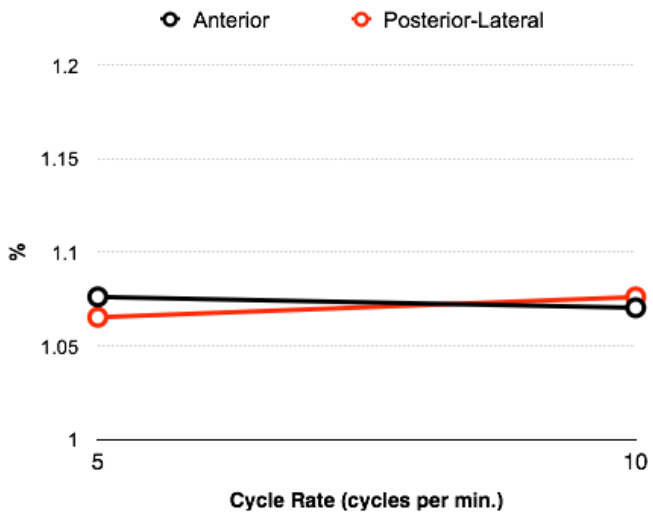

Figure 6-17: Profile plot of collapsed surface strain data across cycle rate and radial location on the intervertebral disc.

6.5 Discussion

Consistent with our hypothesis, there were a number of significant interactions that emerged in the mechanical properties of the AF across different regions of the IVD. Additionally, the mechanical response of excised tissue samples was found to be significantly different about each loading axis. Overall, the circumferential loading direction was associated with higher S-S moduli, resulting in greater peak tensile stress and lower peak surface strains. However, contrary to our hypothesis, AF samples excised from the posterior-lateral region of the IVD exhibited a significant difference in the magnitude of peak stress between cycle rates (p = 0.01) in the posterior-lateral region during the first loading cycle. Moreover, significantly greater peak surface strains at 10 cycles per minute were observed in AF tissue samples excised from the posterior-lateral region of the IVD.

Comparison of the results from this study to previous research is challenging, since the majority of fatigue testing of isolated AF tissue samples has been performed using uniaxial methods. Green et al. (1993) were some of the first to conduct cyclic fatigue testing of human AF tissue using a sawtooth waveform (2 seconds cycle duration) at varying levels of specimens' peak ultimate tensile strength. Vertical slices of AF and bone (5 mm thick and 15 mm wide) obtained from the anterior and posterior margins of human lumbar intervertebral joints were employed for testing; however, the authors failed to report how specimen hydration was maintained across the 10,000 cycle loading protocol. Findings from their work suggest that the AF will not accumulate fatigue damage if the vertical stresses applied to the AF (as would result from forward bending) remain below 45% of the magnitude of force required to cause damage in a single cycle (Green et al., 1993). More recent work conducted by Iatridis et al. (2005) using AF tissue obtained from mature bovine discs has examined the effect of both the number of loading cycles and magnitude of tensile strain on micro-structural tissue damage with cyclic uniaxial testing. The baseline loading protocol, which consisted of 1600 cycles (triangular waveform; strain rate of 2.5% per second; tissue samples submerged in a PBS bath) of uniaxial tensile loading at 40% of specimens' ultimate tensile strength (approximately 8.52% strain) resulted in over a 20% reduction of peak stress, as well as permanent deformation of approximately 3% elongation (Iatridis et al., 2005). Based on these results, the authors hypothesized that these changes

could manifest as sub-catastrophic damage in the AF, by way of an increased neutral zone, IVD disc bulging and loss of intradiscal pressure in FSUs that are typically employed for cyclic mechanical testing. Although the present work was conducted in displacement control, due to the fact that similar magnitudes of peak stretch were used for testing, it is hypothesized that greater magnitudes of residual elongation would emerge under cyclic biaxial tensile loading conditions.

When comparing the stress stretch-ratio profile from the first loading cycle in the present study to previous work conducted by our group using bilayer AF tissue samples (average thickness of 0.36 mm) (Gregory & Callaghan, 2011), it is noted that the peak stresses observed in our 12-20% loading condition were much lower in samples excised from both the anterior and posterior regions; however, the cross-sectional area of our AF tissue samples was larger due to the increased thickness of the multilayer AF tissue sample. However, the S-S moduli that were recorded in the circumferential direction (average of 5.55 and 5.22 MPa for the anterior and posterior-lateral tissue samples, respectively) were of similar magnitude when collapsed across depth in the Gregory and Callaghan (2011) study, despite the lower magnitude of peak axial tissue stretch in the present work. The lack of a defined linear region in 25 AF tissue samples that were assigned to loading conditions with lower magnitudes of peak stretch was not entirely unexpected. With a peak stretch ratio of 1.23 applied over 20 seconds, Gregory and Callaghan (2011) reported that the linear portion of the stress-stretch ratio curve began at a mean stretch ratio of 1.19. Although not examined in the present study, it is likely that the increase rate of stretch that was applied in the present work can be used to explain why a linear region in the stress stretch-ratio curve emerged at lower magnitudes of stretch.

To the best of the authors' knowledge, this investigation represents one of the first studies to characterize the cycle-varying changes in the mechanical properties of the AF with cyclic, biaxial tensile loading. However, there are a number of potential limitations that should be addressed. Unfortunately, due to methodological difficulties in controlling the hydration of the excised tissue samples we were limited in the number of cycles that could be collected. In particular, it was found that even in a temperature and humidity controlled local testing environment the specimens started to exhibit signs of dehydration (e.g.

increased S-S moduli, higher peak stress, etc.) after 100 cycles. This is evident by the significant change in mass that was observed pre and post testing. Although fluid loss is a known physiological response of the IVD *in vivo* (Adams, Dolan, Hutton & Porter, 1990), it must be acknowledged that the local testing environment is likely not a true representation of the *in vivo* physiological conditions in the lumbar spine. However, based on pilot testing results conducted with AF samples submerged in a 0.9% weight/volume saline bath, it was immediately apparent that the cross-sectional thickness of the AF samples increased very rapidly. In fact, controlled testing that was conducted in preparation for this study revealed that the cross-sectional thickness of AF tissue samples (comprised of 3-5 lamellae) excised from the anterior region of the IVD, increased an average of 150% after 30 minutes of submersion in a 0.9% saline bath (Gruevski, Gooyers, Karakolis & Callaghan, 2014).

Our decision to conduct all testing in a temperature and humidity controlled local testing environment was justified based on the preliminary results from this work, which demonstrated that, on average, a 15% (SD = 18) increase in thickness and a 17% (SD = 16%) increase in mass for isolated AF tissue samples (unloaded) that were stored in a temperature (29° C ± 1) and humidity (90% ± 5) controlled local testing environment after 120-minutes (Gruevski et al., 2014). This is consistent with earlier research conducted by Hirsch and Galante (1967), which demonstrated that a temperature and humidity controlled local testing environment was preferred for tensile testing of AF tissue. More recent studies (Ebara et al., 1996; Iatridis et al., 2005) have opted to conduct their mechanical testing of isolated AF tissue in a physiological saline bath, despite the significant swelling and mass gain that occurs; however, a 30 minute pre-soak has been deemed acceptable for tissue samples to reach equilibrium. Interestingly, a recent study conducted by Iatridis et al. (2005) using a scanning electron microscope has identified small tubules parallel to the collagen fibers in the AF of rat-tail IVD tissue, which are similar to those that have been reported in articular cartilage. It has been suggested that the structure of these tubules may contribute to the tensile modulus of the AF, and could provide a mechanism for compartmentalization of water throughout the tissue (Iatridis et al., 2005). A second limitation of the present work is the longer duration of loading cycles (6 seconds) that were included in the present study, compared to the previous chapters of this thesis (Chapter 1 – average lift time was 0.85 seconds for controlled lifting trials; Chapter 2,3 – 2 second loading cycles were employed).

Despite previous research that failed to show a significant effect of loading rate on bi-layer samples of AF tissue (Gregory & Callaghan, 2010), there was a noticeable rate effect observed during pilot testing with multilayer samples, which resulted in technical difficulties in keeping the sharpened tungsten rakes fixed within the specimens, as they slowly work their way up and out of the tissue sample at higher loading rates. For this reason, we decided to extend each stretch/recovery cycle to 6 seconds (three seconds each), corresponding to a maximum loading rate of 4 and 6.66 % (circumferential-axial) respectively. It should also be noted that the lower magnitudes of peak surface strain about each loading axis, when compared to the overall displacement of the linear actuators, were not entirely unexpected. Specimen mounting followed the recommended guidelines that have been previously reported for biaxial testing of soft tissues using the BioTester system (Eilaghi et al., 2009) (i.e. five attachment points per side, apron width equal to 0.6-1.0x the tine spacing). Previous research by Eilaghi et al. (2009) has shown that the reduced magnitude of strain in the central area of the specimen may be, in part, due to relative movement between the tine and the tissue sample as the magnitude of the applied load (or stretch) increases. Moreover, the virtual strain tracking is dependent on the adhesion between the tiny reflective particles and the top surface of the tissue.

6.6 Conclusion

Results from this study emphasize the cycle-varying tensile stress response of the AF, which changed across loading axis and region of the IVD. However, no significant changes were observed in S-S moduli after 100 cycles of biaxial tensile loading. These findings provide novel insight into the cycle-varying stress-relaxation response that occurs in multilayer samples of AF tissue, which may be linked to the known mechanism of failure (i.e. development of fissures and clefts) under cyclic loading conditions. Results from this study may also have important implications for finite element models of the IVD that consider time-varying loading scenarios with no consideration for the cycle-varying changes in the mechanical properties of the AF. Future research should examine longer durations of fatigue loading at higher magnitudes of peak stretch. It will also be important that future work characterize the *in vivo* hydration environment of the IVD in order to more closely mimic the actual physiological conditions for prolonged, cyclic loading protocols.

Chapter 7
Synthesis of Contributions

7.1 Thesis Summary

The global purpose of this thesis was to explore interactions between external task demands (i.e. force, repetition and posture) on *in vivo* joint loading in the lumbar spine and characterize the combined effects of these mechanical exposures on fatigue injury pathways in the intervertebral disc (IVD), a common source of low back pain (Dammers & Koehler, 2002; DePalma et al., 2011; Schwarzer et al., 1995). In particular, the four studies included in this thesis were conducted to:

i. Explore the complex interactions that exist between: (i) magnitude of external load, (ii) speed of movement, and (iii) postural symmetry on estimates of *in vivo* low back joint loading during a simulated occupational lifting task (**study I**).

ii. Examine the combined effects of: (i) the magnitude of the applied compressive force, (ii) frequency of loading (i.e. cycle rate) and (ii) degree of postural deviation on known fatigue injury pathways in porcine cervical functional spinal units (FSUs) at sub-acute-failure magnitudes of peak compressive force and to characterize the micro-structural damage imposed to the IVD in "survivor" specimens using histological staining methods (**study II)**.

iii. Characterize interactions between: (i) the magnitude of the applied compressive force, (ii) cycle rate and (ii) degree of postural deviation on IVD height loss, as well as pre/post changes in AF bulging to better understand the structural changes that occur in the IVD with cyclic compressive loading (**study III)**.

iv. Explore interactions between the magnitude of peak tissue stretch and cycle rate on cycle-varying changes in the mechanical properties of the annulus fibrosus (AF) tissue during cyclic, biaxial tensile loading (**study IV)**.

Study one provided insight into the *in vivo* low back kinetic response to various external task demands during occupational lifting. Using biomechanics data collected from a sample of participants with manual material handling experience (Beach, 2011; Frost et al., 2012), this investigation explored interactions between: (i) the magnitude of the load, (ii) movement speed and (iii) posture on estimates of L4/L5 compression and shear using a dynamic, EMG-assisted, three-dimensional dynamic model of the lumbar spine (Cholewicki & McGill, 1996). Results from this study provide strong evidence that known mechanical low back injury risk factors should not be viewed in isolation. Stated differently, the influence of external demands on *in* vivo estimates of joint loading cannot simply be treated as independent additive factors. Therefore, injury prevention efforts need to consider the complex interactions that exist between external task demands and their combined influence on resultant internal joint loads.

Study two explored the combined effects of: (i) the magnitude of the applied compressive force, (ii) cycle rate and (ii) degree of postural deviation on known fatigue injury pathways in porcine cervical FSUs exposed to sub-acute-failure magnitudes of cyclic compressive force. Using a biofidelic time-varying waveform that was based on the *in vivo* estimate of compressive loading and postural deviation in the lumbar spine during an occupational lifting task, this study provides strong evidence that the mechanism for fatigue injury is dependent on the combined effects of all three mechanical exposures that were investigated. Consistent with previous research (Brinckmann et al., 1988; Parkinson & Callaghan, 2009) it was found that when the magnitude of the applied load was greater than 20% UCT, fatigue fracture of the cartilaginous endplate would occur in less than 5000 loading cycles. Moreover, exaggerated dynamic postural deviation shifted the "weakest link" to either the attachment site of the cartilaginous endplate to the vertebral body (i.e. avulsion injury) or to the pars interarticularis. However, an important contribution of this work is that considerable disruption to the IVD (e.g. clefts, fissures, delamination) was observed through histological analyses in specimens that otherwise would have been considered "survivors" of the cyclic loading protocol. It is noteworthy that a qualitative depiction of emerging interactions could be detected in representative histological images (e.g. interaction between postural deviation and cycle rate in posterior-lateral tissue samples). Although there was no consistent trend in the amount of damage that was observed between 10%

and 20% UCT loading conditions, a noticeable effect of posture was observed, with increased damage in tissue samples from the 300% NZ range condition. Tissue samples excised from the posterior-lateral region were also found to have more disruption in comparison to those excised from the anterior region of the IVD. Similarly, more disruption was observed in sections that were obtained from deeper layers of the IVD, compared to those obtained from the superficial portion of the AF. Results from this study provide novel insight into the combined effects the magnitude of the applied compressive load, frequency of loading, and degree of postural deviation on injury pathways in the lumbar spine. Future efforts in injury prevention should consider more than just the magnitude of the applied force when evaluating risk of low back injury (i.e. the technique employed for lifting should also be considered).

Using the same cohort of porcine FSUs, study three characterized interactions between the same three mechanical exposures (i.e. force, repetition and posture) on the structural changes that occurred in the IVD among "survivor" specimens across loading conditions. Specifically, using a 3D displacement laser sensor system, this investigation quantified pre/post changes in IVD height loss and AF bulging across loading conditions. Three-dimensional surface profiles of the anterior aspect of the IVD were produced for each specimen, which enabled IVD height loss to be partitioned from net changes in specimen height, as calculated from the vertical position of the materials testing system actuator. Moreover, the magnitude of IVD bulging was quantified in a flexed posture pre- and post-cyclic loading. Overall, a significant three-way interaction between the magnitude of peak compressive force, cycle rate and degree of postural deviation was observed in cycle-varying specimen height loss data. However, total specimen height loss was not an accurate depiction of cycle-varying changes in the IVD, since peak compressive force was the only independent factor that influenced IVD height loss. Significant main effects of postural deviation and time were observed in peak measures of AF bulge, with increased AF bulging observed both before the cyclic loading protocol and in the 100% NZ postural condition. Collectively, findings from this study suggest that in the absence of spinal posture measures, estimates of peak and cumulative compressive loading may not be sufficient to describe the risk of injury to the IVD injury.

Study four, the final investigation included in this thesis, further refined the insight gained from studies II and III on the mechanical response of the IVD to cyclic loading in characterizing interactions between the magnitude of peak tissue stretch and cycle rate on the mechanical properties of the AF tissue during cyclic, biaxial tensile loading. Specifically, cycle-varying changes in the stress stretch-ratio profiles were compared across both axial and circumferential loading axes in isolated multilayer AF tissue samples excised from both the anterior and posterior-lateral regions of the IVD. Results from this study showed that significant interactions between the radial locations on the IVD, magnitude of tissue stretch and cycle rate emerged in peak measures of tensile stress and surface strain. However, it is interesting that no significant changes were observed in S-S moduli throughout the cyclic loading protocol. These findings provide novel insight into the cycle-varying stress-relaxation response that occurs in multilayer samples of AF tissue, which may be linked to the known mechanism of failure (i.e. development of fissures and clefts) under cyclic loading conditions.

7.2 Hypotheses Revisited

As outlined in section 1.4, the general hypothesis for this thesis was that a significant interaction between external task demands would emerge in estimates of *in vivo* joint loading in the lumbar spine and that the combined effects of these exposures would have a significant influence on the mechanical response and fatigue injury pathways in the IVD. Collectively, the findings from this thesis indicate that the combined effects of the magnitude of the applied load, cycle rate (which inevitably affects movement speed) and postural deviation interact to modulate both the resultant load in the lumbar spine (*in vivo*), as well as the mechanical response (and resultant injury pathways) of the intervertebral disc under cyclic loading conditions. The following is a summary of the decisions regarding the null hypotheses that were developed for this thesis:

i. There will be no significant interaction between the magnitude of the external load, speed of movement and postural symmetry on estimates of *in vivo* joint loading in the lumbar spine (**study I**).

DECISION: The null hypothesis is rejected.
Significant interactions between load, speed and posture emerged in both peak and cumulative estimates of L4/L5 joint compression and shear.

ii. The mechanism of fatigue injury in isolated FSUs will not differ across levels of peak compressive force, cycle rate and postural deviation (**study II**).

DECISION: The null hypothesis is rejected.
Consistent with previous research, it was found that when the magnitude of the applied load was greater than 20% UCT, fatigue fracture of the cartilaginous endplate occurred in less than 5000 loading cycles. Moreover, exaggerated dynamic postural deviation shifted the "weakest link" to either the attachment site of the cartilaginous endplate to the vertebral body (i.e. avulsion injury) or to the pars interarticularis.

iii. There will be no differences in the magnitude of micro-structural tissue damage imposed to the AF across cyclic compressive loading conditions (**study II)**.

DECISION: The null hypothesis is rejected.
Considerable disruption to the IVD (e.g. clefts, fissures, delamination) was observed through histological analyses in specimens that otherwise would have been considered "survivors" of the cyclic loading protocol. It is noteworthy that a qualitative depiction of emerging interactions could be detected in representative histological images (e.g. interaction between postural deviation and cycle rate in posterior-lateral tissue samples). There was no consistent trend in the amount of damage that was observed between 10% and 20% UCT loading conditions. However, a noticeable effect of posture was observed, with increased damage in tissue samples from the 300% NZ range condition.

vi. There will be no differences in IVD height loss or AF bulging across cyclic loading conditions paired with dynamic flexion/extension (**study III)**.

DECISION: The null hypothesis is rejected.

Total specimen height loss was not an accurate depiction of cycle varying changes in the IVD, since peak compressive force was only independent that influenced IVD height loss. Significant main effects of postural deviation and time were observed in peak measures of AF bulge, with increased AF bulging observed both before the cyclic loading protocol and in the 100% NZ postural condition. Overall a wide range of Pearson product-moment correlation was observed (r = -0.44 to 0.78) between IVD height loss and IVD bulging across experimental conditions.

iv. There will be no cycle-varying changes in the mechanical response of isolated AF tissue exposed to cyclic, biaxial tensile loading (**study IV**).

DECISION: The null hypothesis is rejected.
Significant interactions between the magnitude of tissue stretch and cycle rate emerged in peak measures of tensile stress and surface strain. However, no significant changes were observed in S-S moduli after 100 cycles of biaxial tensile loading.

7.3 Summary of Contributions

The following is a summary of the novel scientific contributions from the research that has been presented in this thesis.

Study I:

i. Results from this study provide strong evidence that known mechanical risk factors linked to low back injury should not be viewed in isolation. Significant interactions between load, movement speed and symmetry of initial load placement (i.e. posture) emerged in every dependent measure that was used to characterize time-varying measures of L4/L5 compression and shear.

ii. A significant contribution from this work is the assessment of lumbar spine joint loads in a large sample of participants with manual materials handling experience across such a wide range of external task demands.

Study II:

i. This investigation represents one of the first efforts to pair *in vitro* biomechanical testing of FSUs with histological staining methods to characterize the combined effects of various mechanical risk factors linked to low back injury and IVD disruption.

ii. Findings from this work underscore the importance that future efforts to prevent low back injury should focus on more than just peak and cumulative loading exposures, since cyclic postural deviation was observed to have the most pronounced effect of the magnitude of micro-structural disruption.

iii. Results from this study highlight that threshold limit values for cumulative load exposure that are based on *in vitro* tests of FSUs that did not experience a fatigue related injury (e.g. endplate fracture) may overestimate the true capacity of the lumbar spine, since considerable disruption to the AF was observed in "survivor" specimens.

Study III:

i. This study represents one of the first efforts to partition of IVD height loss from total specimen height loss, and characterizes pre/post changes in IVD bulging across a wide range of cyclic compressive loading conditions.

ii. Results from this study provide strong evidence that total FSU height loss in *in vitro* spine biomechanics studies is a poor descriptor of the structural changes that occur within the IVD with cyclic compressive loading.

iii. This study also represents one of the first investigations to characterize pre/post changes in AF bulging with cyclic compressive loading.

Study IV:

i. This investigation represents one of the first efforts to characterize cycle-varying changes in mechanical properties of AF tissue with cyclic biaxial tensile loading.

ii. Results from this study provide novel insight into the cycle-varying stress-relaxation response that occurs in multilayer samples of AF tissue, which may be linked to the known mechanism of failure (i.e. development of fissures and clefts) under cyclic loading conditions.

iii. The temperature and humidity controlled local testing environment was a custom accessory that was developed for this study, which had not previous been available for the BioTester system.

7.4 Synthesis of Contributions

To combine some of the scientific contributions that emerged from both the *in vivo* modeling of human movement during simulated occupational lifting (**study I**), as well as the cyclic loading of functional spinal units to characterize the different fatigue injury mechanisms and structural changes that occur across loading conditions (**study II & III**) it was first necessary to normalize the magnitude of peak compressive force estimates (**study I**) to each participant's predicted spinal compression tolerance limit.

The regression equation (**Equation 7-1**) proposed by Genaidy et al. (1993) is one of the most widely adopted methods to predict the human lumbar SCTL. This research was based on the experimental data of Hutton and Adams (1982), Hansson et al. (1987) and Adams and Hutton (1982), and considers the age, gender, lumbar spinal level, and body weight of participants. However, the influence of posture, loading rate (i.e. movement speed) and cycle rate (i.e. number of repetition) – all shown to be important factors in this thesis are not accounted for with this method. Nonetheless, it is the author's opinion that this still represents one of the best prediction methods in the biomechanics literature.

Equation 7-1

$$CS = -13331.2 - (73.7 \times AGE) - (962.6 \times GENDER) + (403.0 \times LMS) + (79.8 \times BW)$$

where:

CS	=	*estimated compressive strength (N)*
AGE	=	*participant's age (years)*
GENDER	=	*participants' gender (male = 1, female = 2)*
LMS	=	*lumbar motion segment*
		(L1/L2 = 44, L2/L3 = 45, L3/L4 = 46, L4/L5 = 47, L5/S1 = 48)
BW	=	*participant's body weight (kg)*

However, to reduce the probability of injury resulting from manual materials handling, Genaidy et al. (1993) recommended that the biomechanical tolerance limit of the spine be set at the damage load, which had been defined as the force that cause the first gross sign of damage (e.g. tissue fluid, blood, localized tissue damage), which could range from 33 to 93% of the compressive strength of the vertebrae, with an average value of 60%. The following equation (**Equation 7-2**) was proposed to describe the relationship between the damage load (DL) and the estimated compressive strength (CS).

Equation 7-2

$$DL = -805.18 + (0.74554 * CS)$$

where:

DL	=	*damage load (N)*
CS	=	*estimated compressive strength (N)*

Therefore, based on the age, gender and body weight of the 34 participants that were included in **study I**, the peak compressive forces that were estimated using a three-dimensional, dynamic, EMG-assisted model of the lumbar spine across lifting conditions (i.e. data presented in **Figure 3-3**, Chapter 3) were normalized to their predicted CS and DL. The ensemble averaged data are shown in **Figure 7-1** and **Figure 7-2**, respectively. It is noteworthy that across external task demands that the average relative percentage of loading (normalized to CS) ranged from 29 to 54%, with the lowest margin of safety (i.e. 1 – normalized peak load) observed in the high-load (24.7 kg), high-speed ("as fast as comfortable) lifting trials with symmetrical load placement. As expected, a similar trend remained when peak estimates of *in vivo* joint loading at L4/L5 were compared to the estimated DL; however, the relative percentage was scaled higher – ranging from 44 to 83% (on average). Although estimates of *in vivo* lumbar spine loading at L4/L5 never exceeded the predicted compressive strength (max = 79.4%; observed during the 2nd trial of a controlled, symmetrical lift of 24.7 kg; male, age = 46 years, weight = 95.25 kg); however, it did surpass the DL by 21.2%.

Considering the survival analysis (**study II)** of porcine FSUs that was conducted across levels of: (i) magnitude of peak compressive force, (ii) cycle rate and (iii) postural deviation, it is noteworthy that the probability of survivorship was less than 67% UCT after 5000 cycles of cyclic loading at 40% UCT. Previous research conducted by Brinckmann et al. (1988) has suggested that 5000 cycles was representative of approximately two weeks of manual materials handling work. For example, based on the 50th percentile lifting frequency (1 cycle per minute) that was presented by Dempsey et al. (2003) that was based on a sample of 547 industrial lifting tasks, this assertion seems reasonable, as 5000 cycles would accumulate in just over two weeks (assuming 480 lifts per day results in 2400 lifts in one week). However, similar to previous studies that have cyclically loaded FSUs to estimate the fatigue life across experimental conditions, fatigue injury was defined as macro-structural to the joint (e.g. endplate fracture); whereas most musculoskeletal disorders do not characterize complete disruption of a tissue. Moreover, the absence of any physiological repair mechanism must be acknowledged; however, the natural healing rate of

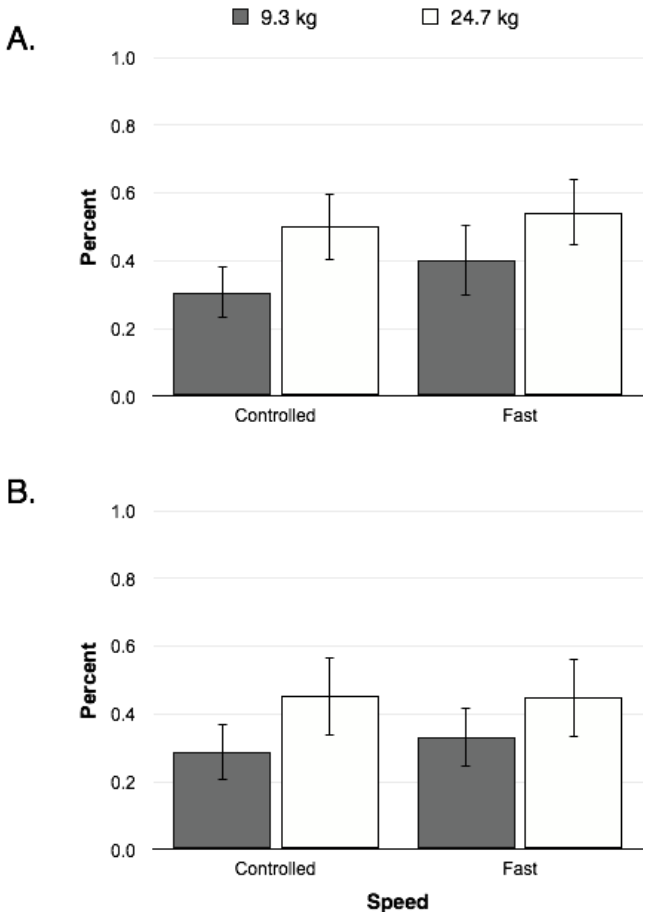

Figure 7-1: Summary of L4/L5 peak compressive joint loading across (A) symmetrical and (B) asymmetrical lifting trials, normalized to individual estimates of L4/L5 compressive strength.

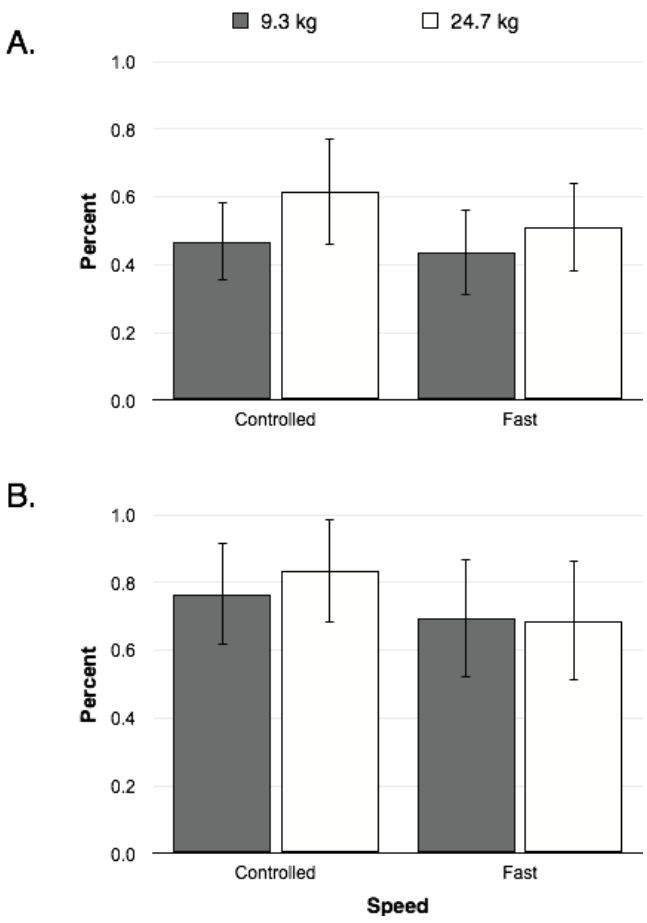

Figure 7-2: Summary of L4/L5 peak compressive joint loading across (A) symmetrical and (B) asymmetrical lifting trials, normalized to individual estimates of L4/L5 damage load.

the intervertebral joints is understood to be rather slow and therefore the accumulation of damage under cyclic loading conditions would be expected to exceed to the rate of repair.

When conducting *in vitro* mechanical experiments with FSUs, it is also important to remember that several structures in the osteoligamentous system (e.g. ligaments, vertebrae, intervertebral disc, cartilaginous endplates, etc.) undergo load. Across each of the mechanical risk factors that were examined in **studies II & III** (i.e. magnitude of force, cycle rate and postural deviation) it is interesting that the mechanism of fatigue injury varied across each of the different exposure conditions. For example, exaggerated postural deviation at 40% UCT was associated with avulsion of the superior endplate, whereas fracture of the pars interarticularis was observed in the 20% UCT condition. Although no macro-structural damage was observed in 10% UCT conditions at 300% neutral zone range, considerable micro-structural damage was observed in the AF across both the anterior and posterior-lateral regions of the IVD. This was an important contribution from this work, since most studies have focused on macro-structure damage when defining fatigue injury.

Pairing our description of the micro-structural damage imposed to the AF at sub-acute-failure magnitudes of cyclic compressive loading (**Figures 4-6, 4-7** and **4-8**) with recent work published by Lama et al. (2014), novel insight into the cycle-varying changes in the mechanical properties of isolated FSUs can be gained. For example, considering the specimen height loss data that were presented in **study III** (see **Figure 5-4,** Chapter 5), the second-order response that is observed, which may have previously been attributed to the time-dependent viscoelastic creep response of the intervertebral disc, cartilaginous endplates and vertebrae, is likely also due to the accumulation of micro-structural damage in each of these components (i.e. micro-cracks in the trabecular bone, micro-fracture of the cartilage endplates, delamination of the inter-lamellar matrix). Collectively, these changes result in a net loss in specimen height, as well as a reduction in the capacity to support load. This hypothesis is supported by recent findings of Lama et al. (2014), that documented cartilage fragments in the extruded material that was surgically removed in 10/21 patients that under lumbar microdisectomy.

Considering our results from **study III,** it is interesting to note that the magnitude of IVD height loss in the 40% UCT condition was 2x that observed in the 10% group (in some cases), however, the resultant specimen height loss after 5000 loading cycles was even greater (over 3x in some 40% UCT survivor specimens). These findings provide further support for the hypothesis that different mechanisms of fatigue damage occurred across each of the experimental conditions that were examined in this thesis, which nicely tie into the different force x repetition quadrants that Drs. Gallagher and Heberger (2013) have proposed for the typical stress-life curve of FSUs (**Figure 7-3**). Based on the insights obtained from this thesis, it is hypothesized that deviated postures would further reduce the number of cycles to failure (across levels % ultimate stress), due to the increased joint loading that occurs (or distribution of the resultant joint force across different axes – increased posterior shear observed in **study I**), as well as the reduce capacity of the lumbar spine in a flexed posture.

The lack of a consistent trend between the magnitude of IVD height loss and AF bulging that was observed in **study III** also deserves further discussion. Based on the results from this work, our hypothesis that increased AF bulging would be observed in specimens assigned to the 300% postural deviation conditions (after 5000 loading cycles) was rejected. However, when considering the significant reduction in intradiscal pressure that was observed in recent work conducted by our group (i.e. Noguchi et al. 2013) with a cyclic flexion/extension loading protocol, previously shown to induce IVD herniation (see Callaghan & McGill, 2001), a potential mechanism for results (or lack thereof) can be raised. The initial response of FSUs that undergo cyclic mechanical loading, is AF bulging (outwards) and the cartilaginous endplates deflecting down/upwards (into the inferior and superior vertebrae, respectively) due to the high magnitudes of hydrostatic pressure that arises within the joint. If the load is held for a sufficient amount of time / number of cycles, fluid from inside the joint is displaced (i.e. exuded), which in turn decreases the magnitude of deflection in the AF / cartilaginous endplate. However, under prolonged loading conditions it has been hypothesized that this lack of hydrostatic pressure on the inner layers of AF may accelerate the disruption that occurs between adjacent lamellae in the IVD, inducing delamination - with some layers folding inwards and others bulging outwards.

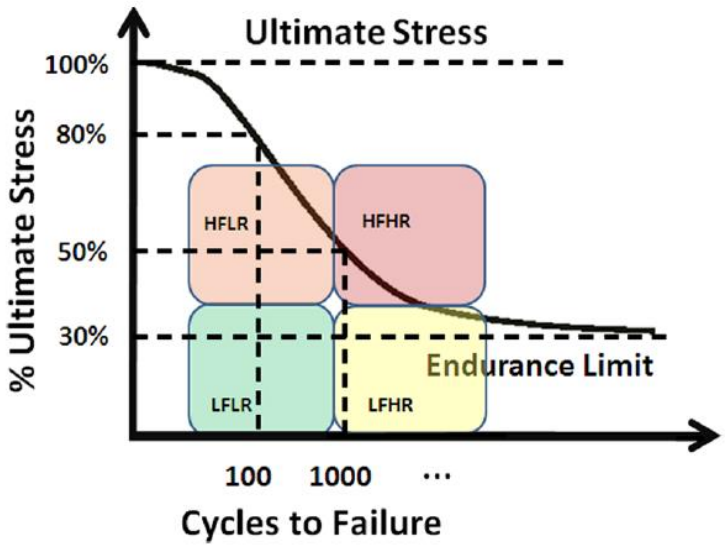

Figure 7-3: Force x Repetition quadrants superimposed on a fatigue failure curve, as proposed by Gallagher & Heberger. *Image obtained from*: Gallagher & Heberger (2013).

Previous research conducted by Adams et al. (2000) has nicely illustrated this potential mechanism in cadaver tissue.

Lastly, it is important to note that the cycle-varying stress relaxation response of the AF to cyclic biaxial tensile loading that was observed in **study IV** sheds interesting light on the known mechanism of AF tissue failure under cyclic loading conditions. Previous research conducted by our group (i.e. Tampier et al. 2007) has shown that the nucleus pulposus broaches through small clefts and fissures that form within individual lamellae (displacing the collagen fiber bundles), and propagates outwards from the inner layers of AF with herniation. It is interesting that the cycle varying changes observed in the may predispose the IVD to this type of fatigue failure; however, the lack of changes that were observed in the S-S moduli may suggest that the damage induced to the multilayer samples of AF tissue that were tested may not be entirely explained by structural changes in the collagen fiber bundles, rather structural changes to elastin fiber network and GAG proteins should also be considered. Therefore, future research efforts using immunohistochemical staining methods to characterize disruption to individual proteins with cyclic mechanical loading may be warranted.

7.5 A Framework of Significant Interactions

As illustrated in Chapter 3 (**Study I**), the combined effects of external task demands (e.g. high forces, fast movement speeds, asymmetrical postures) significantly interact to influence the resultant *in vivo* joint loading that occurs in the lumbar spine. Then in Chapter 4 (**study II**), when these exposures were cyclically applied to isolated FSUs it was discovered that the combined effects of force, repetition (i.e. cycle rate) and postural deviation modulated the mechanism of fatigue injury (e.g. endplate fracture or avulsion), with considerable micro-structural damage observed in specimens where no injury was detected. Using a 3D laser scanner **(study III),** structural changes in the IVD (e.g. height loss, bulging) from the same sample of specimens could be linked to mechanical changes in the isolated joint that occurred due to interactions between each of the exposure variables (i.e. force, repetition, posture), suggested that different mechanisms for fatigue failure may be at a play across each of the various conditions that were examined (i.e. micro-cracks in the trabecular bone, micro-fracture of the cartilage endplates, delamination of the inter-lamellar matrix). Lastly, to better understand the cycle-varying changes that occur in the mechanical properties IVD, excised samples of AF tissue were examined under cyclic, biaxial tension (**study IV**), which provided novel insight into cycle-varying stress relaxation that occurs in the IVD, which may be linked to the known mechanism of fatigue failure. Therefore, the results presented within this thesis can be used to establish a framework of significant interactions that exist between external task demands (e.g. force, speed, posture), the resultant internal mechanical exposure (i.e. compression, shear, postural deviation) and the risk of musculoskeletal injury (**Figure 7-4**).

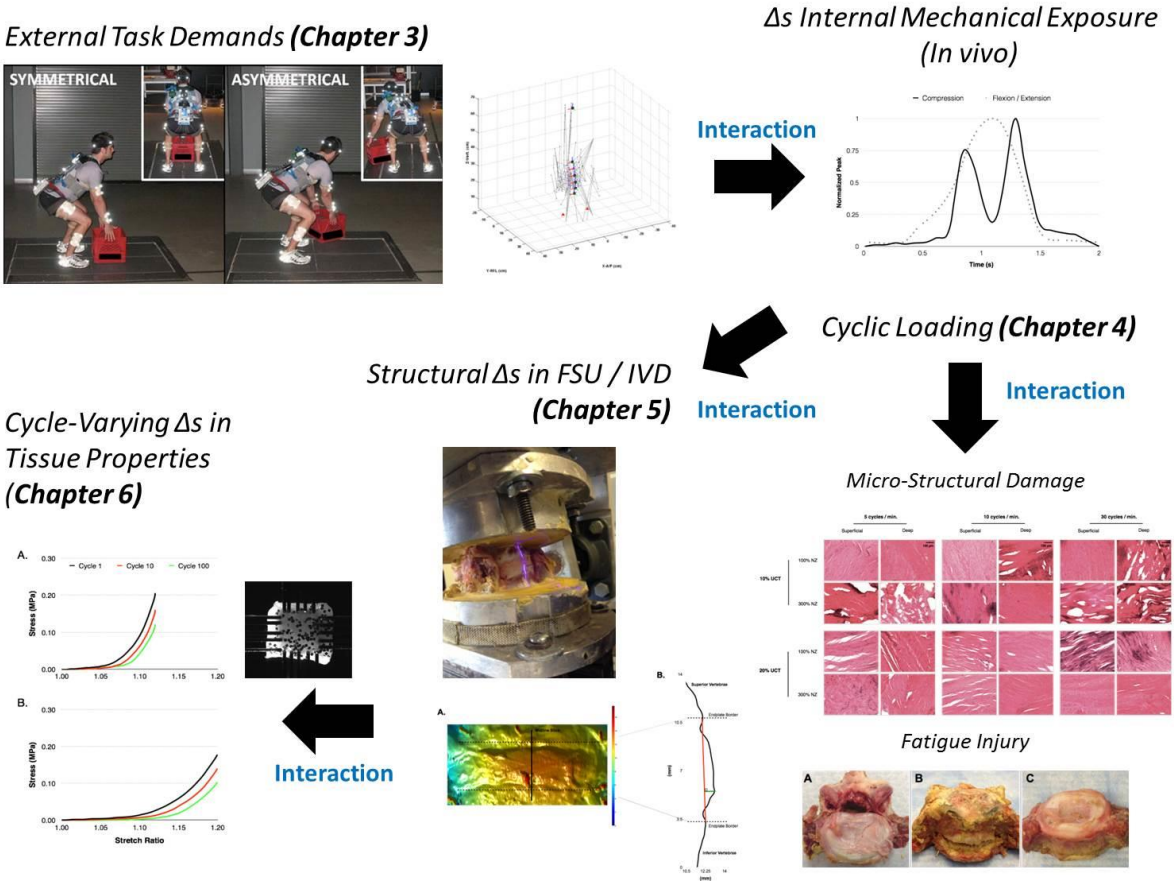

Figure 7-4: A framework of significant interactions between external task demands, internal mechanical exposures and resultant structural/mechanical changes in lumbar spine that could lead to musculoskeletal injury.

Bibliography

Adams, M. A. & Hutton, W. C. (1983). The effect of fatigue on the lumbar intervertebral disc. *The Journal of Bone and Joint Surgery. British Volume*, *65*(2), 199-203.

Adams, M.A., Hutton, W.C. (1982). Prolapsed intervertebral disc. A hyperflexion injury. *Spine*, 7, 184-91.

Adams, M. A., Dolan, P., & Hutton, W. C. (1987). Diurnal variations in the stresses on the lumbar spine. *Spine*, *12*(2), 130-7.

Adams, M. A., Dolan, P., Hutton, W. C., & Porter, R. W. (1990). Diurnal changes in spinal mechanics and their clinical significance. *The Journal of Bone and Joint Surgery. British Volume*, *72*(2), 266-70.

Adams, M. A., Freeman, B. J. C., Morrison, H. P., Nelson, I. W., & Dolan, P. (2000). Mechanical initiation of intervertebral disc degeneration. *Spine*, *25*(13), 1625-36.

Andersson, G. B. (1981). Epidemiologic aspects on low-back pain in industry. *Spine*, *6*(1), 53-60.

Bass, E. C., Ashford, F. A., Segal, M. R., & Lotz, J. C. (2004). Biaxial testing of human annulus fibrosus and its implications for a constitutive formulation. *Ann Biomed Eng*, *32*(9), 1231-42.

Beach, T. A.C. (2012). Firefighter fitness, movement qualities, occupational low back loading demands and injury potential. Ph.D. Dissertation. University of Waterloo. Waterloo, Ontario, Canada.

Beach, T. A., Frost, D. M., & Callaghan, J. P. (2014). FMS™ scores and low-back loading during lifting--whole-body movement screening as an ergonomic tool? *Applied Ergonomics*, *45*(3), 482-9.

Begon, M., Monnet, T., & Lacouture, P. (2007). Effects of movement for estimating the hip joint centre. *Gait & Posture*, *25*(3), 353-9.

Bernard, B.P., Putz-Anderson, V., Burt, S.E., et al. (1997). A critical review of epidemiologic evidence for work-related musculoskeletal disorders of the neck, upper-extremity, and low-back. Available at: http://www.cdc.gov/niosh/dcos/97-141

Bisseling, R. W. & Hof, A. L. (2006). Handling of impact forces in inverse dynamics. *Journal of Biomechanics*, *39*(13), 2438-44.

Bogduk, N. (2005). *Clinical anatomy of the lumbar spine and sacrum.* Churchill Livingstone.

Brereton, L. C. & McGill, S. M. (1998). Frequency response of spine extensors during rapid isometric contractions: Effects of muscle length and tension. *Journal of Electromyography and Kinesiology*, *8*(4), 227-32.

Brinckmann, P. & Horst, M. (1985). The influence of vertebral body fracture, intradiscal injection, and partial discectomy on the radial bulge and height of human lumbar discs. *Spine*, *10*(2), 138-45.

Brinckmann, P., Biggemann, M., & Hilweg, D. (1988). Fatigue fracture of human lumbar vertebrae. *Clinical Biomechanics*, *3*, S1, i-S23.

Brinckmann M, P. & Hilweg, D. (1989). Prediction of the compressive strength of human lumbar vertebrae. *Clinical Biomechanics*, *4*, S2, iii-27.

Brown, S. H. & Potvin, J. R. (2007). The effect of reducing the number of EMG channel inputs on loading and stiffness estimates from an EMG-driven model of the spine. *Ergonomics*, *50*(5), 743-51.

Bruehlmann, S. B., B Rattner, J., R Matyas, J., & A Duncan, N. (2002). Regional variations in the cellular matrix of the annulus fibrosus of the intervertebral disc. *Journal of Anatomy*, *201*(2), 159-171.

Bruehlmann, S. B., Hulme, P. A., & Duncan, N. A. (2004). In situ intercellular mechanics of the bovine outer annulus fibrosus subjected to biaxial strains. *Journal of Biomechanics*, *37*(2), 223-31.

Callaghan, J. P. & McGill, S. M. (1995). Frozen storage increases the ultimate compressive load of porcine vertebrae. *Journal of Orthopaedic Research*, *13*(5), 809-12.

Callaghan, J. P. & McGill, S. M. (2001). Intervertebral disc herniation: Studies on a porcine model exposed to highly repetitive flexion/extension motion with compressive force. *Clinical Biomechanics*, *16*(1), 28-37.

Cassidy, J. D., Carroll, L. J., & Côté, P. (1998). The Saskatchewan health and back pain survey: The prevalence of low back pain and related disability in Saskatchewan adults. *Spine*, *23*(17), 1860-6.

Chan, S. C., Ferguson, S. J., Wuertz, K., & Gantenbein-Ritter, B. (2011). Biological response of the intervertebral disc to repetitive short-term cyclic torsion. *Spine*, *36*(24), 2021-30.

Cholewicki, J. & McGill, S. M. (1996). Mechanical stability of the in vivo lumbar spine: Implications for injury and chronic low back pain. *Clinical Biomechanics*, *11*(1), 1-15.

Chubinskaya, S., Kawakami, M., Rappoport, L., Matsumoto, T., Migita, N., & Rueger, D. C. (2007). Anti-catabolic effect of OP-1 in chronically compressed intervertebral discs. *Journal of Orthopaedic Research*, *25*(4), 517-30.

Coenen, P., Kingma, I., Boot, C. R., Twisk, J. W., Bongers, P. M., & van Dieën, J. H. (2013). Cumulative low back load at work as a risk factor of low back pain: A prospective cohort study. *Journal of Occupational Rehabilitation.* 23(1): 11-18.

Cohen, J. (1988). *Statistical power analysis for the behavioral sciences.* Lawrence Erlbaum.

Cuchanski, M., Cook, D., Whiting, D. M., & Cheng, B. C. (2011). Measurement of occlusion of the spinal canal and intervertebral foramen by intervertebral disc bulge. *International Journal of Spinal Surgery*, *5*(1), 9-15.

Dammers, R. & Koehler, P. J. (2002). Lumbar disc herniation: Level increases with age. *Surgical Neurology*, *58*(3-4), 209-12.

Dempsey, P. G. (2003). A survey of lifting and lowering tasks. *International Journal of Industrial Ergonomics*, *31*(1), 11-16.

Dempsey, P. G., McGorry, R. W., & Maynard, W. S. (2005). A survey of tools and methods used by certified professional ergonomists. *Applied Ergonomics*, *36*(4), 489-503.

Denis, F. & Burkus, J. K. (1992). Shear fracture-dislocations of the thoracic and lumbar spine associated with forceful hyperextension (lumberjack paraplegia). *Spine*, *17*(2), 156-161.

DePalma, M. J., Ketchum, J. M., & Saullo, T. (2011). What is the source of chronic low back pain and does age play a role? *Pain Medicine (Malden, Mass.)*, *12*(2), 224-33.

Dhillon, N., Bass, E. C., & Lotz, J. C. (2001). Effect of frozen storage on the creep behavior of human intervertebral discs. *Spine*, *26*(8), 883-8.

Drake, J. D. & Callaghan, J. P. (2009). Intervertebral neural foramina deformation due to two types of repetitive combined loading. *Clinical Biomechanics,* 24(1), 1-6.

Ebara, S., Iatridis, J. C., Setton, L. A., Foster, R. J., Mow, V. C., & Weidenbaum, M. (1996). Tensile properties of non-degenerate human lumbar annulus fibrosus. *Spine*, *21*(4), 452-61.

Eilaghi, A., Flanagan, J. G., Brodland, W.G., & Ethier, C. R. (2009). Strain uniformity in biaxial specimens is highly sensitive to attachment details. *Journal of Biomechanical Engineering*, *131*(9), 091003.

Elliott, D. M. & Setton, L. A. (2001). Anisotropic and inhomogeneous tensile behavior of the human annulus fibrosus: Experimental measurement and material model predictions. *Journal of Biomechanical Engineering*, *123*(3), 256-63.

Eyre, D. R. & Muir, H. (1976). Types I and II collagens in intervertebral disc. Interchanging radial distributions in annulus fibrosus. *Biochemical Journal*, *157*(1), 267-70.

Faber, G. S., Kingma, I., & van Dieën, J. H. (2011). Effect of initial horizontal object position on peak L5/S1 moments in manual lifting is dependent on task type and familiarity with alternative lifting strategies. *Ergonomics*, *54*(1), 72-81.

Fredericson, M., Lee, S. U., Welsh, J., Butts, K., Norbash, A., & Carragee, E. J. (2001). Changes in posterior disc bulging and intervertebral foraminal size associated with flexion-extension movement: A comparison between L4-5 and L5-S1 levels in normal subjects. *The Spine Journal, 1*(1), 10-7.

Frost, D. M. (2012). Towards the establishment of a worker-centered framework to physically prepare firefighters. Ph.D. Dissertation. University of Waterloo. Waterloo, Ontario, Canada.

Galante, J. O. (1967). Tensile properties of the human lumbar annulus fibrosus. *Acta Orthopaedica Scandinavica*, Suppl 100,1-91.

Gallagher, S. & Heberger, R. (2013). Examining the interaction of force and repetition on musculoskeletal disorder risk: A systematic literature review. *Human Factors*, 55(1), 108-24.

Gallagher, S., Hamrick, C. A., Love, A. C., & Marras, W. S. (1994). Dynamic biomechanical modelling of symmetric and asymmetric lifting tasks in restricted postures. *Ergonomics*, *37*(8), 1289-310.

Gallagher, S., Marras, W. S., Litsky, A. S., & Burr, D. (2005). Torso flexion loads and the fatigue failure of human lumbosacral motion segments. *Spine*, *30*(20), 2265-73.

Garg, A. & Banaag, J. (1988). Maximum acceptable weights, heart rates and reps for one hour's repetitive asymmetric lifting. *Ergonomics*, *31*(1), 77-96.

Genaidy, A.M., Waly, S.M., Khalil, T.M. & Hidalgo, J. (1993). Spinal compression tolerance limits for the design of manual handling operations in the workplace. *Ergonomics,* 36(4), 415-34.

Gooyers, C. E., McMillan, R. D., Howarth, S. J., & Callaghan, J. P. (2012). The impact of posture and prolonged cyclic compressive loading on vertebral joint mechanics. *Spine*, 37(17), E1023-9.

Gooyers, C. E., Frost, D.M., McGill, S.M., & Callaghan, J. P. (2013). Partial rupture of the Achilles tendon during a simulated fire ground task: Insights obtained from a case report for the prevention and reporting of musculoskeletal injury. *Clinical Biomechanics*, 28(4), 436-440.

Green, T. P., Adams, M. A., & Dolan, P. (1993). Tensile properties of the annulus fibrosus II. Ultimate tensile strength and fatigue life. *European Spine Journal, 2*(4), 209-14.

Greenland, K. O., Merryweather, A. S., & Bloswick, D. S. (2013). The effect of lifting speed on cumulative and peak biomechanical loading for symmetric lifting tasks. *Safety and Health at Work*, *4*(2), 105-10.

Gregory, D. E. & Callaghan, J. P. (2010). An examination of the influence of strain rate on sub-failure mechanical properties of the annulus fibrosus. *Journal of Biomechanical Engineering*, *132*(9), 091010.

Gregory, D. E. & Callaghan, J. P. (2011). A comparison of uniaxial and biaxial mechanical properties of the annulus fibrosus: A porcine model. *Journal of Biomechanical Engineering*, *133*(2), 024503.

Gregory, D. E., Veldhuis, J. H., Horst, C., Brodland, W.G., & Callaghan, J. P. (2011). Novel lap test determines the mechanics of delamination between annular lamellae of the intervertebral disc. *Journal of Biomechanics*, *44*(1), 97-102.

Gregory, D. E. & Callaghan, J. P. (2012). An examination of the mechanical properties of the annulus fibrosus: The effect of vibration on the intra-lamellar matrix strength. *Medical Engineering & Physics,* 34(4), 472-7.

Gruber, H. E., Ingram, J., & Hanley, E. N. (2002). An improved staining method for intervertebral disc tissue. *Biotechnic & Histochemistry*, *77*(2), 81-3.

Gruevski, K. M., Gooyers, C. E., Karakolis, T., & Callaghan, J. P. (2014). The effect of local hydration environment on annular thickness and mass temporal changes. *In Proceedings of the 7th World Congress of Biomechanics*. Boston, MA.

Gunzburg, R., Parkinson, R., Moore, R., Cantraine, F., Hutton, W., Vernon-Roberts, B., et al. (1992). A cadaveric study comparing discography, magnetic resonance imaging, histology, and mechanical behavior of the human lumbar disc. *Spine*, *17*(4), 417-26.

Hansson, T. H., Keller, T. S., & Spengler, D. M. (1987). Mechanical behavior of the human lumbar spine. II. Fatigue strength during dynamic compressive loading. *Journal of Orthopaedic Research*, *5*(4), 479-487.

Hasegawa, T., An, H. S., Inufusa, A., Mikawa, Y., & Watanabe, R. (2000). The effect of age on inflammatory responses and nerve root injuries after lumbar disc herniation: An experimental study in a canine model. *Spine*, *25*(8), 937-40.

Hayes, A. J., Benjamin, M., & Ralphs, J. R. (2001). Extracellular matrix in development of the intervertebral disc. *Matrix Biology*, *20*(2), 107-121.

Heuer, F., Schmidt, H., Claes, L., & Wilke, H. J. (2008a). A new laser scanning technique for imaging intervertebral disc displacement and its application to modeling nucleotomy. *Clinical Biomechanics (Bristol, Avon)*, *23*(3), 260-9.

Heuer, F., Schmidt, H., & Wilke, H. J. (2008b). The relation between intervertebral disc bulging and annular fiber associated strains for simple and complex loading. *Journal of Biomechanics*, *41*(5), 1086-94.

Heuer, F., Schmidt, H., & Wilke, H. J. (2008c). Stepwise reduction of functional spinal structures increase disc bulge and surface strains. *Journal of Biomechanics*, *41*(9), 1953-60.

Heuer, F., Schmidt, H., Claes, L., & Wilke, H. J. (2007). Stepwise reduction of functional spinal structures increase vertebral translation and intradiscal pressure. *Journal of Biomechanics*, *40*(4), 795-803.

Heuer, F., Schmitt, H., Schmidt, H., Claes, L., & Wilke, H. J. (2007). Creep associated changes in intervertebral disc bulging obtained with a laser scanning device. *Clinical Biomechanics, 22*(7), 737-44.

Hill, A. B. (1965). The environment and disease: Association or causation? *Proceedings of the Royal Society of Medicine*, *58*(5), 295-300.

Hirsch, C. & Galante, J. (1967). Laboratory conditions for tensile tests in annulus fibrosus from human intervertebral discs. *Acta Orthopaedica Scandinavica*, *38*(2), 148-62.

Hirsch, C. & Nachemson, A. (1954). New observations on the mechanical behavior of lumbar discs. *Acta Orthopaedica Scandinavica*, *23*(4), 254-83.

Ho, G., Leung, V. Y., Cheung, K. M., & Chan, D. (2008). Effect of severity of intervertebral disc injury on mesenchymal stem cell-based regeneration. *Connective Tissue Research*, *49*(1), 15-21.

Holzapfel, G. A., Schulze-Bauer, C. A., Feigl, G., & Regitnig, P. (2005). Single lamellar mechanics of the human lumbar annulus fibrosus. *Biomech Model Mechanobiol*, *3*(3), 125-40.

Hoogendoorn, W. E., van Poppel, M. N., Bongers, P. M., Koes, B. W., & Bouter, L. M. (1999). Physical load during work and leisure time as risk factors for back pain. *Scandinavian Journal of Work, Environment & Health*, *25*(5), 387-403.

Howarth, S. J. & Callaghan, J. P. (2013). Towards establishing an occupational threshold for cumulative shear force in the vertebral joint - an in vitro evaluation of a risk factor for spondylolytic fractures using porcine specimens. *Clinical Biomechanics*, *28*(3), 246-54.

Howarth, S. J., Beach, T. A., & Callaghan, J. P. (2010). Dynamic factors and force-weighting corrections influence estimates of cumulative vertebral joint compression. *Theoretical Issues in Ergonomics Science*, *11*(5), 474-488.

Howarth, S. J., Beach, T. A., Pearson, A. J., & Callaghan, J. P. (2009). Using sitting as a component of job rotation strategies: Are lifting/lowering kinetics and kinematics altered following prolonged sitting. *Applied Ergonomics*, *40*(3), 433-9.

Hubbard, R. D., Chen, Z., & Winkelstein, B. A. (2008). Transient cervical nerve root compression modulates pain: Load thresholds for allodynia and sustained changes in spinal neuropeptide expression. *Journal of Biomechanics*, *41*(3), 677-85.

Hutton, W.C., & Adams, M.A. (1982). Can the lumbar spine be crashed in heavy lifting? *Spine,* 7, 586-90.

Iatridis, J. C. & Gwynn, I. (2004). Mechanisms for mechanical damage in the intervertebral disc annulus fibrosus. *Journal of Biomechanics*, *37*(8), 1165-75.

Iatridis, J. C., MaClean, J. J., & Ryan, D. A. (2005). Mechanical damage to the intervertebral disc annulus fibrosus subjected to tensile loading. *Journal of Biomechanics*, *38*(3), 557-65.

Inoue, H. (1981). Three-dimensional architecture of lumbar intervertebral discs. *Spine*, *6*(2), 139-46.

Kaplan, E.L. & Meier, P. (1958). Nonparametric estimation from incomplete observations. *Journal of the American Statistical Association,* 53(282), 457-481.

Kuga, N. & Kawabuchi, M. (2001). Histology of intervertebral disc protrusion: An experimental study using an aged rat model. *Spine*, *26*(17), E379-84.

Kuijer, P. P., Frings-Dresen, M. H., Gouttebarge, V., van Dieën, J. H., van der Beek, A. J., & Burdorf, A. (2011). Low back pain: We cannot afford ignoring work. *The Spine Journal*, 11(2), 164-6.

Kuiper, J. I., Burdorf, A., Verbeek, J. H. A. M., Frings-Dresen, M. H. W., van der Beek, A. J., & Viikari-Juntura, E. R. A. (1999). Epidemiologic evidence on manual materials handling as a risk factor for back disorders: A systematic review. *International Journal of Industrial Ergonomics*, *24*(4), 389-404.

Kumar, S. (1990). Cumulative load as a risk factor for back pain. *Spine*, *15*(12), 1311-6.

Kuorinka, I., Jonsson, B., Kilbom, A., Vinterberg, H., Biering-Sørensen, F., Andersson, G., et al. (1987). Standardised nordic questionnaires for the analysis of musculoskeletal symptoms. *Applied Ergonomics*, *18*(3), 233-237.

Lama, P. , Urujm Z,m Balkovec, C., Claireaux, H.A., Flower, L., Harding, I.J., Dolan, P., Adams, M.A. (2014). Significance of cartilage endplate within herniated disc tissue. *European Spine Journal.* In Press.

Lavender, S. A., Andersson, G. B. J., Schipplein, O. D., & Fuentes, H. J. (2003). The effects of initial lifting height, load magnitude, and lifting speed on the peak dynamic L5/S1 moments. *International Journal of Industrial Ergonomics*, *31*(1), 51-59.

Lavender, S. A., Li, Y. C., Andersson, G. B., & Natarajan, R. N. (1999). The effects of lifting speed on the peak external forward bending, lateral bending, and twisting spine moments. *Ergonomics*, *42*(1), 111-25.

Leung, V. Y., Chan, W. C., Hung, S. C., Cheung, K. M., & Chan, D. (2009). Matrix remodeling during intervertebral disc growth and degeneration detected by multichromatic FAST staining. *J Histochem Cytochem*, *57*(3), 249-56.

Liu, Y. K., Njus, G., Buckwalter, J., & Wakano, K. (1983). Fatigue response of lumbar intervertebral joints under axial cyclic loading. *Spine*, *8*(8), 857.

Lo, I. K., Chi, S., Ivie, T., Frank, C. B., & Rattner, J. B. (2002). The cellular matrix: A feature of tensile bearing dense soft connective tissues. *Histology and Histopathology*, *17*(2), 523-37.

Lotz, J. C., Colliou, O. K., Chin, J. R., Duncan, N. A., & Liebenberg, E. (1998). Compression-induced degeneration of the intervertebral disc: An in vivo mouse model and finite-element study. *Spine*, *23*(23), 2493-506.

Lü, D. S., Shono, Y., Oda, I., Abumi, K., & Kaneda, K. (1997). Effects of chondroitinase ABC and chymopapain on spinal motion segment biomechanics: An in vivo biomechanical, radiologic, and histologic canine study. *Spine*, *22*(16), 1828.

MacLean, J. J., Owen, J. P., & Iatridis, J. C. (2007). Role of endplates in contributing to compression behaviors of motion segments and intervertebral discs. *Journal of Biomechanics*, *40*(1), 55-63.

Marchand, F. & Ahmed, A. M. (1990). Investigation of the laminate structure of lumbar disc annulus fibrosus. *Spine*, *15*(5), 40210.

Marras, W. S. (2000). Occupational low back disorder causation and control. *Ergonomics*, *43*(7), 880-902.

Marras, W. S. & Davis, K. G. (1998). Spine loading during asymmetric lifting using one versus two hands. *Ergonomics*, *41*(6), 817-34.

Marras, W. S. & Mirka, G. A. (1989). Trunk strength during asymmetric trunk motion. *Human Factors*, *31*(6), 667-77.

Marras, W. S. & Mirka, G. A. (1992). A comprehensive evaluation of trunk response to asymmetric trunk motion. *Spine*, *17*(3), 318-26.

Marras, W. S., Granata, K. P., & Davis, K. G. (1999). Variability in spine loading model performance. *Clinical Biomechanics*, *14*(8), 505-514.

Marras, W. S., Lavender, S. A., Leurgans, S. E., Fathallah, F. A., Ferguson, S. A., Allread, W. G., et al. (1995). Biomechanical risk factors for occupationally related low back disorders. *Ergonomics*, *38*(2), 377-410.

Marras, W. S., Lavender, S. A., Leurgans, S. E., Rajulu, S. L., Allread, W. G., Fathallah, F. A., et al. (1993). The role of dynamic three-dimensional trunk motion in occupationally-related low back disorders. The effects of workplace factors, trunk position, and trunk motion characteristics on risk of injury. *Spine*, *18*(5), 617-28.

McGill, S. (2007). *Low back disorders: Evidence-based prevention and rehabilitation.* Human Kinetics Publishers.

McGill, S., Juker, D., & Kropf, P. (1996). Appropriately placed surface EMG electrodes reflect deep muscle activity (psoas, quadratus lumborum, abdominal wall) in the lumbar spine. *Journal of Biomechanics*, *29*(11), 1503-7.

McGill, S., Seguin, J., & Bennett, G. (1994). Passive stiffness of the lumbar torso in flexion, extension, lateral bending, and axial rotation. Effect of belt wearing and breath holding. *Spine*, *19*(6), 696-704.

McGill, S. M. (1991). Electromyographic activity of the abdominal and low back musculature during the generation of isometric and dynamic axial trunk torque: Implications for lumbar mechanics. *Journal of Orthopaedic Research*, *9*(1), 91-103.

McGill, S. M. (1992). A myoelectrically based dynamic three-dimensional model to predict loads on lumbar spine tissues during lateral bending. *Journal of Biomechanics*, *25*(4), 395-414.

McGill, S. M. (1997). The biomechanics of low back injury: Implications on current practice in industry and the clinic. *Journal of Biomechanics*, *30*(5), 465-75.

McGill, S. M. (2011). Letter to the editor regarding: "Causal assessment of occupational lifting and low back pain: Results of a systematic review" by Wai et al. *The Spine Journal*, *11*(4), 365; author reply 366.

McGill, S. M. & Callaghan, J. P. (1999). Impact forces following the unexpected removal of a chair while sitting. *Accident; Analysis and Prevention*, *31*(1-2), 85-9.

McGill, S. M. & Norman, R. W. (1986). Partitioning of the L4-L5 dynamic moment into disc, ligamentous, and muscular components during lifting. *Spine*, *11*(7), 666-78.

McNally, D. S. & Adams, M. A. (1992). Internal intervertebral disc mechanics as revealed by stress profilometry. *Spine*, *17*(1), 66-73.

Melrose, J., Smith, S. M., Appleyard, R. C., & Little, C. B. (2008). Aggrecan, versican and type VI collagen are components of annular translamellar crossbridges in the intervertebral disc. *European Spine Journal*, *17*(2), 314-24.

Moon, D. K., Abramowitch, S. D., & Woo, S. L. (2006). The development and validation of a charge-coupled device laser reflectance system to measure the complex cross-sectional shape and area of soft tissues. *Journal of Biomechanics*, *39*(16), 3071-5.

Noguchi, M. (2013). Examining changes in intradiscal pressure during intervertebral disc herniation. M.Sc. Thesis. University of Waterloo. Waterloo, Ontario, Canada.

Norman, R., Wells, R., Neumann, P., Frank, J., Shannon, H., & Kerr, M. (1998). A comparison of peak vs cumulative physical work exposure risk factors for the reporting of low back pain in the automotive industry. *Clinical Biomechanics*, *13*(8), 561-573.

Olczyk, K. (1994). Age-related changes of elastin content in human intervertebral discs. *Folia Histochem Cytobiologica*, *32*, 41-4.

Oxland, T. R., Panjabi, M. M., Southern, E. P., & Duranceau, J. S. (1991). An anatomic basis for spinal instability: A porcine trauma model. *Journal of Orthopaedic Research*, *9*(3), 452-462.

Parkinson, R. J. & Callaghan, J. P. (2007a). Can periods of static loading be used to enhance the resistance of the spine to cumulative compression? *Journal of Biomechanics*, *40*(13), 2944-52.

Parkinson, R. J. & Callaghan, J. P. (2007b). The role of load magnitude as a modifier of the cumulative load tolerance of porcine cervical spinal units: Progress towards a force weighting approach. *Theoretical Issues in Ergonomics Science*, *8*(3), 171-184.

Parkinson, R. J. & Callaghan, J. P. (2008). Quantification of the relationship between load magnitude, rest duration and cumulative compressive tolerance of the spine: Development of a weighting system for adjustment to a common injury exposure level. *Theoretical Issues in Ergonomics Science*, *9*(3), 255-268.

Parkinson, R. J. & Callaghan, J. P. (2009). The role of dynamic flexion in spine injury is altered by increasing dynamic load magnitude. *Clinical Biomechanics (Bristol, Avon)*, *24*(2), 148-54.

Parkinson, R. J., Durkin, J. L., & Callaghan, J. P. (2005). Estimating the compressive strength of the porcine cervical spine: An examination of the utility of DXA. *Spine*, *30*(17), E492-8.

Pei, B. Q., Li, H., Li, D. Y., Fan, Y. B., Wang, C., & Wu, S. Q. (2014). Creep bulging deformation of intervertebral disc under axial compression. *Bio-medical Materials and Engineering*, *24*(1), 191-8.

Pezowicz, C. A., Robertson, P. A., & Broom, N. D. (2005). Intralamellar relationships within the collagenous architecture of the annulus fibrosus imaged in its fully hydrated state. *Journal of Anatomy*, *207*(4), 299-312.

Pezowicz, C. A., Schechtman, H., Robertson, P. A., & Broom, N. D. (2006). Mechanisms of annular failure resulting from excessive intradiscal pressure: A microstructural-micromechanical investigation. *Spine*, *31*(25), 2891-903.

Potvin, J. R., McGill, S. M., & Norman, R. W. (1991). Trunk muscle and lumbar ligament contributions to dynamic lifts with varying degrees of trunk flexion. *Spine*, *16*(9), 1099-107.

Reuber, M., Schultz, A., Denis, F., & Spencer, D. (1982). Bulging of lumbar intervertebral disks. *Journal of Biomechanical Engineering*, *104*(3), 187-92.

Roffey, D. M., Wai, E. K., Bishop, P., Kwon, B. K., & Dagenais, S. (2010a). Causal assessment of awkward occupational postures and low back pain: Results of a systematic review. *The Spine Journal, 10*(1), 89-99.

Roffey, D. M., Wai, E. K., Bishop, P., Kwon, B. K., & Dagenais, S. (2010b). Causal assessment of occupational pushing or pulling and low back pain: Results of a systematic review. *The Spine Journal*, *10*(6), 544-53.

Roffey, D. M., Wai, E. K., Bishop, P., Kwon, B. K., & Dagenais, S. (2010c). Causal assessment of workplace manual handling or assisting patients and low back pain: Results of a systematic review. *The Spine Journal*, *10*(7), 639-51.

Sahlman, J., Inkinen, R., Hirvonen, T., Lammi, M. J., Lammi, P. E., Nieminen, J., et al. (2001). Premature vertebral endplate ossification and mild disc degeneration in mice after inactivation of one allele belonging to the col2a1 gene for type II collagen. *Spine*, *26*(23), 2558-65.

Schollum, M. L., Robertson, P. A., & Broom, N. D. (2008). ISSLS prize winner: Microstructure and mechanical disruption of the lumbar disc annulus: Part I: A microscopic investigation of the translamellar bridging network. *Spine*, *33*(25), 2702-10.

Schwartz, M. H. & Rozumalski, A. (2005). A new method for estimating joint parameters from motion data. *Journal of Biomechanics*, *38*(1), 107-16.

Schwarzer, A. C., Aprill, C. N., Derby, R., Fortin, J., Kine, G., & Bogduk, N. (1995). The prevalence and clinical features of internal disc disruption in patients with chronic low back pain. *Spine*, *20*(17), 1878-83.

Seidler, A. (2001). The role of cumulative physical work load in lumbar spine disease: Risk factors for lumbar osteochondrosis and spondylosis associated with chronic complaints. *Occupational and Environmental Medicine*, *58*(11), 735-746.

Seidler, A. (2003). Occupational risk factors for symptomatic lumbar disc herniation; a case-control study. *Occupational and Environmental Medicine*, *60*(11), 821-830.

Skaggs, D. L., Weidenbaum, M., Iatridis, J. C., Ratcliffe, A., & Mow, V. C. (1994). Regional variation in tensile properties and biochemical composition of the human lumbar annulus fibrosus. *Spine*, *19*(12), 1310.

Smeathers, J. E. & Joanes, D. N. (1988). Dynamic compressive properties of human lumbar intervertebral joints: A comparison between fresh and thawed specimens. *Journal of Biomechanics*, *21*(5), 425-33.

Smith, G. (1989). Padding point extrapolation techniques for the butterworth digital filter. *Journal of Biomechanics*, *22*(8-9), 967-71.

Smith, L. J. & Elliott, D. M. (2011). Formation of lamellar cross bridges in the annulus fibrosus of the intervertebral disc is a consequence of vascular regression. *Matrix Biol*, *30*(4), 267-74.

Smith, L. J. & Fazzalari, N. L. (2006). Regional variations in the density and arrangement of elastic fibers in the annulus fibrosus of the human lumbar disc. *Journal of Anatomy*, *209*(3), 359-67.

Smith, L. J., Byers, S., Costi, J. J., & Fazzalari, N. L. (2008). Elastic fibers enhance the mechanical integrity of the human lumbar annulus fibrosus in the radial direction. *Ann Biomed Eng*, *36*(2), 214-23.

Smits, P. (2003). Sox5 and sox6 are required for notochord extracellular matrix sheath formation, notochord cell survival and development of the nucleus pulposus of intervertebral discs. *Development*, *130*(6), 1135-1148.

Snook, S. H. & Ciriello, V. M. (1991). The design of manual handling tasks: Revised tables of maximum acceptable weights and forces. *Ergonomics*, *34*(9), 1197-213.

Standaert, C. J. & Herring, S. A. (2000). Spondylolysis: A critical review. *British Journal of Sports Medicine*, *34*(6), 415-22.

Stokes, I. A. (1987). Surface strain on human intervertebral discs. *Journal of Orthopaedic Research*, *5*(3), 348-55.

Stokes, I. A. (1988). Bulging of lumbar intervertebral discs: Non-contacting measurements of anatomical specimens. *J Spinal Disord*, *1*(3), 189-93.

Takala, E. P. (2010). Lack of "statistically significant" association does not exclude causality. *The Spine Journal*, *10*(10), 944; author reply 944-5.

Tampier, C. (2006). Progressive disc herniation: An investigation of the mechanism using histochemical and microscopic techniques. M.Sc. Thesis. University of Waterloo. Waterloo, Ontario, Canada.

Tampier, C., Drake, J. D., Callaghan, J. P., & McGill, S. M. (2007). Progressive disc herniation: An investigation of the mechanism using radiologic, histochemical, and microscopic dissection techniques on a porcine model. *Spine*, *32*(25), 2869-74.

Thompson, R. E., Barker, T. M., & Pearcy, M. J. (2003). Defining the neutral zone of sheep intervertebral joints during dynamic motions: An in vitro study. *Clinical Biomechanics (Bristol, Avon)*, *18*(2), 89-98.

Tsuji, H., Hirano, N., Ohshima, H., Ishihara, H., Terahata, N., & Motoe, T. (1993). Structural variation of the anterior and posterior annulus fibrosus in the development of human lumbar intervertebral disc. A risk factor for intervertebral disc rupture. *Spine*, *18*(2), 204.

van Dieën, J.H., Kuijer, P.P., Burdif, A., Marras, W.S., Adams, M.A. (2012). Non-specific low back pain. Lancet, 19; 379(9829):1874; author reply 1874-5.

van der Veen, A. J., Mullender, M. G., Kingma, I., van Dieën, J. H., van, J. H., & Smit, T. H. (2008). Contribution of vertebral bodies, endplates, and intervertebral discs to the compression creep of spinal motion segments. *Journal of Biomechanics*, *41*(6), 1260-8.

van Deursen, D. L., Snijders, C. J., Kingma, I., & van Dieën, J. H. (2001). In vitro torsion-induced stress distribution changes in porcine intervertebral discs. *Spine*, *26*(23), 2582-6.

Wai, E. K., Roffey, D. M., Bishop, P., Kwon, B. K., & Dagenais, S. (2010a). Causal assessment of occupational bending or twisting and low back pain: Results of a systematic review. *The Spine Journal*, *10*(1), 76-88.

Wai, E. K., Roffey, D. M., Bishop, P., Kwon, B. K., & Dagenais, S. (2010b). Causal assessment of occupational carrying and low back pain: Results of a systematic review. *The Spine Journal*, *10*(7), 628-38.

Wai, E. K., Roffey, D. M., Bishop, P., Kwon, B. K., & Dagenais, S. (2010c). Causal assessment of occupational lifting and low back pain: Results of a systematic review. *The Spine Journal*, *10*(6), 554-66.

Ward, A. C. (2009). The role of causal criteria in causal inferences: Bradford hill's "aspects of association". *Epidemiologic Perspectives & Innovations*, 6, 2.

Waters, T. R., Putz-Anderson, V., Garg, A., & Fine, L. J. (1993). Revised NIOSH equation for the design and evaluation of manual lifting tasks. *Ergonomics*, *36*(7), 749-76.

Wenger, K. H. & Schlegel, J. D. (1997). Annular bulge contours from an axial photogrammetric method. *Clinical Biomechanics*, *12*(7-8), 438-444.

The Workplace Safety and Insurance Board of Ontario Statistical Supplement to the 2013 Annual Report. (2013). Toronto, ON, Canada.

Yasuma, T., Arai, K., & Yamauchi, Y. (1993). The histology of lumbar intervertebral disc herniation: The significance of small blood vessels in the extruded tissue. *Spine*, *18*(13), 1761-1765.

Yasuma, T., Koh, S., Okamura, T., & Yamauchi, Y. (1990). Histological changes in aging lumbar intervertebral discs. Their role in protrusions and prolapses. *The Journal of Bone and Joint Surgery*, *72*(2), 220-9.

Yingling, V. R., Callaghan, J. P., & McGill, S. M. (1997). Dynamic loading affects the mechanical properties and failure site of porcine spines. *Clinical Biomechanics*, *12*(5), 301-305.

Yingling, V. R., Callaghan, J. P., & McGill, S. M. (1999). The porcine cervical spine as a model of the human lumbar spine: An anatomical, geometric, and functional comparison. *Journal of Spinal Disorders*, *12*(6), 501-8.

Yu, J., Fairbank, J. C., Roberts, S., & Urban, J. P. (2005). The elastic fiber network of the annulus fibrosus of the normal and scoliotic human intervertebral disc. *Spine*, *30*(16), 1815-20.

Yu, J., Tirlapur, U., Fairbank, J., Handford, P., Roberts, S., Winlove, C. P., et al. (2007). Microfibrils, elastin fibers and collagen fibers in the human intervertebral disc and bovine tail disc. *Journal of Anatomy*, *210*(4), 460-71.

Yu, J., Winlove, P. C., Roberts, S., & Urban, J. P. (2002). Elastic fiber organization in the intervertebral discs of the bovine tail. *Journal of Anatomy*, *201*(6), 465-75.

Zander, T., Krishnakanth, P., Bergmann, G., & Rohlmann, A. (2010). Diurnal variations in intervertebral disc height affect spine flexibility, intradiscal pressure and contact compressive forces in the facet joints. *Computer Methods in Biomechanics and Biomedical Engineering*, *13*(5), 551-7.

Zou, J., Yang, H., Miyazaki, M., Morishita, Y., Wei, F., McGovern, S., et al. (2009). Dynamic bulging of intervertebral discs in the degenerative lumbar spine. *Spine*, *34*(23), 2545-50.

APPENDIX A - Individual Specimen Data from Studies II & III

Table A-1: Summary of individual functional spinal unit data from studies II & III.

Specimen	Level	Force	Repetition	Posture	NZ Range	Endplate Area (mm2)	Peak Force (kN)	Cycles	Height Loss (mm)
Survivor Specimens									
4	2	3	3	1	9	611.79	3.59	5000	4.41
9	2	1	1	1	3	689.77	1	5000	1.04
12	2	3	3	1	7	607.3	3.57	5000	10.28
16	1	3	3	1	7	711.99	4.14	5000	7.36
18	2	1	3	1	5	746.29	1.08	5000	1.42
20	1	2	1	1	5	698.44	2.03	5000	2.60
22	2	1	1	1	7	609.6	0.9	5000	1.71
34	1	1	1	1	9.5	826.26	1.19	5000	1.70
35	1	2	3	1	13	772	2.23	5000	3.72
41	1	2	1	1	14	714.28	2.08	5000	3.16
47	2	1	2	2	19.5	760.02	1.1	5000	2.28
49	2	2	3	2	22.5	725.22	2.11	5000	4.14
51	2	1	2	2	24	697.75	1.02	5000	2.55
52	2	2	3	2	18	745.46	2.16	5000	4.05
53	1	1	1	2	21	688.74	1	5000	1.57
55	1	2	3	2	31.5	762.62	2.21	5000	3.57
58	1	2	1	2	19.5	796.73	2.3	5000	2.88
59	2	3	2	1	5	769.16	4.45	5000	5.78
61	1	1	3	1	6	650.66	0.95	5000	1.28
65	1	1	1	1	9	789.63	1.14	5000	0.87
66	1	1	3	2	21	769.52	1.11	5000	1.42
74	1	1	2	2	21	736.07	1.07	5000	1.52
75	2	1	3	2	16.5	740.17	1.07	5000	1.83
76	1	3	1	2	16.5	729.73	4.23	5000	7.63
77	2	1	3	1	5.5	695.85	1.01	5000	1.81
78	1	2	3	1	7	752.8	2.18	5000	3.71
79	1	1	1	2	22.5	708.86	1.03	5000	1.31
80	2	2	3	1	6	793.02	2.29	5000	4.33

81	2	2	1	2	18	689.95	2.01	5000	4.30
83	1	1	2	1	8.5	717.83	1.04	5000	1.31
84	1	3	2	1	10	708.84	4.12	5000	5.18
85	1	1	3	2	24	708.84	1.03	5000	1.65
87	1	1	2	2	30	673.82	0.98	5000	2.33
89	1	2	2	1	7	739.04	2.14	5000	3.42
90	1	2	3	2	27	716.62	2.08	5000	2.70
91	1	2	2	2	21	718.86	2.09	5000	4.17
92	2	3	3	2	15	780.86	4.51	5000	6.44
93	1	2	3	1	5.5	760.71	2.2	5000	3.42
94	2	2	1	1	5	765	2.21	5000	3.36
95	2	1	2	1	8	619.56	0.91	5000	1.62
96	2	2	2	1	6.5	817.55	2.36	5000	4.36
98	1	1	2	1	8	749.31	1.09	5000	1.97
102	2	2	2	1	6.5	724.56	2.1	5000	3.76
103	1	1	3	2	24	725.78	1.05	5000	2.12
105	1	2	1	1	11	657.74	1.92	5000	2.55
106	1	3	3	1	7	758.74	4.39	5000	6.39
107	2	2	1	2	18	788.84	2.28	5000	3.34
108	2	2	3	1	5	724.31	2.1	5000	4.11
111	2	2	2	2	18	705.92	2.05	5000	4.57
112	2	2	2	2	22.5	736.33	2.14	5000	4.26
115	1	3	3	2	27	726.38	4.22	5000	7.02
116	1	1	3	1	9	734.35	1.06	5000	2.24
117	2	1	1	2	24	729.06	1.06	5000	2.07
118	2	1	2	2	18	731.53	1.06	5000	2.51
119	1	1	2	1	6.5	711.95	1.03	5000	2.06
120	2	2	1	1	4	819.95	2.36	5000	1.59
121	1	1	1	2	18	815.75	1.18	5000	1.59
122	2	2	2	1	5	732.66	2.13	5000	3.49
123	1	2	1	2	21	723.93	2.1	5000	3.40
124	2	3	3	2	15	759.44	4.4	5000	9.09
126	2	2	3	2	18	687.7	2	5000	3.84

128	2	1	3	1	4	728.51	1.06	5000	1.53
129	1	3	2	1	10	672.87	3.93	5000	7.32
130	2	3	2	2	19.5	623.63	3.66	5000	5.18
131	1	2	2	1	7	624.8	1.83	5000	3.32
132	2	3	3	1	5.5	597.03	3.51	5000	6.04
133	2	2	1	2	21	625.68	1.83	5000	2.75
134	2	1	2	1	4	837.36	1.21	5000	2.30
135	1	3	2	2	15	870.77	5	5000	6.36
136	2	1	1	2	18	644.3	0.94	5000	1.85
139	2	1	3	2	21	640.04	0.94	5000	2.20
145	1	1	2	2	18	727.15	1.06	5000	1.89
146	1	1	1	2	30	770.5	1.11	5000	2.60
147	1	1	3	2	18	672.4	0.98	5000	2.31
148	2	1	1	2	15	733.09	1.06	5000	1.38
149	1	2	2	1	6	735.03	2.13	5000	3.07
150	1	2	2	2	13.5	705.87	2.05	5000	3.95
151	2	1	3	2	12	702.29	1.02	5000	2.03
153	2	2	2	1	6	671.95	1.96	5000	3.57
154	2	1	3	1	5	749.2	1.09	5000	2.04
155	2	1	2	2	18	783.22	1.13	5000	2.23
156	2	1	2	1	6	618.02	0.91	5000	2.21
158	1	2	3	2	18	828.79	2.39	5000	4.48
159	2	2	3	1	5	703.11	2.04	5000	3.65
160	1	1	2	1	8	680.44	0.99	5000	2.00
161	1	1	3	1	4.5	692.45	1.01	5000	2.11
162	1	2	2	2	18	716.27	2.08	5000	3.43
165	2	3	3	1	6	690.45	4.02	5000	5.84
167	2	2	1	1	5	760.92	2.2	5000	2.66
168	1	3	2	1	5	768.84	4.45	5000	5.66
169	1	3	3	1	8.5	688.43	4.01	5000	7.18
172	1	2	3	1	9	806.76	2.33	5000	4.43
173	2	2	1	2	27	685.75	2	5000	3.55
175	1	2	1	1	7	720.38	2.09	5000	2.84

176	2	2	3	2	21	719.37	2.09	5000	5.13
177	1	3	1	2	27	796.49	4.6	5000	7.72
179	2	1	1	1	6	772.71	1.12	5000	1.87
180	1	2	1	2	22.5	764.66	2.21	5000	4.30
181	1	1	1	1	5	840.72	1.21	5000	1.97
Specimens that experience Fatigue Injury									
7	1	3	1	1	4	618.62	3.63	2318	1.04
11	2	3	1	1	5	820.51	4.73	343	10.28
17	1	3	1	1	6	715.53	4.16	1006	7.36
24	2	3	2	1	4	714.62	4.15	586	1.42
56	1	3	3	2	16.5	777.99	4.5	583	2.60
63	1	3	2	2	18	767.74	4.44	471	1.71
68	1	3	2	2	33	798.23	4.61	1570	1.70
69	1	3	3	2	21	767.74	4.44	127	3.72
99	1	3	1	2	21	766.81	4.44	515	3.16
109	2	3	1	1	6	638.1	3.74	288	2.28
114	2	3	1	2	18	726.34	4.22	1733	4.14
127	1	3	1	2	21	758.63	4.39	3998	2.55
137	2	3	1	1	9	751.06	4.35	43	4.05
138	2	3	1	2	24	720.09	4.18	129	1.57
143	2	3	2	1	8	703.49	4.09	267	3.57
144	1	3	3	2	21	763.52	4.42	943	2.88
152	2	2	2	2	18	752.08	2.18	3139	5.78
163	2	3	2	2	21	761.76	4.41	1869	1.28
164	2	3	2	2	21	743.61	4.31	62	0.87
166	1	3	1	1	7	717.98	4.17	2506	1.42
170	2	3	2	2	21	697.53	4.06	1230	1.52
171	2	3	3	2	15	636.99	3.73	21	1.83
178	2	3	1	2	21	757.24	4.38	504	7.63
182	2	3	1	1	6.5	855.51	4.92	597	1.81

Note: Level (1 = c34; 2 = c56), Force (1 = 10% UCT, 2 = 20% UCT, 3 = 40% UCT), Cycle Rate (1 = 5 cycles per minute, 2 = 10 cycles per minute, 3 = 30 cycles per minute), Posture (1 = 100% neutral zone range, 2 = 300% neutral zone range).